GRATE BOILER MODELING FOR SOFT SENSOR BASED CONTROL

REPORT 2018:490

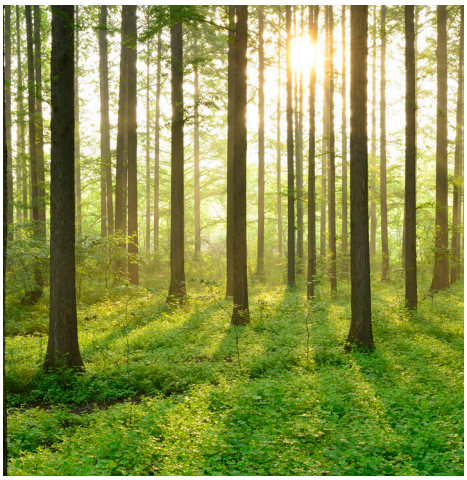

BRÄNSLEBASERAD EL- OCH VÄRMEPRODUKTION

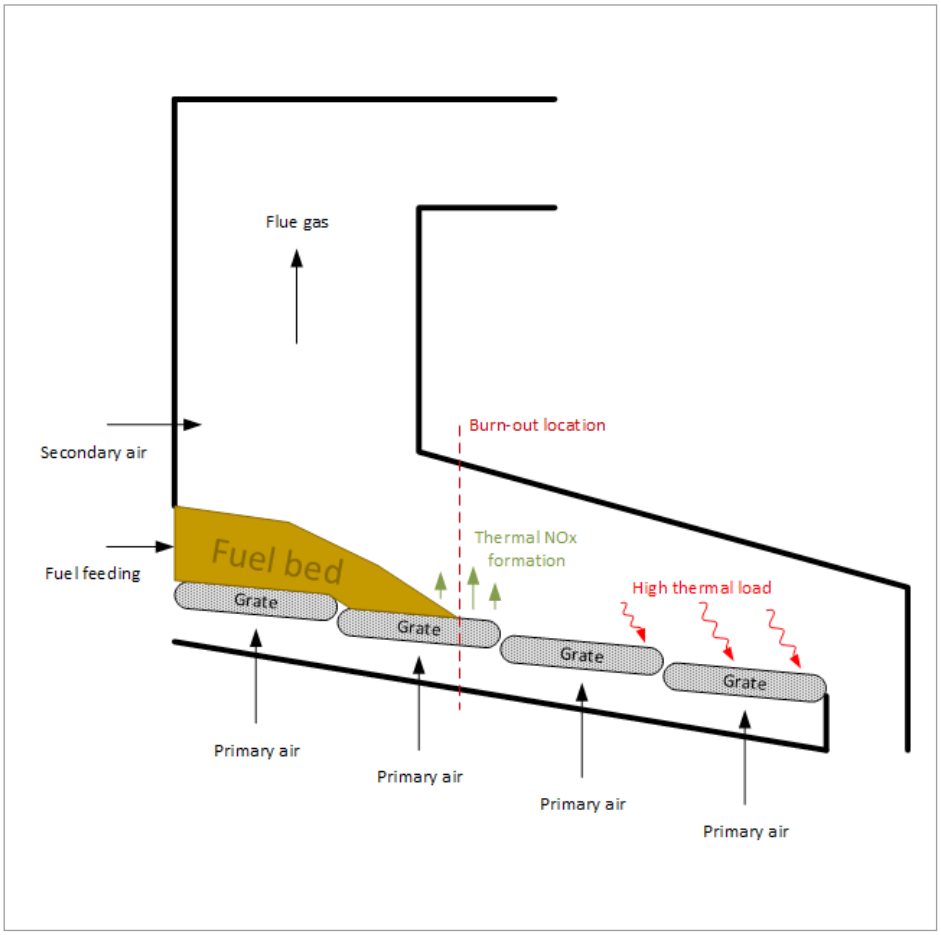

Energiforsk

Grate Boiler Modeling for Soft Sensor Based Control

RENÉ JUST NIELSEN
KASPER VINTHER
HÅKAN RUNVIK
EDWARD EKSTEDT
JOHAN WINDAHL
STÉPHANE VELUT

ISBN 978-91-7673-490-2 | © Energiforsk October 2018
Energiforsk AB | Phone: 08-677 25 30 | E-mail: kontakt@energiforsk.se | www.energiforsk.se

Foreword

Denna rapport är slutrapportering av projekt P43455 Soft-sensor för rostförbränning (Energimyndighetens projektnummer 43455-1) inom SEBRA, samverkansprogrammet för bränslebaserad el- och värmeproduktion.

Programmets övergripande mål är att bidra till långsiktig utveckling av effektiva miljövänliga energisystemlösningar. Syftet är att medverka till framtagning av flexibla bränslebaserade anläggningar som kan anpassas till framtida behov och krav. Programmet är indelat i fyra teknikområden: anläggnings- och förbränningsteknik, processtyrning, material- och kemiteknik samt systemteknik. Programmet är en samverkan mellan Energiforsk och Energimyndigheten. Ingående projekt finansieras av Energimyndigheten och av de parter som Energiforsk samlar i programmet.

Detta projekt har haft som syfte att öka förståelsen för förbränning i rosterpannor och bättre kunna kontrollera den. En soft-sensor för bestämning av flamfrontspositionen har utvecklats baserat på detaljerade pannmodeller i Modelica. Det Modelica-bibliotek som projektet utvecklat finns att tillgå hos Energiforsk och hos Modelon som varit utförare av projektet. Huvudprojektledare har varit Stéphane Velut.

Projektet har följts av en referensgrupp bestående av:

Per Eriksson, Göteborg energi
André Hallberg, E.ON
Nader Padban, Vattenfall
Fredrik Johansson, Holmen
Per Johnsson, Sweco Energuide
Martin Råberg, E.ON

Stockholm oktober 2018

Helena Sellerholm
Områdesansvarig
Termisk energiomvandling, Energiforsk AB

Exekutiv sammanfattning

Med den ökande andelen förnyelsebara energikällor i Europa, ställs nya krav för driften av kraftvärmeverk. Fokus skiftas mot ökad flexibilitet, såsom transienta driftsituationer och drift vid lägre last. För att möjliggöra denna förändring måste pannans beteende analyseras, så att effekterna av drift vid de nya arbetspunkterna kan utvärderas och begränsande faktorer kan identifieras.

Användningen av rosterpannor är utbredd inom kraftproduktionsindustrin. De är flexibla då deras konstruktion möjliggör drift med bränsle med varierande sammansättning, såsom biobränslen eller hushållsavfall. Denna flexibilitet leder också till att kraftverken, åtminstone i teorin, kan drivas med det för stunden billigaste fasta förnyelsebara bränslet som finns tillgängligt. En av nackdelarna med rosterpannor är den relativt långa uppehållstid bränslet har på rosten, vilket tillsammans med variationer i bränslets sammansättning gör processen svår att reglera.

Ett av reglerproblemen för en panna av denna typ rör flamfrontspositionen, det vill säga positionen där allt bränsle har förbränts. För att optimera pannans prestanda och inte skada komponenter får flamfrontspositionen inte avvika för mycket från sitt nominella läge. Om förbränningen är avslutad för tidigt utsätts rosten för påfrestande strålning och pannans kapacitets utnyttjas inte till fullo. Om bädden å andra sidan överfylls riskerar oförbränt material att följa med i askutmatningen, vilket slösar med bränslet och kan skada transportbanden för askan. Av dessa anledningar är det till stor nytta att kunna styra flamfrontspositionen, men i praktiken görs detta sällan på grund av att mätningar av flamfrontspositionen saknas. Detta då utrustningen för att göra sådana mätningar, som IR-kameror och bildbehandlingsmjukvara, är dyr och kräver underhåll.

I detta projekt har en soft-sensor som kan uppskatta bäddhöjd och flamfrontens position baserat på existerande mätningar av bränsle-, luft- och rökgasflöden och av ugntemperatur utvecklats. På detta sätt tillåts reglering av flamfrontspositionen utan dyr mätutrustning. Detta genomfördes genom att modeller utvecklades i Modelica, som tillsammans med svartlådemodellering användes för att ta fram en observerare. Modellerna är baserade på Modelica Standard Library, samt tidigare projekt inom området.

Modellerna i detta projekt avviker från de typiska modelleringsmetoder som normalt används på området. Dessa är antingen detaljerade CFD-modeller som beskriver förbränningen i detalj, men inte kan användas i systemsimuleringar på grund av sin komplexitet, eller kraftigt förenklade modeller för reglerdesign, som bara kan representera processen översiktligt. Med den fysikaliska modellering som Modelica tillåter eftersöks en medelväg mellan dessa båda metoder, där den viktiga fysiken fångas i en enklare modell.

En förenklad modell av en rosterpanna har tagits fram för att kvalitativt validera ett generiskt reglersystem samt för att testa de metoder som ska användas i

projektet på ett enklare system. Målet med modellen är ett kvalitativt rimligt beteende både statiskt och dynamisk.

Den förenklade modellen har primärt- och sekundärt luftflöde samt bränsleflöde som insignaler och mätsignaler på temperatur och syrehalt i rökgasen, samt total frigjord värme som utsignaler. Utöver dessa är den viktigaste signalen i modellen flamfrontspositionen, som är vad projektet som helhet kretsar kring.

Den förenklade pannan består av tre delar: torkning, förbränning och rökgasspädning. Torkningsprocessen för bränslet är modellerad med en konstant hastighet som är proportionell mot den totala mängden vatten på bädden. För att modellera den tid det tar för bränslet att värmas till vattnets kokpunkt används en fördröjningsfunktion. Värmeflödet som krävs för att hetta upp bränslet och förånga vattnet tas från förbränningsmodellen.

Förbränningsmodellen är modellerad som en integrator, där balansen mellan det inkommande bränsleflödet och den stökiometriska förbränningen med det primära luftflödet avgör om massan bränsle på bädden ökar eller minskar. Bränslet på bädden antas vara triangulärt fördelat i riktningen mellan bränsleintaget och askuppsamlingen med en konstant vinkel. Detta innebär att massan bränsle är proportionell med längden och höjden av bränslet. Flamfrontens position antas vara samma som bränslets längd. Förhållandet mellan luft och bränsle vid komplett förbränning sattes initialt konstant. Detta gav dock upphov till att flamfrontens position inte blev observerbar, på grund av att flera bäddlängder kan ge upphov till samma utsignaler. För att åtgärda detta infördes därför effektivitet i förbränningen, som är en funktion av bäddens längd. Massan som förbränns bildar tillsammans med den primära luften och vattenångan från torkningsprocessen rökgasflödet. Detta blandas upp med det sekundära luftflödet i rostermodellens tredje del. Här sänks rökgasens temperatur och syre tillsätts (då förbränningen med den primära rökgasen antogs stökiometrisk innehåller gasen som bildats vid förbränningen inget syre) genom enkla fysikaliska samband.

Den kompletta förenklade modellen har fyra dynamiska tillstånd. Den uppvisar tillfredsställande kvalitativa resultat, men är otillräcklig för en mer detaljerad analys, framförallt på grund av att bränslets relativa fördelning på bädden är konstant, för att förbränningsmodellen där endast primärluften används är orealistisk, samt på grund av effektivitetsfaktorn som lades till i förbränningsmodellen, som endast har lösa fysikaliska grunder.

Ett förenklat generiskt reglersystem har utvecklats för att undersöka beteendet för den förenklade rosterpannemodellen med en sluten reglerloop. Detta system kommer även ligga till grund för reglersystemet för den komplexa modellen. Reglerstrukturen är baserad på standardmetoder inom kraftverksreglering, där styrningen bestäms genom en kombination av framkoppling och återkoppling. För modellerna som är utvecklade i detta projekt används två av utsignalerna som angivits för den förenklade processen som insignaler till reglersystemet; det totala värmeflödet och syrehalten i rökgasen.

Tre PID regulatorer används i systemet för att styra last/bränsleflöde, last/primärluft och syrehalt. Deras funktion summeras nedan.

- Last/bränsleflöde: Framförallt integralverkande reglering med långsam tidskonstant. Dess syfte är att motverka variationer i bränslets värmevärde över längre tid (timmar). Ger tillsammans med framkopplingssignalen för lasten bränsleflödet till pannan.
- Last/primärluft: Framförallt P- och D-reglering med syftet att motverka variationer i ångtryck. Ger tillsammans med motsvarande framkopplingsterm det primära luftflödet.
- Syrereglering: Reglerar förbränningens stökiometri genom att styra det sekundära luftflödet. Regulatorn är relativt långsam och är inställd för att bibehålla ett överflöd av syre över längre tidsperioder.

Noterbart är att ingen hänsyn tas till bränslets fördelning i pannan i denna typ av reglersystem.

Då den förenklade modellen är otillräcklig för att beskriva dynamiken i en verklig panna på ett tillfredställande sätt utvecklades en detaljerad modell utifrån grundläggande fysikaliska principer. Kärnan i denna modell är bäddsegment, som beskriver de olika processer som sker när bränslet torkas och omvandlas till brännbara gaser, samt förbränningsmodellen. Dessa komponenter ingår i ett större system som beskriver pannan som helhet och därför även innefattar modeller för rosten, pannans väggar, värmeöverföringsmodeller, gasvolymer samt randvillkor för värme- och massflöden. Utöver dessa tillkommer även mediamodeller, som används för att beskriva de termodynamiska egenskaperna hos bränsle, luft och rökgas. De viktigaste delarna i detta system presenteras härnäst.

Luft- och rökgasmediet modelleras som en ideal gasblandning, med hjälp av interfaceklasser som finns tillgängliga i MSL. Mediet består av kväve, syre, kolmonoxid, koldioxid, vattenånga och metan.

Bränslets sammansättning beskrivs med hjälp av en kombination av ultimat och proximat analys. Båda beskrivningarna är nödvändiga då sammansättningen både på atomnivå och molekylär nivå behövs för att kemiska balanser och energiinnehåll ska kunna representeras korrekt. Varje kategori i den proximata beskrivningen av bränslet modelleras genom enkla antaganden såsom konstant värmekapacitet, förutom vattnet, som representeras med det färdiga tvåfasmediet IF97, som finns i MSL.

Varje Bäddsegment har fyra portar, där bränsle och gas kommer in och leds ut. Utöver dessa finns även värmeportar som möjliggör värmeutbyte med omgivningen via strålning och konduktion. Modellen består av tre undermodeller som beskriver hur bränslet torkas och devolatiliseras samt förgasningen av det förkolnade bränslet. Var och en dessa är modellerade enligt följande:

- Torkning: När massan vattenånga i ett bränslesegment överstiger noll, överförs ett flöde ånga från bränslet till gasvolymen, som är proportionell med ångans massa.
- Devolatilisering: Flyktiga ämnen i bränslet flödar till gasvolymen i form av väte, kolmonoxid, vattenånga, koldioxid och metan. Processen drivs av Arrhenius ekvation. Andelen vattenånga och koldioxid i den producerade gasen bestäms av fixa massfraktioner, medan övriga ämnen bestäms av massbalanser utifrån bränslets sammansättning.

- Förgasning: Baserat på den tillgängliga mängden koldioxid, syre och vattenånga i gasen och reaktionshastigheter tagna från litteratur, reagerar dessa ämnen med kol i bränslet, vilket resulterar i produktion av kolmonoxid, koldioxid och väte.

Med hjälp av mass- och energibalanser för bränslet och gasen beräknas hur stora respektive massflöden ut ur modellen ska vara, samt vid vilka temperaturer de sker. Gasflödena är drivna av tryckskillnader, medan bränslet drivs framåt med hjälp av rostens rörelse, som beskrivs av en hastighet som ges av en insignal. Geometriskt beskrivs bränslet i varje bäddsegment som ett rätblock med fix längd och bredd, medan höjden beräknas från den totala mängden bränsle i segmentet.

Förbränningsmodellen är statisk och uppdelad i tre olika fall, baserat på mängden tillgängligt syre. Med hjälp av stökiometri, antaganden om ordningen reaktionerna sker i och vatten-gas skift-ekvationen förbränns de brännbara ämnena i gasen. Den frigjorda energin beräknas med hjälp av formationsentalpin för respektive ämne.

Bäddsegmenten kopplas samman i serie och bildar på detta sätt bränslebädden. Under varje segment i bädden finns ett rostsegment som är sammankopplat med bädden genom luftflödet, som går genom rosten och via en termisk port, för att fånga värmeöverföringen mellan dem båda. Rostsegmenten består av termiska massor och rörmodeller för luftflödet.

Gaserna som frigörs i bädden leds tillsammans med det primära luftflödet till den primära förbränningsmodellen, blandas med det sekundära luftflödet och sedan vidare till den sekundära förbränningsmodellen. Förbränningsmodellerna, bäddsegmenten samt termiska modeller för pannans väggar är alla kopplade till en generell strålningsmodell, som representerar de viktigaste värmeflödena mellan dessa delar.

Flamfrontens position beräknas med hjälp av förgasningsmassflödet från segmenten. Flamfrontens position antas vara där 90 procent av det totala förgasningsmassflödet skett.

För att validera modellen användes data från Sysavs avfallskraftvärmeverk vid Spillepengen i Malmö. En svårighet med denna validering var den begränsade mängden dynamiska mätdata från anläggningen, vilket ofta är fallet för denna typ av kraftverk. För att kringgå att det momentana bränsleflödet inte mäts och att bränslets sammansättning inte är känt användes standarden EN-12952-15 för att validera modellen statiskt. Vidare finns inte heller mätningar av rostens hastighet och flamfrontens position, vilket innebar att valideringen av flamfrontspositionen mot det verkliga verket endast gjordes indirekt, genom kvalitativ och kvantitativ analys av modellens övergripande beteende.

Den fullständiga modellen parametriserades för att matcha Sysavs anläggning enligt ovan. Den har tio bädd- och rostersegment, vilket tillsammans med övriga modeller ger en modell med cirka 300 tillstånd och 3700 variabler. Simuleringar av modellen visade att de kvalitativa och kvantitativa resultaten överensstämmer med förväntningarna. De olika underprocesserna i bädden sker vid de förväntade temperaturerna och massflöden, energiflöden och temperaturer i övrigt är också rimliga. Vissa transienta beteenden i temperatur och syrehalt i rökgasen

identifierades som orsakade av bäddens diskretisering. Modellen kan simuleras cirka 40 gånger snabbare än realtid, men den har vissa robusthetsproblem, vilket visar sig begränsande i vissa senare moment i projektet. En begränsad modelleringsinsats förväntas dock vara tillräcklig för att lösa dessa problem.

För att estimera flamfrontens position utifrån mätsignaler användes ett artificiellt neuralt nätverk (ANN). Detta är implementerat i Python med paketet NeuroLab. Att utveckla en observerare med hjälp av unscented kalman-filter (UKF) undersöktes även under projektet, men på grund av det stora antalet tillstånd bedömdes det som orimligt att använda den komplexa modellen direkt i detta syfte, framförallt på grund av observerbarhetsproblematik, men även på grund av beräkningstiden, som skulle blivit oerhört lång på grund av de många sigma-punkterna processen skulle ge upphov till och den relativt långsamma simuleringshastigheten. Att använda en förenklad modell i Kalman-filtret och den detaljerade modellen för att simulera processen hade dock kunnat vara en möjlig lösning på detta spår.

Det neurala nätverket använder mätsignaler som är tillgängliga i den riktiga processen för att hitta vikter som minimerar skillnaden mellan nätverkets utsignal och flamfrontens position i modellen. Då ett ANN normalt är statiskt används samplade signaler som fördröjs för att fånga systemets dynamik.

Träningsdata togs fram genom att processens insignaler exciteras vid olika lastförhållanden med en pseudo-random binary signal (PRBS) med varierande amplitud. För att uppnå tydliga variationer i flamfrontens position kombinerades dessa med trapetsformade variationer av det primära luftflödet. Träningsdata motsvarande cirka 25 timmar genererades på detta sätt och importeras till NeuroLab.

Olika parametriseringar av det neurala nätverket utvärderades genom att nätverkets förmåga att observera ett separat scenario med samma typ av variationer i insignalerna som för träningsdatan, men drivet av ett annat random seed. De bästa resultaten erhölls från ett system med 20 noder i ett lager, med samplingstiden 120 sekunder och där insignalerna till nätverket är fördröjda med noll, ett och två tidssteg. Resultaten visar att nätverket kan reproducera det generella beteendet hos variationerna i flamfrontspositionen, men att brus och spikar gör att signalens tillförlitlighet inte kan garanteras generellt.

Ett förslag till förbättrad pannreglering togs fram från det generiska reglersystem som tidigare presenterats. Den estimerade flamfrontspositionen adderades tillsammans med en PID-regulator till systemet. Styrsignalen denna krets genererar används i styrningen av bränsleflöde och primärluft, genom att styrsignalerna för dessa multipliceras med en faktor framfrontsregleringen genererar. Experiment på den förenklade rostermodellen användes för att validera metodens giltighet. Dessa visar att metoden förbättrar reglerprestandan för systemet. På grund av robusthetsproblem med den komplexa modellen kunde denna inte användas vid simulering i sluten loop. Av denna anledning är inte heller flamfrontsestimeringen medtagen i detta system, istället används det faktiska värdet.

Summary

As renewable energy production is increasing, the demands of thermal power plants is changing. More flexibility is required, such as transient operation and operation at lower load. This project is aimed at this issue for grate boilers, by investigating how better control of the flame front position can be achieved.

Flame front position control have traditionally only been possible by using cameras and image processing to estimate the location of the combustion. However, since this solution is quite expensive it is rarely found. An alternative approach, which is the focus of this project, is to utilize existing measurements to estimate the flame front position. This discipline is also referred to as state observation and inherently relies on a physical model to calculate the immeasurable process variables.

Since the estimated variable of interest (the flame front position) is not measured the validation of the soft-sensor must also rely on adjacent measurements under the assumption that "if the physics-based model reproduces these measurements well, then the estimate of immeasurable variables also matches the physical values". This approach is commonly found in power plant control in, e.g., coal mill control, where the mass flow of pulverised coal is usually not measured (see e.g. [Andersen et al., 2005]). A detailed Modelica model of a grate boiler have thus been created for this purpose. Using physics-based modelling, the model was created in a bottom-up approach, where submodels are combined into a complete representation of the bed, the grate, fuel combustion and transfer of heat and mass.

The bed is the main part of the model, which consists of bed segments which form a discretization along the flow direction of the fuel. Inside each segment, the processes of vaporization, pyrolysis and char conversion are modelled. Another important part of the model is the combustion model, which calculates the production and composition of flue gas and the released heat, based on the gaseous fuel composition and temperature. The model also contains a complex radiation model, to capture the heat transfer between different parts of the bed and furnace.

To estimate the position of the flame front in the model, an artificial neural network is used. Training data with random excitation is created and used for training of the network, which only gets signals that are typically measured in a real plant as input. The network is implemented in python, using simulation results imported from Dymola. Experiments with the trained network reveals that it is likely possible to retrieve the desired information about the flame front from already existing measurements. Limits in the implementation makes it hard to draw conclusions about whether the results from the model are applicable in a real process too, but the limited number of measured signals used in the model is a promising sign, as additional measurements could simplify the estimation task considerably.

To verify the usefulness of estimating the flame front position, an improvement over a generic control scheme developed in the project is proposed, utilizing this

information. The controller is tested on a simplified grate boiler model, showing that improvements in performance is achieved with the added information.

List of content

1 Introduction

1.1 BACKGROUND

With an increasing penetration of renewable energy in Europe over the last two decades the volatility of electricity prices has increased. At the same time, increased competition within district heat production forces asset owners to review their production portfolio toward higher production flexibility both in terms of transient operation (balancing services, day-ahead and intraday markets), reduction of minimum stable generation (MSG) and choice of fuel. This has resulted in an increased focus on optimizing plant operation and agility on all levels from component to systems to portfolio level.

A necessary approach for successful achievement of these improvements is to identify and mend the restricting (and often underlying) components or processes in the hierarchy. In thermal heat and power plants restricting components (ignoring faulty components) are equal to the components with large time constants (slow) or stochastic behaviour. That is to say the boiler.

Grate boilers are widely used in the power generation industry as they allow for combustion of heterogeneous fuels such as biomass or household waste, providing a good fuel flexibility and tolerance against variations in fuel water contents and heating value. They have the advantage to accept almost any solid fuel and, in theory, make it possible to select the cheapest renewable fuel available. The price for this flexibility and tolerance is a big inertia in the combustion dynamics due to a high residence time of the fuel of 10–20 minutes (grate entry to slag hopper). Furthermore, in practice a long commissioning time and fine-tuning is the reality due to the stochastic properties of the fuel (moisture, heating value and ash content) in combination with a lacking understanding of the dynamic behaviour under different working conditions.

The main problem is to control the burn-out location or flame front on the grate and ensure an evenly decreasing bed thickness towards the slag discharge without exposing or over-filling the grate. Figure 1 shows an illustration of the problems that can occur if there is insufficient fuel on the grate, such as increased formation of thermal NO_X near the burn-out location (too much air), higher thermal load on the exposed part of the grate (radiation), and under-utilization of the grate capacity.

Figure 2 shows an illustration of the problems that can occur in the opposite scenario, with an over-filled grate. In this case unburnt fuel enters the slag discharge (waste of money and risk of fire in the slag conveyor system), the CO formation is higher due to insufficient primary air (can lead to explosions), the mechanical load is higher, and the furnace temperature is lower.

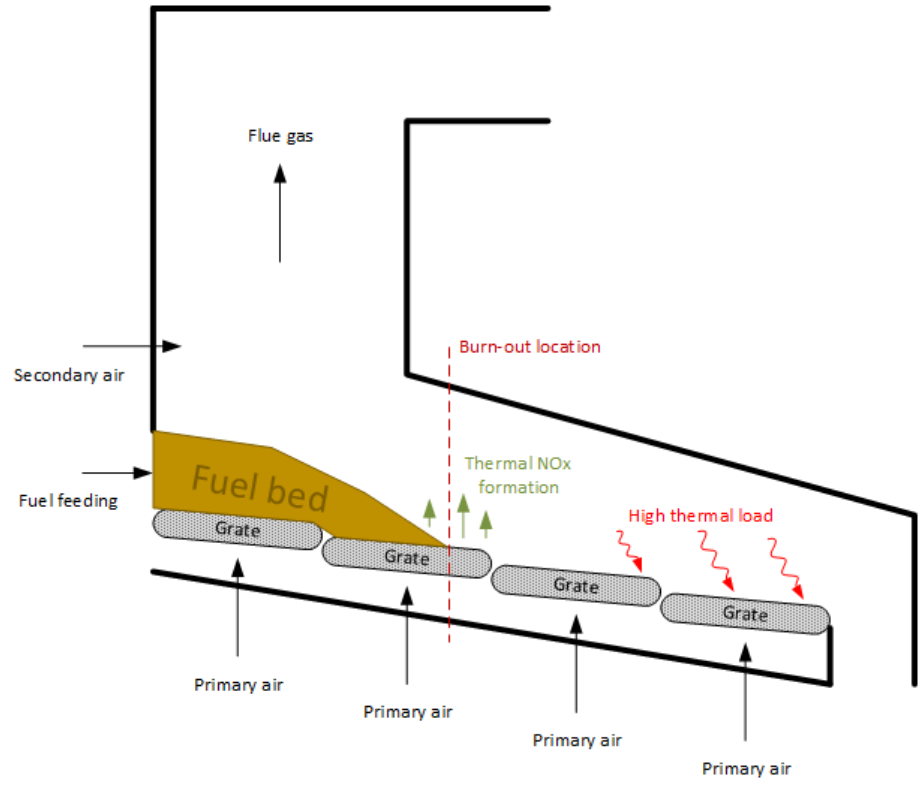

Figure 1. Illustration of exposed grate with insufficient fuel.

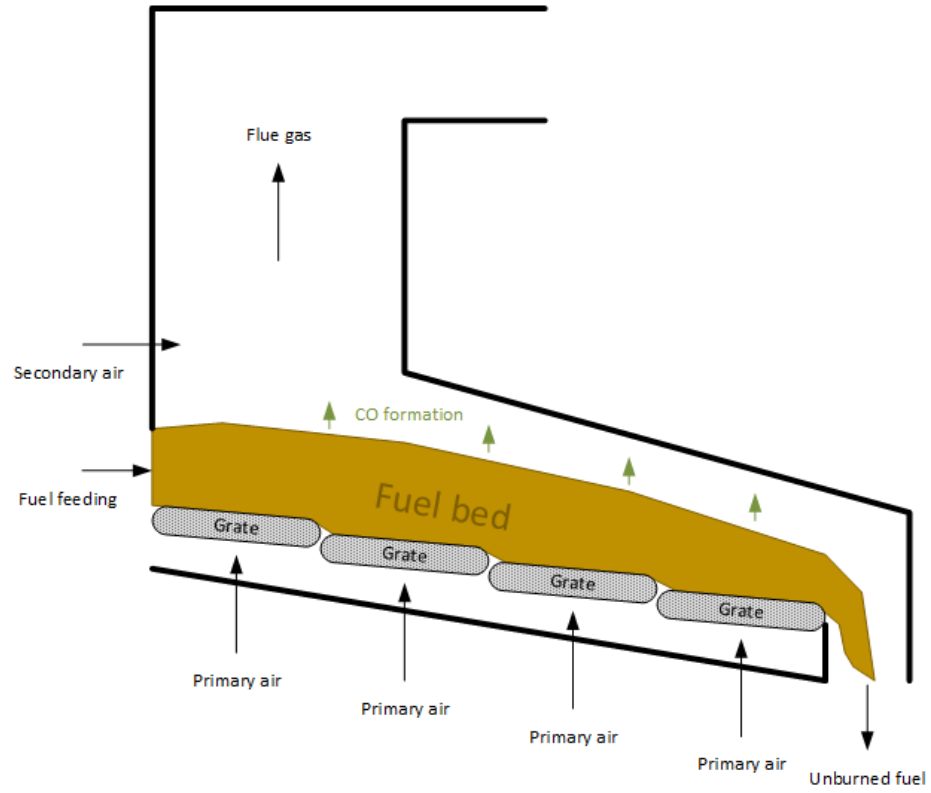

Figure 2. Illustration of over-filled grate with unburned fuel entering the slag hopper.

Good control of the burn-out location and an evenly decreasing bed thickness would result in a better utilization of the grate with a narrower safety margin. These quantities can unfortunately not be measured online very well, and plants are not commonly equipped with the state-of-the-art and expensive technology such as IR cameras and image processing software. Moreover, those measurements do not provide any information about the process behaviour to support the boiler control design. A grate boiler exhibits indeed a complex dynamical behaviour that should be well understood for the design and tuning of the control system; instabilities (from fuel/air imbalance) and non-minimum phase behaviour (increasing fuel flow causes temporarily a decrease in power output). Consequently, the boiler control is often tuned in a very conservative way, making the overall boiler control slow and sensitive to disturbances, causing large variations in NO_x and CO emissions. This calls for a model-based soft sensor that can estimate the flame front by combining a physical model of the plant and commonly available measurements, see illustration of the concept in Figure 3. The model-based soft sensor can additionally improve the understanding of the furnace behaviour and thereby the design and tuning of the boiler control system. This, in turn, can lead to a better use of the boiler capacity, the utilization of cheap low-grade fuels (high ash and moisture contents, low heating value) and more stable emissions.

The main processes taking place in grate fired boilers are illustrated in Figure 4. Wet fuel is heated and dried on the first part of the grate. The fuel then undergoes a devolatilization process where volatiles are removed through pyrolysis. Char then reacts with the surrounding gases at high temperature, resulting in gasification of the substance and release of heat. The remaining ash is finally cooled down on the last part of the grate. The gases released from the fuel on the grate is subsequently combusted above the grate with the addition of secondary air through air-staging.

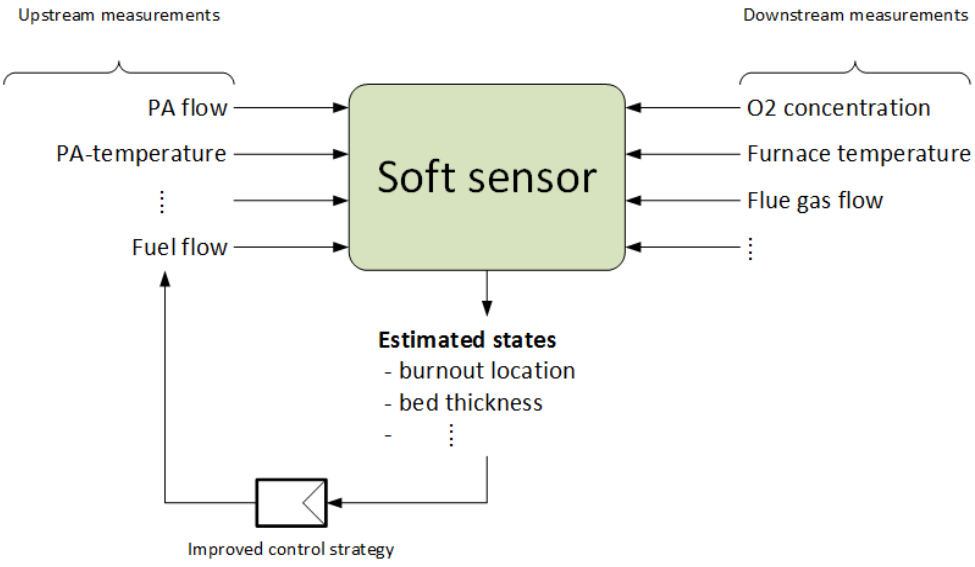

Figure 3. Illustration of the soft sensor concept for estimation of, e.g., burn-out location.

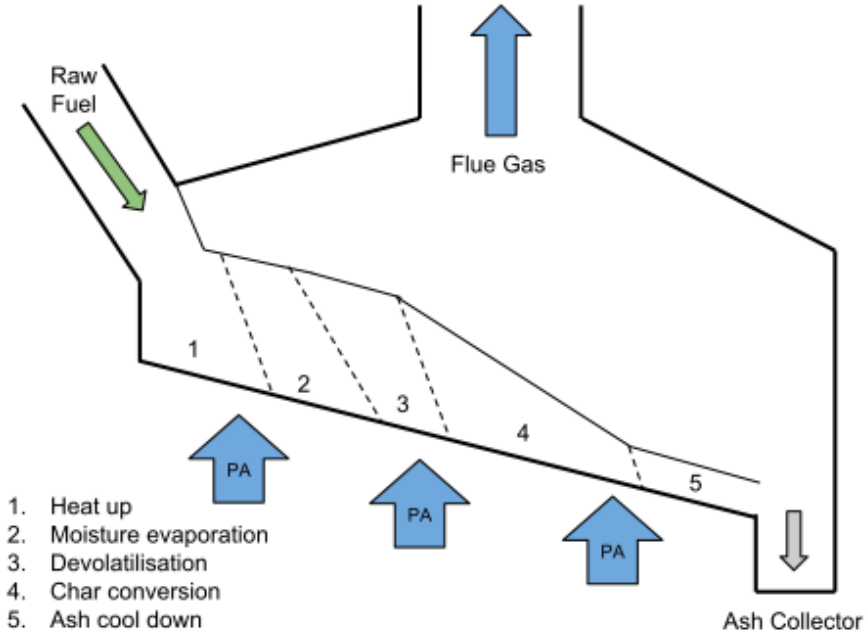

Figure 4. Illustration of the main processes taking place in grate fired boilers.

Prior studies of grate combustion typically fall into one of two categories:

1. Highly detailed models (CFD), e.g., see [Yin et al., 2008], describing the combustion part on either a short time scale (reaction kinetics) or in steady state. These models do not consider the dynamic changes in inputs that occur in normal closed-loop operation of a grate boiler. They require detailed information about plant geometry, boundary conditions and parameter values and are too computationally expensive for online use.
2. Simple, causal transient models used for control purposes. They have the advantage of high simulation speed and a limited number of parameters. However, their simplicity means that they only capture the overall dynamics and not the restricting details of the process that limit the grate operation (burnout zone, thermal/mechanical load etc.). The models are most often implemented in a non-standardized and structurally rigid way (manual equation rewriting) making them difficult to reuse and practically impossible to reconfigure and adapt to other plants/fuels. See, e.g., [Ramström et al., 2004] and [Paces et al., 2011].

The gap between the two categories calls for a setup that captures the right level of detail for the plant in question. Since the required scope/fidelity and available measurements will vary from plant to plant (even with similar boiler configurations) the dynamic model that constitutes the foundation for a soft sensor must be highly adaptable. In the field of soft sensors, implementation is predominantly done with highly customized code conforming, at most, to external interfacing standards. This makes it hard to adapt the internal models used for the estimation to new conditions. The aim has therefore been to make use of a standardized modelling language (Modelica), model interfacing technologies

(Functional Mock-up Interface) and measurement signal interfaces (OPC) to provide a transparent workflow.

The soft sensor plant model derived in this work is used for two purposes with their specific constraints:

1. Building a soft sensor that estimates flame front. Need for real-time performance.
2. Designing a control strategy that fully exploits the bed capacity and results in stable and low emissions.

A requirement has thus been that the model must be structurally compatible with both purposes, i.e. share the same interface to external measurements and internal submodels (grate metal, bed segment, gas combustion etc.). Furthermore, a requirement has also been that it must be easy to replace a simple formulation of, e.g., fuel drying with a more complex one and vice versa as well as to specify, say, the spatial discretization of the bed.

Modelica is an open and equation-based language for physical modelling that inherently supports this modular and component-based way of constructing models of varying complexity. The Functional Mock-up Interface (FMI) is an industrial standard interface that allows models of any complexity to be compiled into a single block accepting, e.g., plant measurements as inputs and producing estimated states as outputs. It takes care of the transition from a tool/language specific model to a standardized implementation. Furthermore, the combination of multiple physical domains (mechanical, chemical, thermal, thermo-fluid, etc.) in the same modelling framework is usually done in an ad-hoc way. Modelica is a true multi-domain language that has a clear interface between different physical domains making it easy to adjust model details, e.g., in heat transmission correlations, while keeping the same details in the hydraulic domain.

The description and quantification of the chemical processes taking place in combustion are extremely complicated and much time can be spent in this field. A key effort in this project has therefore been to balance detailedness and simplicity. The work here thus builds on previous modelling efforts published in, e.g., [Ramström et al., 2005], [Kuijk, 2008], [Bauer et al., 2010]. Additionally, Added Values has previously developed a model together with Aalborg University, Institute of Energy Technology dealing with the modelling and simulation of biomass combustion in a grate fired boiler. In this work a flexible model structure was specifically considered, see [Veje, 2016a] and [Veje, 2016b].

1.2 REPORT OUTLINE

To begin with, a preliminary, simple grate boiler model has been set up from the requirements of a generic grate boiler control system. The purpose is to validate the behaviour of the closed-loop control and to get initial experience with state observation of the process in question.

Subsequently, detailed models have been developed from a first principles approach and continuing experience from previous work in the same field, e.g. [Ullum, 2000], [Veje, 2016a], [Veje, 2016b]. The used modelling framework adhere

to the requirements outlined in Section 1.1 and is based on the Modelica modelling language.

The models are then used to construct a detailed grate boiler simulation environment, which is used as “the truth” in the following estimator design. The Simulation model is parameterized according to approximate dimensions and layout of the Sysav WtE plant in Malmö. Since measurements in the fuel and flue gas path in power plants are always very limited — and the Sysav plant is no exception — it is not possible to make a complete validation of the dynamic combustion model against measurement data. However, to address this common problem in power plant modelling, the EN-12952-15 norm has been used to recover steady state values of some of the missing boundary values for the model using measurements from Sysav. Given the scope of the project, the intent is not to provide an exact replica model of Sysav since this is an extensive task itself, even with existing simulation tools. Rather, the purpose of the model is to reproduce realistic dynamic behaviour of immeasurable quantities such as the flame front position such that soft-sensor ideas can be tested on a conceptual level.

Several approaches for estimating the flame front have been considered, finally settling on an Artificial Neural Network (ANN) solution as the full model developed in the project was too complex to use directly in a Kalman filter implementation.

Finally, an extended control concept is presented — based on the initial, generic grate boiler control — that stabilizes the flame front location, in simulations with the simplified grate boiler model.

2 Preliminary Grate Boiler Model

A preliminary simple model has been set up to qualitatively validate a generic grate combustion control scheme and to be able to make a comparison between a simple and a complex model. The model should simply reproduce the steady-state and transient responses that can be immediately reasoned to justify the behaviour of the controlled process. The simple model also serves as a tool to test soft sensor implementations and designs and to find potential limitations and solutions in an early stage of the project.

2.1 MODEL REQUIREMENTS

The model was designed using a top-down approach from the input/output requirements of the generic control structure resulting in the following inputs;

- fuel mass flow rate,
- primary air (PA) mass flow rate,
- secondary air (SA) mass flow rate,

and the following outputs;

- oxygen concentration ("O2 contents") in the flue gas,
- flue gas temperature after final combustion stage (SA injection),
- total heat release from combustion,

as shown in Figure 5 below.

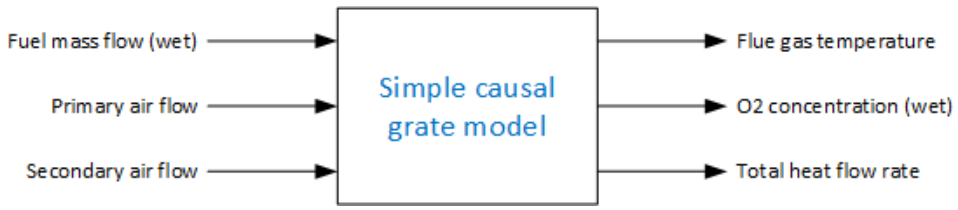

Figure 5. I/O requirements for a simple grate combustion model.

In addition to the input /output signals, fuel and air properties (temperature, moisture contents etc.) are given as parameters.

No chemical reactions are considered in the simple preliminary model, as such considerations quickly grow in complexity. However, this is the focal point in subsequent modelling work.

2.2 MODEL CONSTRUCTION

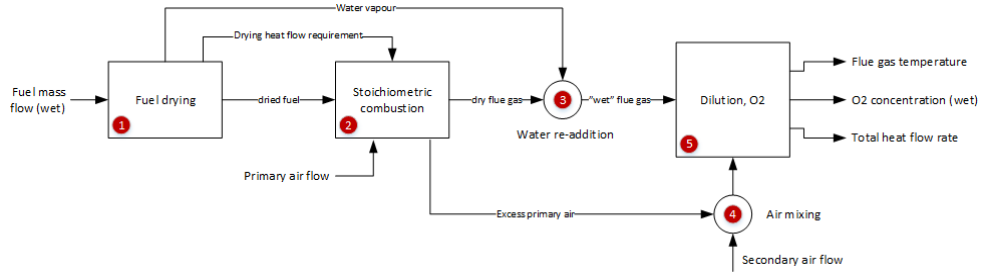

Figure 6. Total process of simple grate combustion model.

Figure 6 shows the internal sub-processes of the simplified model, which consists of the following blocks:

1. Fuel drying.
2. Stoichiometric combustion of dry fuel.
3. Re-addition of vaporized moisture.
4. Mixing of excess primary air from combustion with secondary air.
5. Addition of total secondary air to increase oxygen contents in flue gas to a specified value.

The process and its submodels were constructed from the following assumptions and behavioural requirements. All submodels contain equations for conservation of mass and energy.

2.2.1 Fuel Drying

Wet fuel enters the grate and is continuously dried at a constant rate k_e multiplied by the total accumulated mass of water m_w on the grate. A variable delay is used to simulate a "dead zone" in the start of the grate, where the cold wet fuel is heated to the water vaporization temperature (see also [Bauer et al., 2010]). The delay T_d is set to

$$T_d = \frac{k_d m_w}{m_{wf}(1 - x_{H2O})}$$

where m_{wf} is the wet fuel inlet mass flow, x_{H2O} is the water content ratio (0–1), and k_d is a parameter, which can be used to tune the delay (e.g., 30 seconds at nominal steady state load). The delay will thus go to zero when the accumulated water mass approaches 0 and the delay will also depend on the dryness of the fuel added. Given the moisture contents and temperature of the fuel, the heat required to raise the temperature to 100 °C and vaporize the water is calculated and exposed as an output signal. This value must later be subtracted from the heat release in the stoichiometric combustion. The mass flow rates of dried fuel and water vapor, respectively, are also given as output signals. Figure 7 below shows the responses of a step in wet fuel input. The change in dry fuel flow is delayed approximately 27 seconds relative to the step change and the vapor flow only slowly starts to increase after the delay time, since it is a function of the accumulated mass (changes very slowly). The required heat (Q_flow) immediately increases with the

step in wet fuel flow (cold wet fuel enters the bed) and then gradually increases with the increasing vapor flow.

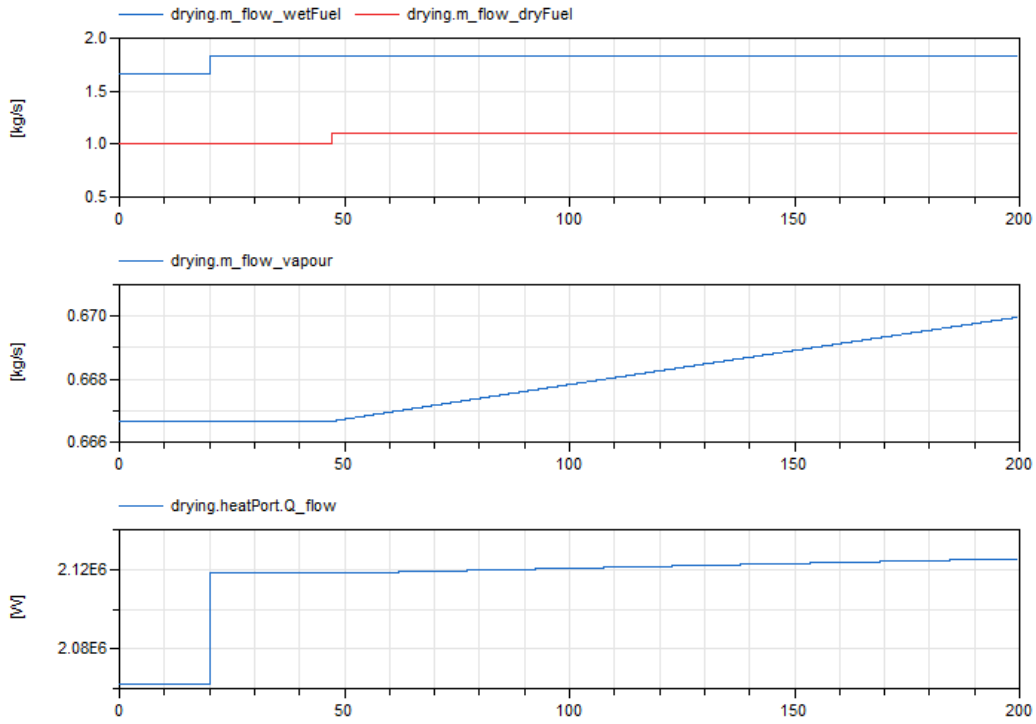

Figure 7. Responses of a step in wet fuel input.

2.2.2 Stoichiometric Combustion

Figure 8 below shows the idea behind the stoichiometric combustion and bed buffering.

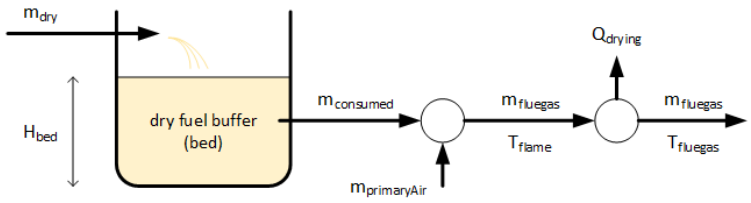

Figure 8. Bed buffer concept.

Dried fuel enters the grate in a buffer (the bed). The grate speed is not considered. Primary air (PA) also enters the block and consumes a certain amount of fuel from the buffer per kg/s of PA. Thus, if the inputs of dry fuel and air are not matched, fuel on the grate will accumulate or decrease resulting in an integrating behaviour of the bed height, H_{bed}. Given the heating value of the fuel and the temperatures of fuel and PA, the adiabatic flame temperature is estimated. Finally, the heat flow rate required for the fuel drying is subtracted, thus lowering the flue gas temperature.

The relation between the fuel consumption and the PA flow was taken from [Sadaka et al., 2009] in which it is stated that the stoichiometric combustion of one kg of dry biomass requires 4.58 kg of air. If this ratio is fixed during the simulation the bed height will become unobservable since the same solution of the grate model can appear for different bed heights. To make the model observable there should be a coupling between the bed height and the rate of fuel consumption. This is done by introducing a quadratic air efficiency ratio n_{PA} (0-1) as a function of the bed filling, which determines how much of the PA air is available for the combustion;

$$n_{PA} = \min\left(1, \max\left(0, \left(\frac{L_{bed}}{L_{nom}}\right)^2\right)\right)$$

where L_{bed} represent how much of the grate length is filled with fuel and L_{nom} is the nominal length (efficiency is 1 if L_{bed}=L_{nom}). It is assumed that the fuel on the bed has a triangular shape, with decreasing height along the grate away from the fuel inlet, so that the bed length L_{bed} is equal to 5*H_{bed}.

Figure 9 shows the step responses from PA and fuel flow to bed height, air efficiency, and flue gas heat flow rate.

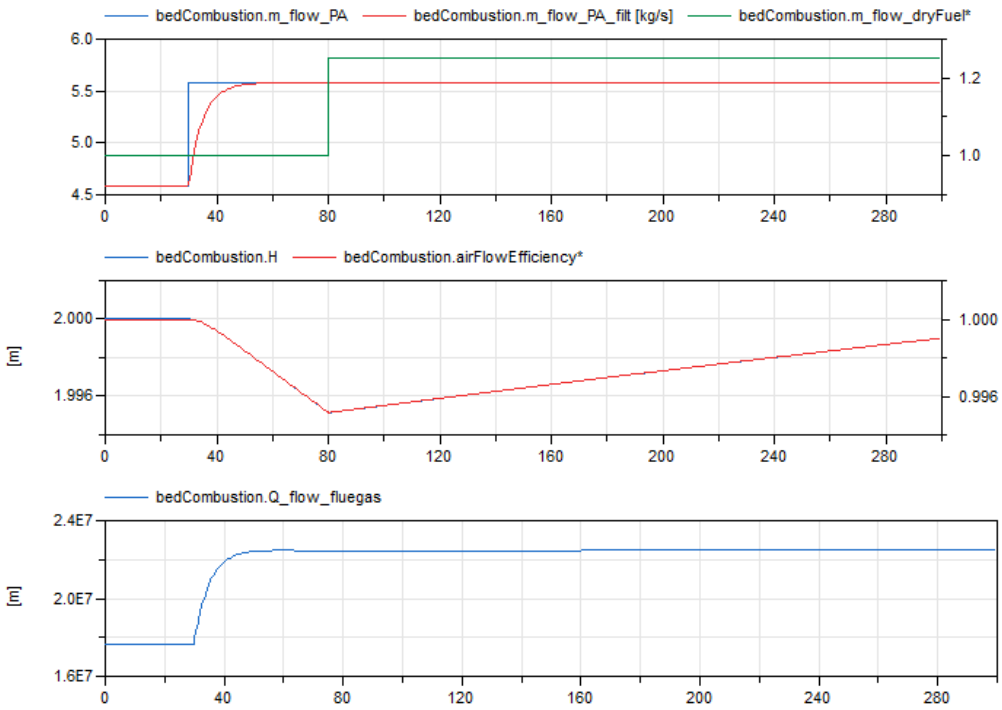

Figure 9. Step responses.

As expected, increasing PA flow causes an increased consumption of the bed buffer and a decreasing bed height. Likewise, increasing the inflow of dried fuel changes the rate of change in bed height — in this case such that the bed height increases again. The air efficiency also changes with the bed height and the heat transfer rate is tied to the consumption rate on the bed (PA flow).

The flue gas temperature calculated in this block is unrealistically high (> 2,700 °C). This is due to the two following model deficiencies, which are remedied in the subsequent blocks:

1. The water vapor has been removed but not yet re-added to the flue gas.
2. The combustion is strictly adiabatic.

2.2.3 Water Re-addition

After the combustion the water vapor from the drying process (at 100 °C) is re-added to the flue gas, lowering the flue gas temperature further. The specific heat capacities of dry and wet flue gas are provided as parameters, which can be used to fit the resulting flue gas temperature to a desired value.

2.2.4 Flue Gas Dilution

Since the secondary air flow is required to control the oxygen contents in the flue gas and since the combustion block only produced zero excess air (stoichiometric combustion), secondary air is mixed with the flue gas to increase O2 contents. The assumption is that SA contains 21 % of oxygen and the incoming flue gas 0 %. During this "dilution" the temperature is decreased further. Since, normally, the secondary air makes up a large part of the combustion air compared to PA, the PA and SA mass flows in the simplified model will be unrealistic. However, to assess the dynamic behaviour around a working point this has no consequence.

2.3 STEP RESPONSES

To validate the simplified model open-loop step responses have been performed.

2.3.1 Primary Air Flow Step

The responses of a step increase in PA flow is shown in Figure 10 below.

- The bed height decreases (ramp) as the fuel/air balance is compromised and the increased primary air consumes fuel from the buffer.
- The O2 contents in flue gas decreases as the increase in PA produces more flue gas but starts to increase again when excess primary air is mixed into the secondary air due to a decreasing air efficiency.
- The flue gas temperature increases, because increased PA flow consumes more dry fuel from the bed buffer, without an increased drying heat flow demand.
- The heat flow rate increases due to an increased flue gas temperature and flow.

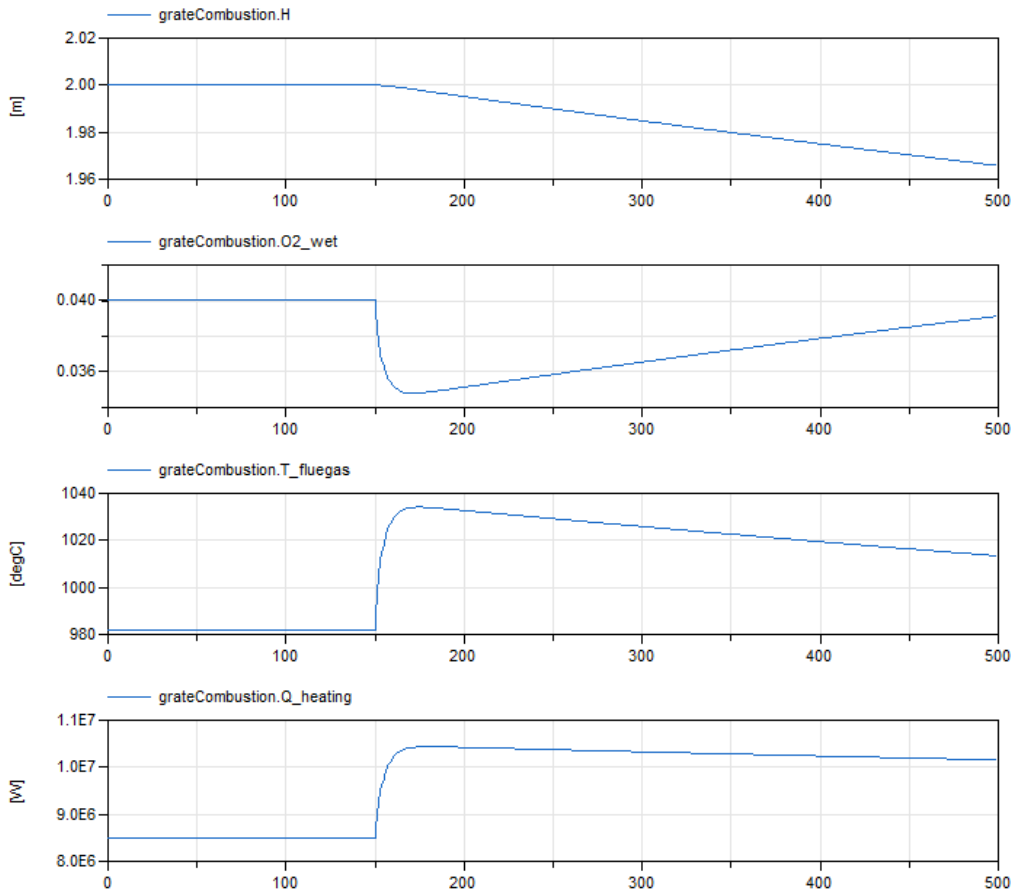

Figure 10. PA step response.

2.3.2 Fuel Flow Step

The responses of a step increase in fuel flow is shown in Figure 11 below.

- The bed height increases (ramp) as the fuel/air balance is compromised.
- The O2 contents in flue gas decreases as more flue gas is generated due to an increased vapor flow (in wet fuel) while the SA flow remains constant.
- The flue gas temperature and generated heat transfer rate decrease as more heat is needed to dry the increasing flow of fuel.

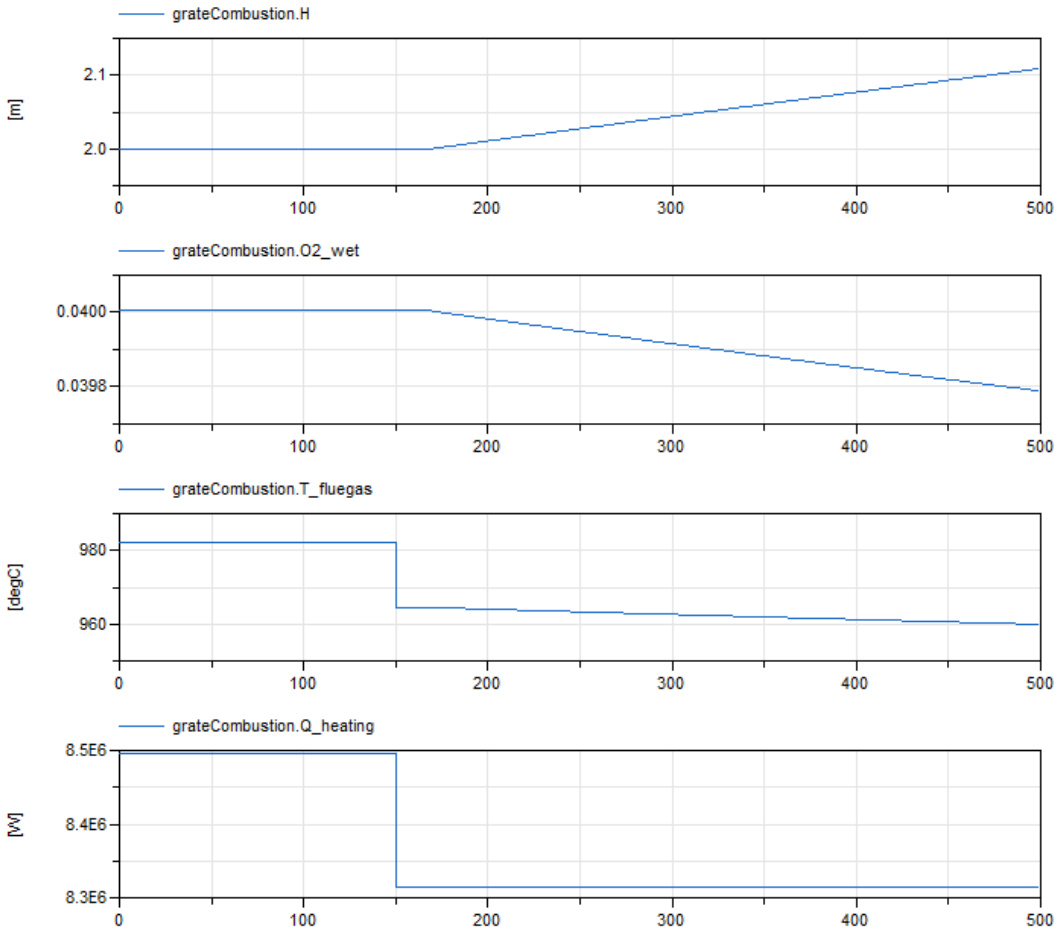

Figure 11. Fuel flow step response.

2.3.3 Secondary Air Flow Step

The responses of a step increase in secondary air flow is shown in Figure 12 below.

- The bed height approximately remains constant.
- The O2 contents in flue gas increases.
- The flue gas temperature and heat transfer rate decreases as the flue gas is diluted with "cold" (120 °C) secondary air.

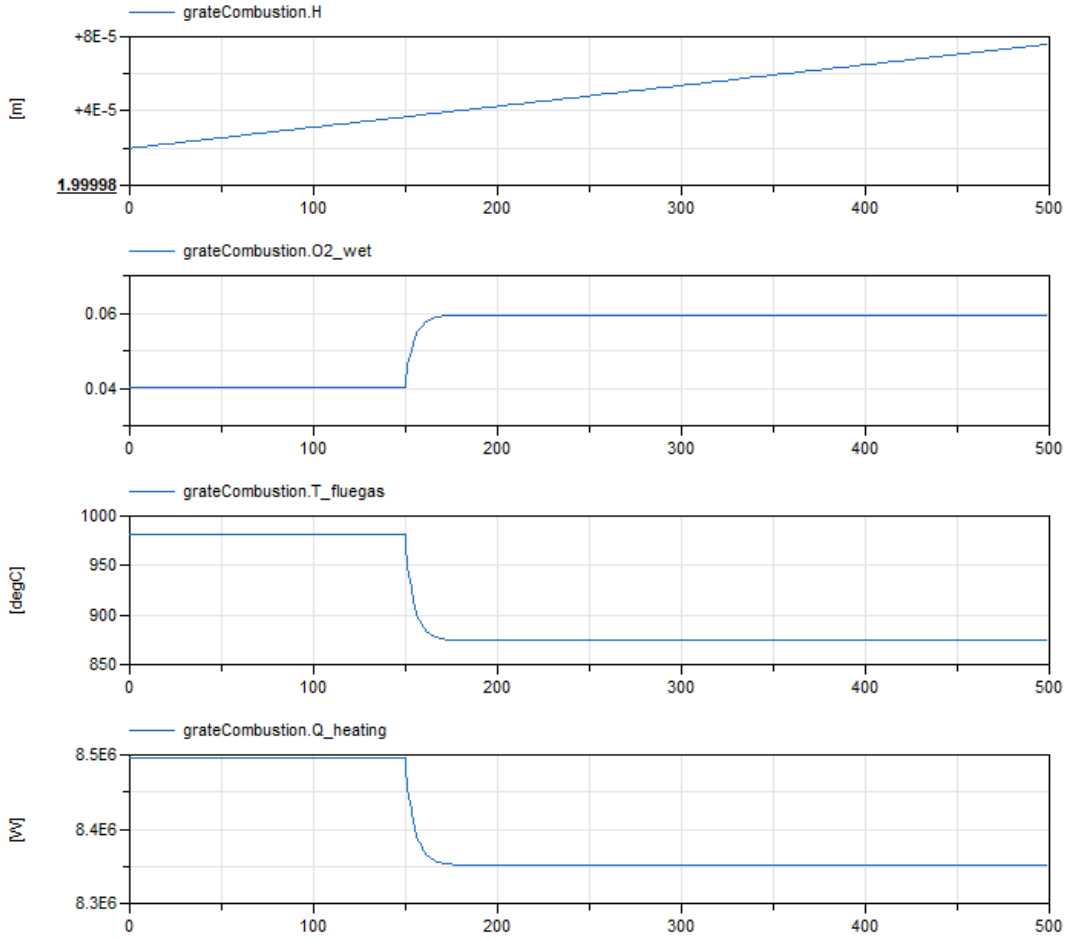

Figure 12. SA flow step responses.

2.3.4 Load Step response

Figure 13 shows the responses of a step increase in load — i.e. when fuel, PA and SA flows are doubled and thus maintaining the same ratio before and after the step.

- The bed height initially decreases and then increases. The decrease is caused by the slower filtering of the fuel input, through the vaporization process, compared to the faster air flow inputs (a higher PA flow consumes more dry fuel from the bed before an equivalent amount is generated).
- The flue gas temperature and total heat transfer rate initially decreases a bit due to the step change in wet cold fuel which takes heat from the process. The increased air flows then eventually cause an increase.

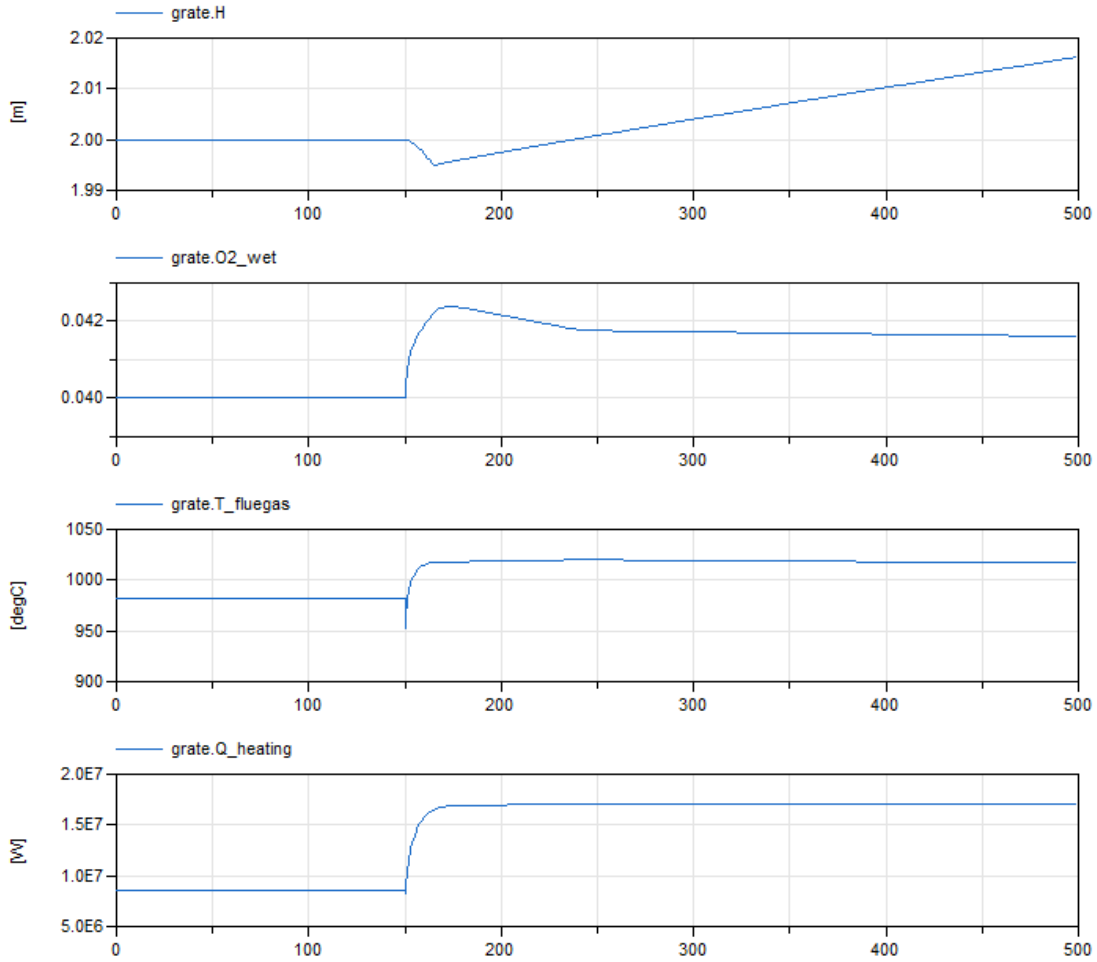

Figure 13. Load step response.

2.4 CONCLUDING REMARKS ON PRELIMINARY MODEL

A simple preliminary grate combustion model has been derived, implemented, and simulated in Dymola. Through exposed parameters it is possible to tune the behaviour of the model to provide a qualitatively realistic dynamic response to changes in fuel and air inputs.

The model can be used for evaluation of initial control and observer designs, as the dynamic behaviour is intuitive and easier to comprehend than with more complex models.

Initial investigations on the preliminary model revealed that the bed height (or length) was un-observable in the outputs as there were no coupling to the combustion taking place. A coupling between the bed height/length and the rate of fuel consumption was therefore added to be able to design a soft sensor for bed height/length estimation. Emphasis in subsequent modelling has therefore been placed in verifying that the heuristic observability solution can be replaced by real physical couplings between height/length and measurable quantities in the grate boiler.

3 Generic Grate Control and Analysis

3.1 CONTROL STRUCTURE

A simplified generic combustion control scheme has been set up to test the closed-loop behaviour of the preliminary grate model. Figure 14 shows the generic control scheme.

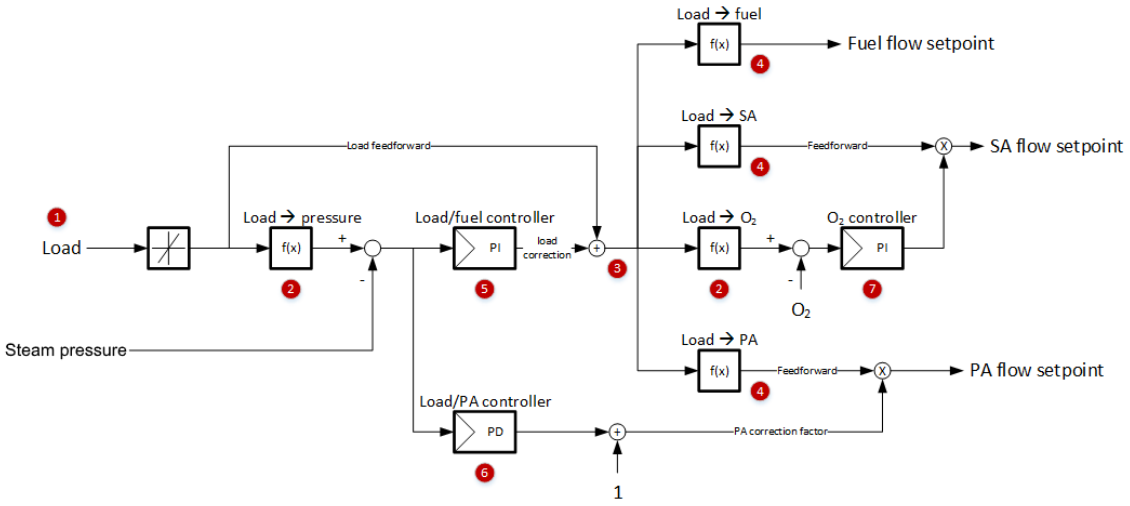

Figure 14. Generic grate boiler control scheme

The control scheme complies with standard power plant control practice in which it should be possible to set feedback controllers in manual mode and still have the process "survive" by means of pure feedforward control. In this kind of implementation, the resulting control signal to an actuator (or actuating process) is the sum (or product) of the feedforward signal and an additive or multiplicative correction signal. Both cases are shown in Figure 14. Please note that the design shown in the figure is greatly simplified.

In the example control scheme, the boiler controls the live steam pressure. This could also be any other measure of the boiler output power, e.g., steam flow or heat flow rate.

Below the control will be explained, referring to the circled numbers in Figure 14. The boiler to be controlled is assumed to have a thermal output of approximately 12 MJ/s.

The boiler load percentage setpoint ① is rate limited and used as a feedforward value for all other actuating signals (mass flow rates). Thus, setting the boiler load to 100 percent (and omitting the feedback loops) will result in the following output values:

- nominal fuel mass flow rate (1,667 kg/s)
- nominal SA mass flow rate (1,47 kg/s)
- nominal PA mass flow rate (4,58 kg/s)

This means that in the simplest case the contents of the "f(x)" blocks ④ will be constant gains of 1.667/100, 1.47/100 and 4.58/100 respectively.

The "f(x)" blocks ② produce the live steam pressure set point and excess O2 setpoint respectively which are, typically, not constant gains but rather load dependent functions (e.g. high O2 setpoint at low loads and low values at high load).

The feedback controls consist of three PID controllers. The load/fuel controller ⑤ is slow (mainly integral action) and is used to suppress deviations in fuel heating value over a longer period (hours). When added to the load feedforward signal the resulting fuel load ③ is generated. If the fuel has a lower heating value than expected the resulting fuel load will be greater than the desired load setpoint, e.g. 105 percent to produce 100 percent boiler load.

The load/PA controller ⑥, on the other hand, mainly consists of derivative and proportional action and utilizes the bed buffer of dried fuel to suppress transient variations in steam pressure. It corrects the feedforward value of the PA flow setpoint.

The O_2 controller corrects the SA flow setpoint to obtain the right combustion — measured by the amount of excess air after the boiler. By the time the O_2 sensor measures a deviating value the combustion has already taken place upstream. Thus, the controller is quite slow to maintain the excess oxygen value over a longer period.

None of the inputs in the control scheme in figure 14 relate "closely" to bed size (height or position of burnout zone). Therefore, it cannot be guaranteed that the grate always has a proper bed shape. For example, if the grate is nearly empty and the steam pressure is too low the load/PA controller will react by increasing the PA flow causing the bed size to reduce further.

3.2 CLOSED LOOP STEP RESPONSE

Figure 15 shows the responses from a step change in boiler load reflected in the following process variables:

- The topmost figure shows that the bed height is constant, 2 meters, until the load step at t=200 seconds. The dynamic coordination of air and fuel inputs causes the bed height to reduce a bit before starting a steady increase. If the model is simulated for long time, the bed height will converge to a value of above 2 meters (not shown).
- The second figure shows the flue gas oxygen contents and its constant setpoint. The oxygen controller manages to maintain the O2 contents after the load change.
- The third figure shows the flue gas temperature increasing with increasing load. The small drop in temperature just after the load step is caused by the step in wet fuel flow, requiring immediate increase in heat consumption for drying.
- The bottom figure shows the heat released from the combustion — the main controlled variable in the grate controller. The response in the figure shows a settling time of just about 10 seconds which seems quite unrealistic. The initial drop in heat flow rate is a consequence of the initial drop in flue gas temperature.

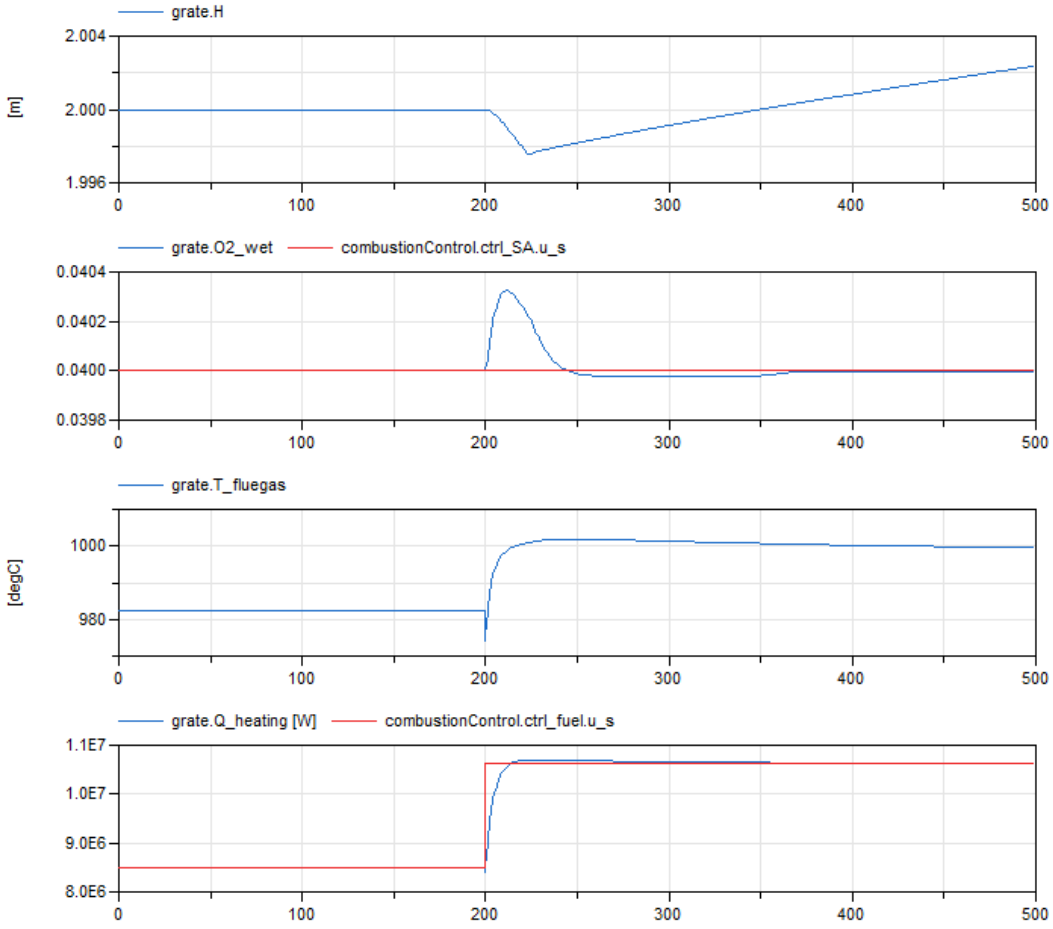

Figure 15. Closed-loop step response.

3.3 CONCLUDING REMARKS ON GENERIC GRATE CONTROL

The step responses in Figure 15 show that the simplified generic grate boiler control essentially works. However, the simplified grate model has some shortcomings that should be addressed in a more detailed and physically founded model.

In the simplified model the primary air acts almost immediately with dried fuel available on the grate and is thus capable of producing a fast and effective heat flow response (bottom plot in Figure 15). In reality, the primary air will help with drying of the wet fuel at the inlet of the grate, while it will accelerate the pyrolysis and combustion at the outlet of the grate. Also, the bed will contain a mixture of wet and dry fuel and adding a small additional amount of wet fuel will not cause a sudden drop in flue gas temperature. This flaw is caused by the modelling assumption that the bed only contains dry fuel and that wet fuel entering the grate is dried immediately.

Many more flaws can be found in the preliminary model and this underlines the need for a more detailed model based on physical principles.

4 Detailed Grate Boiler Model

The preliminary model provides a measure of the bed height/length, and displays reasonable qualitative results, but some quantitative results, such as dynamic settling times for step responses, are not realistic. It is also missing essential physical phenomena as it does not contain information about what happens along the grate in the fuel flow direction, e.g., fuel propagation dynamics, flame front (burn-out location), ash cooling, temperature gradients, combustion air pressure drop, etc. A heuristic coupling between the bed length and the combustion taking place also had to be applied to the preliminary model to ensure observability. Furthermore, missing combustion air dynamics makes controller tuning trivial and limits the models use in control design.

The purpose of the detailed grate boiler modelling is to alleviate some of the shortcomings of the preliminary model. This is achieved by using a staggered grid approach with spatial discretization of the bed and systematic and rigorous application of conservation equations (mass, energy, species, momentum).

4.1 MODEL REQUIREMENTS

The input/output requirements of the generic control structure results in the same minimum list of inputs and outputs as in the preliminary model. An additional output requirement is a measure of the flame front (burn-out location), which needs to be observed/estimated and subsequently utilized in a more advanced grate controller.

It is important that the detailed grate boiler model has a high degree of;

- scalability, e.g., through spatial discretization possibilities,
- reusability, e.g., through use of common media models and splitting of large models into sub-components,
- variable detailedness, e.g., through replaceable models with common interface definition (simple combustion equations vs. reaction kinetics etc.).

The modelling framework should also have the potential to provide the possibility of modelling dynamic behaviour such as fuel “waves” (movement behaviour of the fuel on the grate), combustion air pressure drop and burn-through zones on the bed (air distribution problematics).

4.2 MODELING OVERVIEW

Detailed modelling of the grate boiler is split up into the following sub-components/models to ensure a high degree of reusability and to allow for variable detailedness in modelling:

- Media models — Specification of solid fuel and gas mixture including equations for calculation of media properties such as specific heat capacity, enthalpy, density, etc.

- Bed model — This model describes the behaviour of the fuel on the grate and interaction with the gas mixture located in the void space surrounding the fuel. The main subprocesses taking place are vaporization, pyrolysis (devolatilization), and char conversion. These subprocesses are placed in individual sub-components to further strengthen reusability and variable detailedness in modelling.
- Combustion model — The gas mixture (flue gas) generated in the bed contains unburnt constituents from pyrolysis and char conversion, which is subsequently burnt in a combustion model under the presence of oxygen. This allows for modelling of furnace air-staging by having multiple combustion models in series with addition of secondary air in between.
- Grate model — This model describes the pressure loss of the combustion air as it passes through the air holes in the grate and the thermal inertia of the grate.
- Furnace wall model — The thermal inertia and conductive resistance of the furnace wall is described in this model, which can be comprised of multiple layers of different material (tiles, concrete, metal).
- Radiation heat transfer model — A framework for calculation of radiation heat transfer inside the furnace between all facing surfaces and the flue gas. The model is scalable in the sense that it allows for choosing an arbitrary number of discretizations of the bed surface, furnace wall surface, and combustion volumes.

The sub-components are aggregated into a complete grate boiler simulation for demonstration purposes and partly validated using norm EN-12952-15 and measurement data from Sysav waste grate boiler.

The water/steam side of the grate boiler (drum boiler, evaporator, superheaters, economizers, etc.) and air distribution components (fans, dampers, etc.) are not modelled in this work. However, standard components from the Modelica Fluid library can be used for this purpose.

4.3 MEDIA MODELS

The subcomponents utilize two medium package models with functions for calculation of heat capacity, enthalpy, density, etc.:

- Solid fuel — Defined in this project (utilizing IAWPS97 [Wagner et al., 2000] for the water contents).
- Gas mixture — Ideal gas mixtures (using NASA coefficients [McBride et al., 2002].

During interaction of the media — e.g., water in solid fuel vaporizes and is mixed with flue gas — it is important to use the same reference temperatures and enthalpies for the three medium models. It was chosen to use the reference of the ideal gas mixture, specific enthalpy=0 at 25 °C, 1 bar. This means that the enthalpies of water/steam and solid fuel must be offset accordingly. Likewise, the enthalpy of formation is omitted in the ideal gas mixtures, since it is not defined in the water/steam and solid fuel media. However, enthalpy of formation is considered in models with chemical reactions occurring (pyrolysis, char conversion, and combustion).

4.3.1 Solid Fuel specification

Solid fuels can be specified both in terms of proximate analysis (volatiles, water, fixed carbon, and inerts) and ultimate analysis (e.g., C-H-O-N-S-Ash). In this project, both proximate and ultimate analysis capabilities of the solid fuel are needed. The proximate information is used to split the fuel into subcomponent models for vaporization, pyrolysis and char conversion. The ultimate information is also needed in the pyrolysis and char conversion models to calculate the resulting constituents transferred to the flue gas and the generated heat.

The fuel specification vector X_{fuel} is defined as

$$X_{fuel} = \{x_{vol}, x_{H2O}, x_C, x_H, x_O, x_N, x_S, x_{ash}\}$$

This vector does not satisfy the typical assumption in medium models that all species sum to unity, as some atoms are accounted for in more than one category (e.g. oxygen is not only in the fraction x_O, but also in x_{vol} and x_{H2O}). Therefore, care must be taken when the fuel composition is modified, so that it remains consistent. The ultimate information x_C, x_H, x_O, x_N, x_S and x_{ash} is typically used as a base in calculation as it accounts for all atoms in the wet fuel and sums to unity. The assumption that the proximate composition also sums to unity is used to infer the fraction of fixed carbon in the fuel from x_{vol}, x_{H2O} and x_{ash}. Finally, the specific atomic compositions of the different proximate categories can be retrieved by utilizing the known composition of water and the assumption that char consists entirely of coal. The sulphur and nitrogen in the fuel were considered inert in all chemical processes, if these were to be included, extra assumptions regarding these, or additional information in the fuel medium model, would be needed.

Table 1 provides the composition of different types of fuel for simulation purposes, with specification based on dry moisture free fuel. Helper functions have been implemented to easily convert between specification on wet and dry basis. Note that the volatile mass fraction for the given municipal solid waste (MSW) was not available. Furthermore, general functions for specific heat capacity, enthalpy and density are also difficult to obtain for MSW as these values are very dependent on the composition of the waste (paper, plastic, etc.). The present work will thus be limited to biomass fuels, but with the possibility of easily switching to other types of fuel (functions contained in interchangeable media models).

Table 1. Composition of different types of fuel, with specification based on dry moisture free fuel (DF). Ash accounts for all other constituents not part of CHONS. *Composition based on [DK06]. **Composition based on [Bech et al., 1996]. ***Composition based on statistical analysis of Danish MSW from 1991.

	Wood Chips				**Straw**		**MSW**
	Typical. *	Beech*	Pine*	Fir*	Wheat*	Barley**	DK***
Vol. (% DF)	81	83.9	81.8	80	81	79.9	NA
H_2O (%)	40	40	40	40	12.5	12.1	18.5
C (% DF)	50	49.3	51	50.9	47.4	47.2	35.6
H (% DF)	6.2	5.8	6.1	5.8	6	4.6	5.06
O (% DF)	43	43.9	42.3	41.3	40	44.4	35.7
N (% DF)	0.3	0.22	0.1	0.39	0.6	0.8	0.95

	Wood Chips				Straw		MSW
	Typical. *	Beech*	Pine*	Fir*	Wheat*	Barley**	DK***
S (% DF)	0.05	0.04	0.02	0.06	0.12	0.0	0.17
Ash (% DF)	0.45	0.74	0.48	1.55	5.88	3.0	22.6
LHV (MJ/kg DF)	19.4	18.7	19.4	19.7	17.9	17.9	10.5

The specific enthalpy of the fuel is calculated as a function of temperature and the proximate composition;

$$h_{fuel} = x_{vol}h_{vol} + x_{ash}h_{ash} + x_{char}h_{char} + x_{H2O}h_{H2O}$$

For ash and char, the following expressions are used for the specific heat and enthalpies [Hobbs et al., 1992], [Ullum, 2000]:

$$c_{p,char} = 710$$
$$h_{char} = c_{p,char}\left(T_{fuel} - T_{ref}\right)$$
$$c_{p,ash} = \frac{1}{T_{fuel} - T_{ref}}\left(\frac{0.586}{2}\left({T_{fuel}}^2 - {T_{ref}}^2\right) + 594\left(T_{fuel} - T_{ref}\right)\right)$$
$$h_{ash} = c_{p,ash}\left(T_{fuel} - T_{ref}\right)$$

The specific enthalpy of volatiles h_{vol} is based on a standard proximate composition of unpyrolyzed biomass in the following expression:

$$h_{vol} = \left(\frac{0.6}{0.486}c_{p,com} - \frac{0.1101}{0.486}c_{p,char} - \frac{0.0039}{0.486}c_{p,ash}\right)\left(T_{fuel} - T_{ref}\right)$$

Where the specific heat of biomass before pyrolysis is given by [Dupont et al., 2014]:

$$c_{p,com} = \frac{1}{T_{fuel} - T_{ref}}\left(\frac{5.340}{2}\left({T_{fuel}}^2 - {T_{ref}}^2\right) - 299\left(T_{fuel} - T_{ref}\right)\right)$$

Water medium properties are calculated using the IF97 medium model in Modelica Standard library, which is based on the IAWPS97 standard [Wagner et al., 2000].

The density of the fuel is also calculated from the proximate composition, assuming the fixed densities $\rho_{vol} = 400\ kg/m^3$, $\rho_{ash} = 721\ kg/m^3$, $\rho_{char} = 600\ kg/m^3$ and $\rho_{H2O} = 1000\ kg/m^3$.

4.3.2 Gas Mixture Specification

The gas mixture media package extends from *Modelica.Media.IdealGases.Common.MixtureGasNasa* and the gas specification vector X_{gas} (must sum to 1) is defined as

$$X_{gas} = \{x_{N2}, x_{H2}, x_{CO}, x_{O2}, x_{H2O}, x_{CO2}, x_{CH4}\}$$

These are the species considered for the flue gas.

4.4 BED MODEL

The bed model describes the behaviour of the fuel on the grate and interaction with the gas mixture located in the void space surrounding the fuel. The model structure is important, since the bed model is comprised of individual bed segments used in a 2D discretization scheme. Both segment and discretized model should conform with the staggered-grid topology.

4.4.1 Bed Topology

A staggered-grid model contains a grid of alternately *flow* and *volume* models. *Flow models* generally contain static models describing a flow (mass, heat, displacement etc.) as a function of a potential difference (pressure, temperature, force etc.). *Volume models* generally contain dynamic conservation equations in which, e.g., pressure, temperature or mass are dynamic state variables. The states can be regarded as potentials that can create a flow. If two volume models are directly connected, then the connection enforces the potentials to be equal. This can cause numerical problems for instance during initialization if the state variables are given different initial values.

Figure 16 shows the chosen bed segment topology. The details of the flow and volume models will be described in the following sections. Volume and flow models are always connected alternatingly. The black circles left and right in the figure represent the solid fuel connectors through which fuel enters and leaves the segment. The flow of fuel enters a volume model, indicated by the brown circle, in which the common bed temperature, T, and the masses of C, H, O, N, S, ash, volatiles, fixed carbon are expressed as dynamic state variables. Unlike a hydraulic flow model, the mass flow rate of fuel leaving the segment is not expressed as a function of a pressure difference but rather is forced out of the segment by the movement of the grate, given by the grate velocity, v_{grate}, shown as a blue triangle on the left. The blue circles represent the gas mixture connectors (Modelica stream connectors) through which primary air or generated combustibles flow from bottom to top. Primary air (or flue gas generated by the previous bed segment below) enters a volume model that holds the masses of N_2, H_2, CO, O_2, CH_4 etc., the flue gas temperature leaving the segment and the inlet pressure — all as dynamic state variables. The flue gas volume model is connected to a flow model describing the relationship between pressure difference and mass flow rate. A convective heat flow model is used to model the heat transfer between solid fuel and flue gas with a constant heat transfer coefficient α. Similarly, heat transfer between two vertically connected bed segments would go through the heat transfer model “UA”.

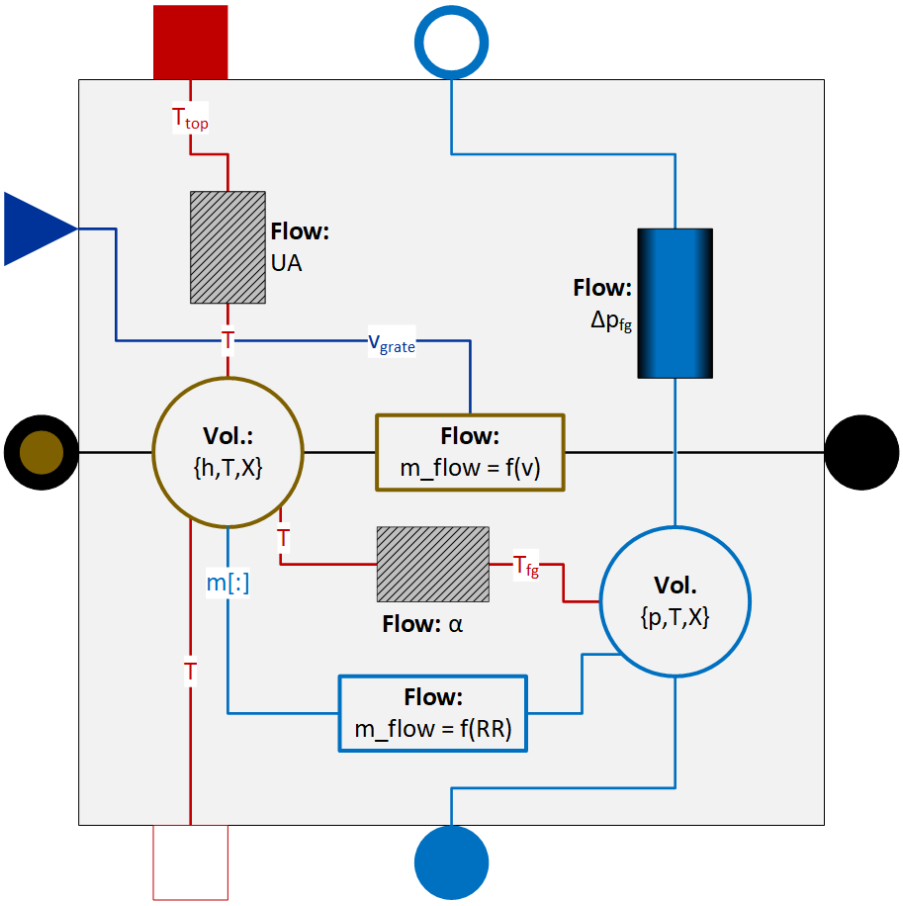

Figure 16. Bed Segment Topology

The discretized bed model can be constructed by connecting M times N bed segment models — M being the number of vertical segments, counting from the grate upwards and N being the number of horizontal segments, counting from fuel inlet towards ash discharge. Because each bed segment model is constructed as a volume-flow model the interconnection of the segments is straightforward, as illustrated in figure 17.

The solid fuel connectors consist of M individual connectors. The vertical fuel distribution at the inlet must be handled by a fuel splitter model that explicitly determines the fuel split. The gas mixture connector consists of N gas mixture ports connected to the segments as shown in Figure 17. If, for instance, one PA fan is connected to the discretized model its outlet connector must be connected directly to each of the N inlet connections. The hydraulic properties (flow resistances) will then calculate the PA flow distribution accordingly given a fixed furnace pressure connected to each of the N outlet connectors. The grate speed input is connected directly to all M times N segments. The upper segments individually expose their temperature through Modelica heat port connectors upwards such that different heat flows can be irradiated from the furnace to the bed. The lower segments individually expose their temperature through heat port connectors downwards such that heat can be conducted horizontally through the grate model.

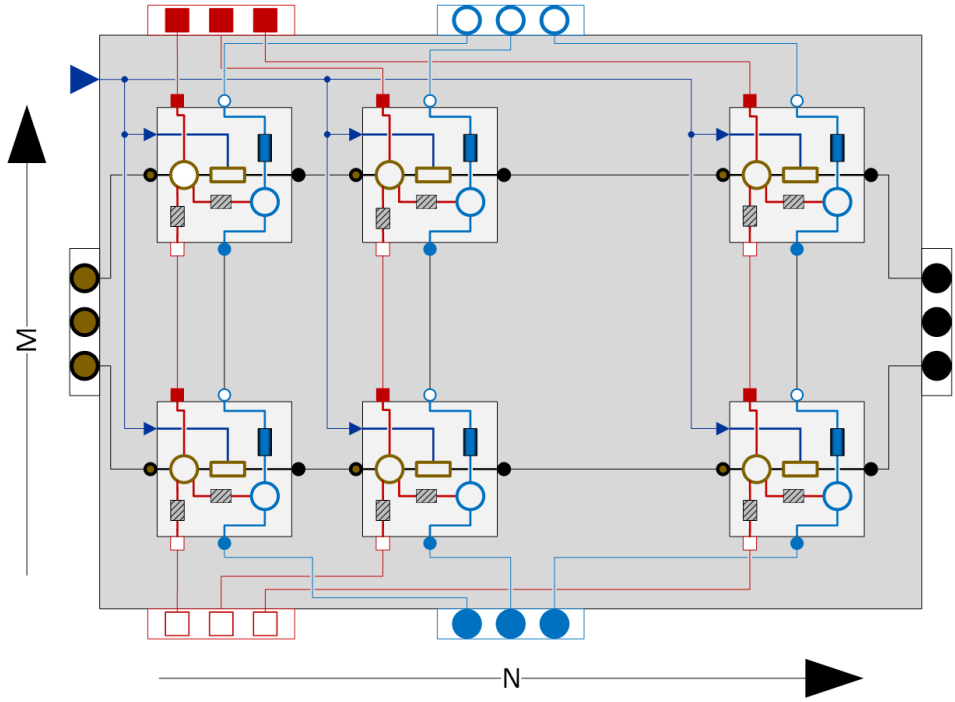

Figure 17. Bed model discretized in M times N bed segments.

4.4.2 Bed Segment Model

Figure 18 shows a Dymola diagram view of the bed segment model with replaceable models for vaporization, pyrolysis and char conversion.

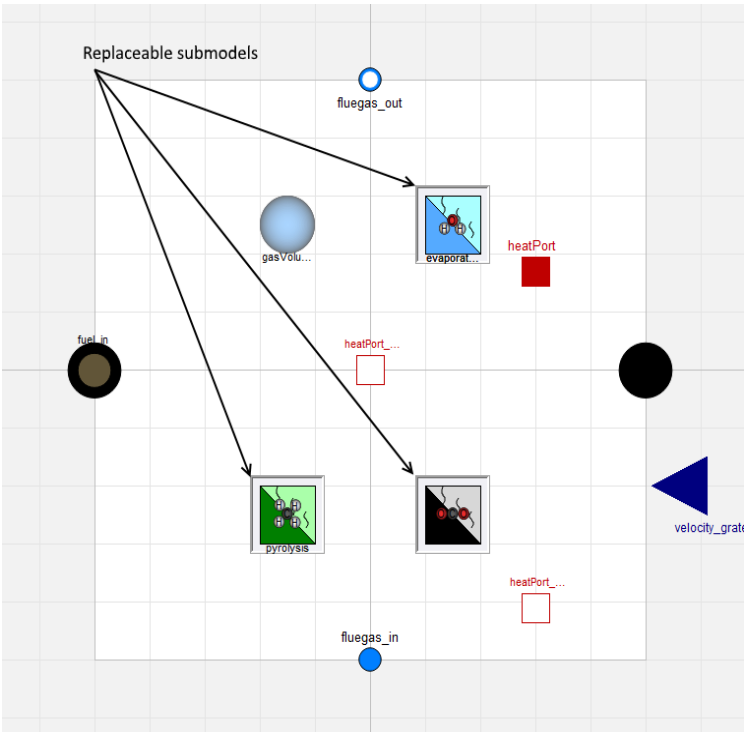

Figure 18. Dymola diagram view of the bed segment model with indication of replaceable submodels for vaporization, pyrolysis, and char conversion.

The governing equations in the bed segment model are presented in the following, starting with the mass balances on the fuel proximate components;

$$\frac{dm_{H2O}}{dt} = \dot{m}_{fuel,in}x_{H2O,in} - \dot{m}_{fuel,out}x_{H2O} - \dot{m}_{H2O,evap}$$
$$\frac{dm_{vol}}{dt} = \dot{m}_{fuel,in}x_{vol,in} - \dot{m}_{fuel,out}x_{vol} - \dot{m}_{vol,pyro}$$
$$\frac{dm_{char}}{dt} = \dot{m}_{fuel,in}x_{char,in} - \dot{m}_{fuel,out}x_{char} - \dot{m}_{char,conv}$$
$$\frac{dm_{inert}}{dt} = \dot{m}_{fuel,in}x_{inert,in} - \dot{m}_{fuel,out}x_{inert,out}$$

where the inlet mass flow of each proximate component is given upstream (boundary condition) and the outlet mass flow is calculated from the grate velocity v_{grate}, the fuel height d_{fuel}, the grate width w_{fuel} and density ρ_{fuel}, according to

$$\dot{m}_{fuel,out} = d_{fuel}w_{fuel}\rho_{fuel}v_{grate}$$

The extra outgoing flows ($\dot{m}_{H2O,evap}$, $\dot{m}_{vol,pyro}$and $\dot{m}_{char,conv}$), from the fuel in the bed segment, are calculated in the submodels for vaporization, pyrolysis and char conversion, respectively. As explained in Section 4.3.1, the char part of the fuel assumed to consist entirely of carbon and that the inert part of the fuel is the sum of nitrogen N, sulphur S, and ash. Fuel bound N and S mass fractions are small and do not contribute much to the general combustion dynamics. However, N and S are important for emission calculations and could be added later if needed.

Mass balances for the ultimate components have the same form as the proximate balance equations above. There is however not a need for implementing dynamic balance equations for every ultimate component, instead algebraic relations can be used in some instances, based on the assumptions mentioned above.

The fuel energy balance is defined as

$$\frac{dE_{fuel}}{dt} = \dot{m}_{fuel,in}h_{fuel,in} - \dot{m}_{fuel,in}h_{fuel} - \dot{H}_{fuel,evap} - \dot{H}_{fuel,pyro} - \dot{H}_{fuel,cov} + Q_{up,fuel} + Q_{down,fuel} + Q_{aux,fuel} + Q_{fg,fuel}$$

where h is specific enthalpy, Q is heat flow rate and $\dot{H}$ is enthalpy flow rate caused by removal of water, volatiles, and char from the fuel (note that $\dot{H}$ should also include any change in enthalpy due to chemical reactions, which is calculated in submodels). $Q_{up,fuel}$ and $Q_{down,fuel}$ are the heat transfer rates from upward and downward direction to the fuel, respectively, and $Q_{aux,fuel}$ is an optional additional heat input directly to the fuel, e.g., to simulate the presence of auxiliary burners during start-up (from cold conditions). The final heat transfer rate from the flue gas surrounding the fuel to the fuel, $Q_{fg,fuel}$, is approximated by

$$Q_{fg,fuel} = \alpha A_{fg,fuel}(T_{fg} - T_{fuel})$$

Where α is the convective heat transfer coefficient and the heat transfer area $A_{fg,fuel}$ is approximated by the volume of the void space inside the fuel, $V_{fuel,void}$, and a conversion factor from volume to surface area, r_{VSA}, according to the equation

$$A_{fg,fuel} = V_{fuel,void}r_{VSA}$$

The void space is calculated as

$$V_{fuel,void} = \frac{m_{H2O}}{\rho_{H2O}}\alpha_{H2O} + \frac{m_{vol}}{\rho_{vol}}\alpha_{vol} + \frac{m_{char}}{\rho_{char}}\alpha_{char} + \frac{m_{inert}}{\rho_{inert}}\alpha_{inert}$$

With α_{H2O}, α_{vol}, α_{char} and α_{inert} representing the faction of void space per unit volume of liquid water, volatiles, char and inerts, respectively.

The equations for the interacting gas mixture (flue gas) surrounding the fuel are provided in the following. The individual flue gas mass balances are;

$$\frac{dm_{H2}}{dt} = \dot{m}_{fg,in}x_{H2,in} - \dot{m}_{fg,out}x_{H2} + \dot{m}_{vol,pyro}x_{H2,pyro} - \dot{m}_{H2,conv}$$
$$\frac{dm_{CO}}{dt} = \dot{m}_{fg,in}x_{CO,in} - \dot{m}_{fg,out}x_{CO} + \dot{m}_{vol,pyro}x_{CO,pyro} - \dot{m}_{CO,conv}$$
$$\frac{dm_{O2}}{dt} = \dot{m}_{fg,in}x_{O2,in} - \dot{m}_{fg,out}x_{O2} + \dot{m}_{vol,pyro}x_{O2,pyro} - \dot{m}_{O2,conv}$$
$$\frac{dm_{H2O}}{dt} = \dot{m}_{fg,in}x_{H2O,in} - \dot{m}_{fg,out}x_{H2O} + \dot{m}_{H2O,evap} + \dot{m}_{vol,pyro}x_{H2O,pyro} - \dot{m}_{H2O,conv}$$
$$\frac{dm_{CO2}}{dt} = \dot{m}_{fg,in}x_{CO2,in} - \dot{m}_{fg,out}x_{CO2} + \dot{m}_{vol,pyro}x_{CO2,pyro} - \dot{m}_{CO2,conv}$$
$$\frac{dm_{CH4}}{dt} = \dot{m}_{fg,in}x_{CH4,in} - \dot{m}_{fg,out}x_{CH4} + \dot{m}_{vol,pyro}x_{CH4,pyro}$$

Note that char conversion flows can both be positive and negative depending on if the specific gas mixture constituent is consumed or produced. The equation for N_2 finally ensures conservation of mass;

$$\frac{dm_{N2}}{dt} = \dot{m}_{fg,in} - \dot{m}_{fg,out} + \dot{m}_{H2O,evap} + \dot{m}_{vol,pyro} + \dot{m}_{fg,conv} - \frac{dm_{H2}}{dt} - \frac{dm_{CO}}{dt} - \frac{dm_{O2}}{dt} - \frac{dm_{H2O}}{dt} - \frac{dm_{CO2}}{dt} - \frac{dm_{CH4}}{dt}$$

The energy balance equation is defined as

$$\frac{dE_{fg}}{dt} = \dot{m}_{fg,in}h_{fg,in} - \dot{m}_{fg,in}h_{fg} + \dot{H}_{fg,evap} + \dot{H}_{fg,pyro} + \dot{H}_{fg,cov} - Q_{fg,fuel}$$

where the enthalpy flow rates $\dot{H}$ are due to addition of gas from the fuel to the flue gas. Finally, the fuel height and fuel porosity factor dependent flue gas pressure drop is approximated by

$$\Delta p = 0.5k_{fuel}\frac{d_{fuel}}{\rho_{fg}\left(l_{fuel}w_{fuel}\alpha_{avg}\right)^2}\dot{m}_{fg,out}\left|\dot{m}_{fg,out}\right|$$

where k_{fuel} is the flue gas flow resistance and the average porosity factor α_{avg} is calculated using the void space factors;

$$\alpha_{avg} = x_{vol}\alpha_{vol} + x_{inert}\alpha_{inert} + x_{char}\alpha_{char} + x_{H2O}\alpha_{H2O}$$

4.4.3 Vaporization Model

The purpose of the vaporization model is to calculate the mass and enthalpy flow rate of water vapor leaving the solid fuel, given an average fuel temperature in the bed segment in question. No vaporization occurs when the temperature is below the saturation temperature of water. When the temperature exceeds the saturation temperature, the vaporization mass flow is assumed to be proportional to the available volume of steam. The enthalpy flow rate is calculated based on this mass flow, using the enthalpy of the water/steam mixture. This is not a very accurate representation of the physical process, but this is not expected to be a big problem as it does satisfy mass and energy balances and captures the qualitative behaviour correctly, which will result in the reasonable overall behaviour of complete vaporization of the water in the fuel once sufficient heat is applied.

The model is replaceable and has the following standard inputs/outputs from/to the bed segment model:

- Saturation pressure (input).
- Specific enthalpy of the water in the fuel (input).
- Mass of the water in the fuel (input).
- Mass flow of vaporized water steam (output).
- Specific enthalpy of vaporized water steam (output).
- Vaporization enthalpy flow rate (output).

4.4.4 Pyrolysis Model

Pyrolysis is the process of thermal decomposition of material in inert atmosphere, where the material undergoes an irreversible change in chemical composition. In the pyrolysis model the volatiles fraction of the solid fuel is assumed to be converted to the ideal gas products {H2, CO, H2O, CO2, CH4}, leaving only char (fixed C) and ash. The constituents of the pyrolysis are unknown and are defined as $C_C H_H O_O$, where subscripts denote the specific composition which depends on the chosen fuel. Tar and smaller amounts of higher hydrocarbons than methane is also formed, but both are neglected in the analysis, e.g., see [Ullum, 2000].

Pyrolysis is a complex process, where the mass fractions of formed gas products depend mostly on temperature, but also on factors such as fuel particle size, heat-up rate and fuel type (e.g., for biomass it depends on the ratio of lignin, cellulose, and hemicellulose). Different approaches for modelling of pyrolysis has been used in the literature, e.g., see [Ullum, 2000] for a discussion.

Temperature Dependent Pyrolysis Model

A temperature dependent pyrolysis model has been implemented based on the approach used in [Thunman et al., 2001] and [Ullum, 2000]. The volatile mass flow rate $\dot{m}_{vol,pyro}$ is determined using an Arrhenius expression [Ullum, 2000];

$$\dot{m}_{vol,pyro} = A_0 e^{\frac{ER}{T}} m_{vol}$$

where m_{vol} is the mass of volatiles, T is fuel temperature, A_0 is set to 650, and ER is set to 6500. These parameters mean that most of the pyrolysis happens between

200 ℃ to 600 ℃. Atomic mass balance equations can be derived based on the volatile fuel composition defined by the mass fractions $x_{C,vol} + x_{H,vol} + x_{O,vol} = 1$,

$$x_{C,vol} = x_{CO,pyro}\frac{M_C}{M_{CO}} + x_{CO2,pyro}\frac{M_C}{M_{CO2}} + x_{CH4,pyro}\frac{M_C}{M_{CH4}}$$
$$x_{H,vol} = x_{H2,pyro}\frac{2M_H}{M_{H2}} + x_{H2O,pyro}\frac{2M_H}{M_{H2O}} + x_{CH4,pyro}\frac{4M_H}{M_{CH4}}$$
$$x_{O,vol} = x_{CO,pyro}\frac{M_O}{M_{CO}} + x_{H2O,pyro}\frac{M_O}{M_{H2O}} + x_{CO2,pyro}\frac{2M_O}{M_{CO2}}$$

which can be complemented by an equation for conservation of energy,

$$\begin{aligned} LHV_{vol}(X_{vol}) + h_{vol}(T) + h_{pyro} \\ = (LHV_{H2} + h_{H2}(T))x_{H2,pyro} + (LHV_{CO} + h_{CO}(T))x_{CO,pyro} \\ + (LHV_{H2O} + h_{H2O}(T))x_{H2O,pyro} + (LHV_{CO2} + h_{CO2}(T))x_{CO2,pyro} \\ + (LHV_{CH4} + h_{CH4}(T))x_{CH4,pyro} \end{aligned}$$

where the lower heating value (LHV) of the gas components are provided by the ideal gas mixture media package and the reaction enthalpy h_{pyro} is set to 400 kJ/kg ([Ullum, 2000] states that it is typically between 200 and 600). The mass fraction vector of the volatiles X_{vol} is used to calculate the lower heating value of the volatiles, LHV_{vol}, with the addition of a unified correlation for estimation of HHV of solid, liquid, and gaseous fuels, which is valid for almost all dry fuels [Channiwali et al., 2002];

$$LHV = HHV - h_{latent}\frac{M_{H2O}}{M_{H2}}x_{H,vol}$$
$$HHV = \left(34.91x_{C,vol} + 117.83x_{H,vol} - 10.34x_{O,vol} - 1.51x_{N,vol} + 10.05x_{S,vol} - 2.11x_{ash,vol}\right) * 10^6$$

where h_{latent} is the latent heat of vaporization. An additional equation is still needed to be able to solve the equation system. For this purpose, an empirical temperature dependent relationship for devolatilization of wood is provided in [Thunman et al., 2001] (based on results in [Blasi et al., 2001]);

$$x_{CO,pyro} = 1.94 * 10^{-6}T^{1.87}x_{CO2,pyro}$$

Alternatives for the above relationship equation can be found in [Thunman et al., 2001];

$$x_{CH4,pyro} = 1.305 * 10^{-11}T^{3.39}x_{CO2,pyro}, x_{H2O,pyro} = 0.95x_{CO2,pyro}$$

and [Ullum, 2000] instead assumes that the mass fraction of water is always 0.13 %. A temperature dependent pyrolysis model could potentially also be based on the empirical work in [Neves et al., 2011], which is a continuation of the work reported in [Thunman et al., 2001].

Figure 19 shows the temperature dependent composition of the volatile gas for different types of fuel.

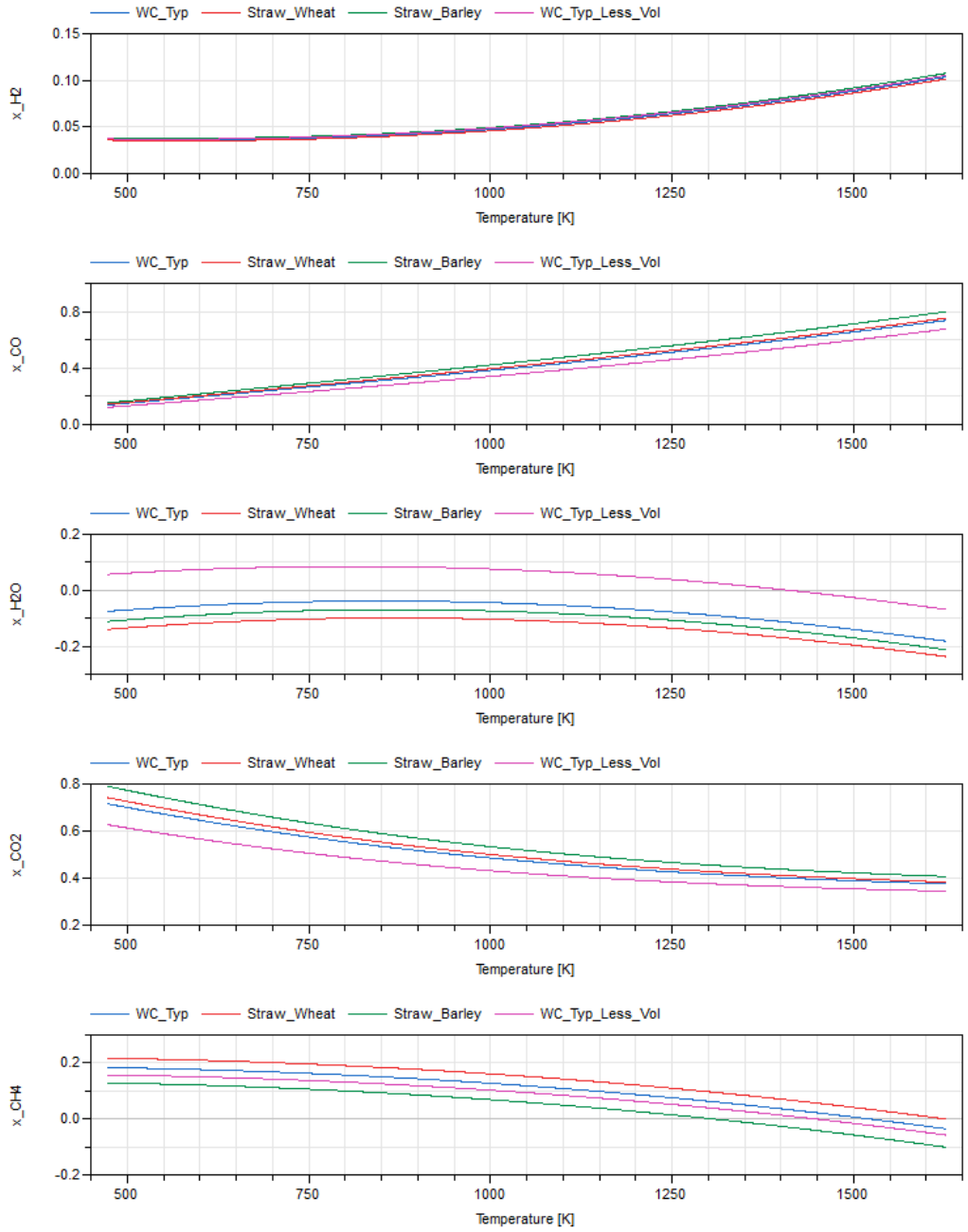

Figure 19. Volatiles mass fraction as a function of temperature for four different biomass compositions using a pyrolysis modelling approach similar to the one used in, e.g., [Thunman et al., 2001]. The biomass fuel composition can be found in table 1 (WC_TYP = Typical wood chips, WC_TYP_Less_Vol = Typical wood chips with 75% volatiles instead of 81%).

Note that the mass fractions of methane and water are negative at high pyrolysis temperatures and that the mass fraction of water is always negative using the biomass composition of typical wood chips, wheat straw, and barley straw. However, the water mass fraction is positive for the fuel specification used in [Ullum, 2000], where the volatile fraction is only 75% (pyrolysis model needs at least 20% fixed C on dry basis to work properly).

Table 2 provides the total end product result after finished pyrolysis reported in literature (the mass fractions in figure 19 would have to be integrated over temperature for a direct comparison). Large differences can be observed in the literature, which indicate the general difficulties in determining the correct gas composition.

Table 2. Volatiles mass fraction reported in [Ullum, 2000] from different sources and from simulation. *Simulated values (straw composition dry fuel; fixed carbon = 0.2, ash = 0.051, volatiles = 0.749, x_C = 0.472, x_H = 0.061, x_O = 0.408). **Water content not measured but fixed to 0.130.

Volatiles mass fraction	[Henriksen et al., 1991] (Straw)	[Bech et al., 1996] (Barley straw - see Table 1)	[Brandt et al., 1997] (Straw)	[Ullum, 2000] (Straw)*
x_{H2}	0.055	0.045	0.013	0.018
x_{CO}	0.716	0.630	0.193	0.258
x_{H2O}	0.133	0.131	0.130**	0.130
x_{CO2}	0.084	0.143	0.444	0.396
x_{CH4}	0.011	0.051	0.220	0.198

Simplified Pyrolysis Model

An alternative, simplified temperature independent pyrolysis model has been implemented, with focus on getting the result in terms of total amount of species correct. This simplification is reasonable if gases from pyrolysis in each bed segment are mixed before combustion (only serial and no parallel gas combustion is taking place above the bed).

Fixed mass fraction for H_2O and CO_2 are used in the simplified model, together with the Arrhenius expression for calculation of the volatile mass flow rate. The remaining mass fractions then only has one solution given a certain volatile composition. The measured H_2O mass fraction is 0.131 in [Bech et al., 1996], 0.133 in [Henriksen et al., 1991], and [Ullum, 2000] uses a fixed value of 0.13. The other mass fractions are not consistent in the literature and the CO_2 mass fraction, measured in [Bech et al., 1996], is therefore chosen (gives approximately the same ratio between H_2O and CO_2 as used in [Thunman et al., 2001]). This results in the following equations calculated in the given order;

$$x_{H2O,pyro} = 0.13$$

$$x_{CO2,pyro} = 0.143$$

$$x_{CO,pyro} = \left(x_{O,vol} - \frac{M_O}{M_{H2O}} x_{H2O,pyro} - \frac{2M_O}{M_{CO2}} x_{CO2,pyro}\right) \frac{M_{CO}}{M_O}$$

$$x_{CH4,pyro} = \left(x_{C,vol} - \frac{M_C}{M_{CO}} x_{CO,pyro} - \frac{M_C}{M_{CO2}} x_{CO2,pyro}\right) \frac{M_{CH4}}{M_C}$$

$$x_{H2,pyro} = x_{H,vol} - \frac{4M_H}{M_{CH4}} x_{CH4,pyro} - \frac{2M_H}{M_{H2O}} x_{H2O,pyro}$$

It can be necessary to iteratively decrease the H2O mass fraction until H2 is just above 0, if the amount of H in the fuel is very low (to avoid negative mass fractions).

Table 3 shows the mass fraction of volatile gases for different types of biomass fuels using the simplified pyrolysis model. The result for typical wood chips with a reduced amount of volatiles is similar to the results reported in [Bech et al., 1996] (75% volatiles was adopted from this reference).

Table 3. Volatiles mass fraction using a fixed ratio of H2O and CO2 in the pyrolysis model. The biomass fuel composition can be found in table 1 (*Typical wood chips with 75% volatiles instead of 81%).

Volatiles mass fraction	Wood chips					Straw	
	Typical	Beech	Pine	Fir	Typical*	Wheat	Barley
x_{H2}	0.020	0.009	0.011	0.010	0.057	0.000	0.016
x_{CO}	0.548	0.534	0.521	0.523	0.623	0.489	0.601
x_{H2O}	0.131	0.131	0.131	0.131	0.131	0.130	0.131
x_{CO2}	0.143	0.143	0.143	0.143	0.143	0.143	0.143
x_{CH4}	0.158	0.183	0.194	0.193	0.046	0.238	0.109

Both the temperature dependent and the simplified pyrolysis model adhere to the same input/output interface and are therefore interchangeable in the bed segment model. The inputs and outputs are;

- fuel temperature (input),
- ultimate composition of the volatile part of solid fuel (input),
- mass of volatiles (input),
- flue gas pressure (input),
- mass flow rate of volatiles (output),
- composition of flue gas from pyrolysis (output),
- enthalpy flow rate out of fuel due to pyrolysis (output),
- enthalpy flow rate into flue gas due to pyrolysis (output).

4.4.5 Char Conversion Model

The conversion of char is a process where fixed carbon in the fuel reacts with surrounding gases, resulting in gasification of the substance. The following reactions are considered in the char conversion model:

$$C + O_2 \rightarrow CO_2$$
$$C + H_2O \rightarrow CO + H_2$$
$$C + CO_2 \rightarrow 2CO$$

The reaction $C + 2H2 \rightarrow CH4$ generally also occurs during the gasification, but as this reaction is significantly slower than the rest of the reactions [Laurendeau, 1978], it will not be included in the model.

The conversion of char is usually divided into the following three regimes, depending on the temperature:

- The **chemical** regime, where the kinetics is limiting the reaction rate
- The **diffusion** or **transport-controlled** regime, where the diffusion of gases to the fuel particles and through its pores is limiting
- The **combined** regime, which is the region where both effects are present

The char conversion model includes reaction rates in the chemical regime and the diffusion regime. The combined regime is modelled using a smoothened min function of the two reaction rates, an example of this is illustrated in figure 20. The reaction rate calculation for the two regimes are presented next.

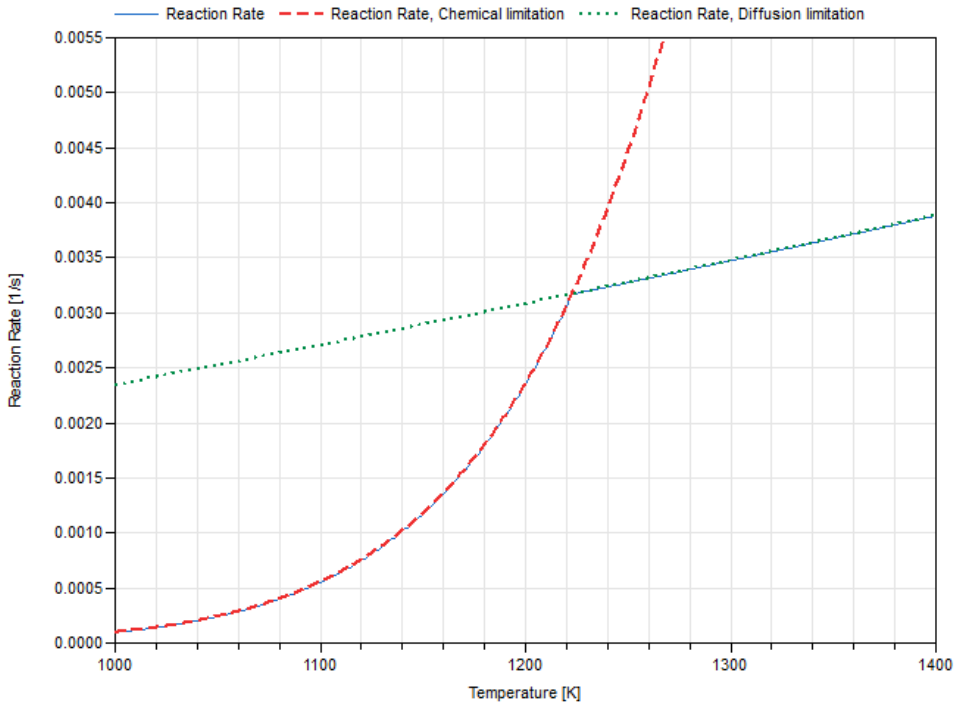

Figure 20. Reaction rate for CO2 at different temperatures.

Chemical Regime

In the chemical regime, it is assumed that the reaction rate r is given by the Arrhenius equation [Ullum, 2000]

$$r(T,x) = A_0 e^{\frac{ER}{T}} x^n$$

Where x is the concentration of the reactant in the gas and n is the reaction order. The constant A_0 varies for the different reactions and is retrieved from literature [Ullum, 2000], [Tanner et al., 2016].

Diffusion Regime

In the diffusion regime, the reaction rate is formulated as in [Ullum, 2000]:

$$r(T,x) = A_1 T^{1.5} x$$

Where A_1 is chosen so that the reaction rate given by the two different equations is equal at the transition temperature T_t:

$$A_1 = \frac{A_0 e^{\frac{ER}{T_t}} x^n}{{T_t}^{1.5} x}$$

In conclusion, the reaction rate over the entire interval can be summarized as

$$r(T,x) = \begin{cases} A_0 e^{\frac{ER}{T}} x^n & \text{if } T \leq T_t \\ A_1 T^{1.5} x & \text{if } T > T_t \end{cases}$$

4.4.6 Flame Front Calculation

The position of the flame front is calculated based on the char conversion mass flows in each segment. During normal operating conditions the char conversion occurs in several segments, with the mass flow in each determined by the reaction speed, which in turn is given by the temperature, and the amount of available char in the segment, as illustrated in Figure 21.

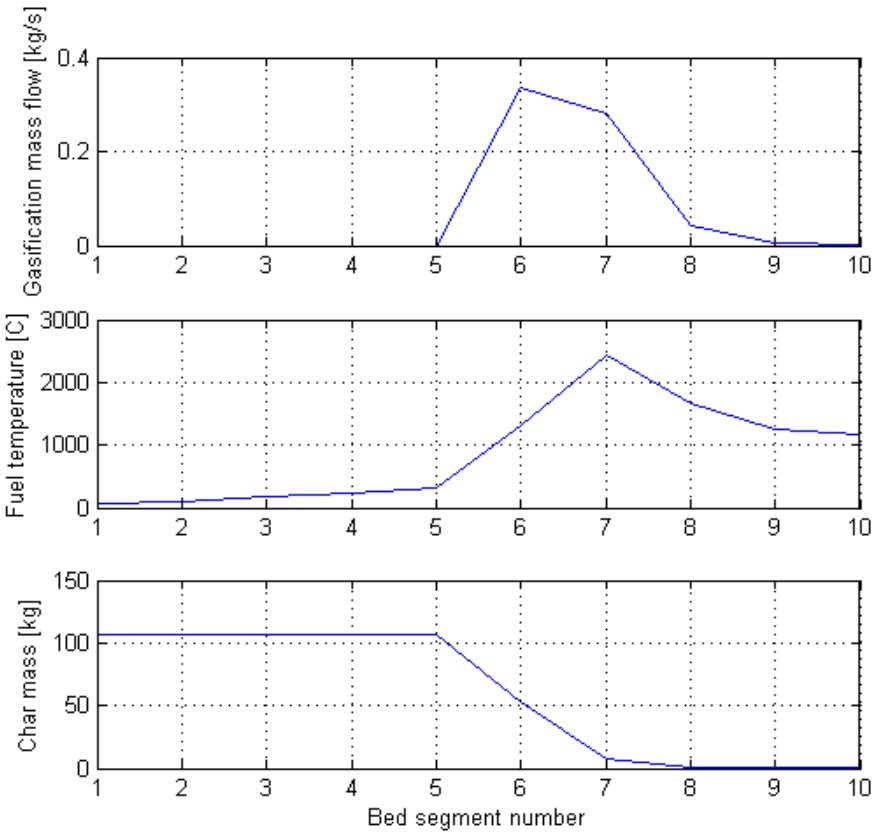

Figure 21. Char conversion mass flow, fuel temperature and char mass in each segment of the bed.

The flame front position is calculated from the distribution of char conversion mass flows, assuming that the location coincides with the position where a predefined fraction (chosen to be 90 percent in our case) of the total char conversion mass flow has occurred, as visualized in Figure 22.

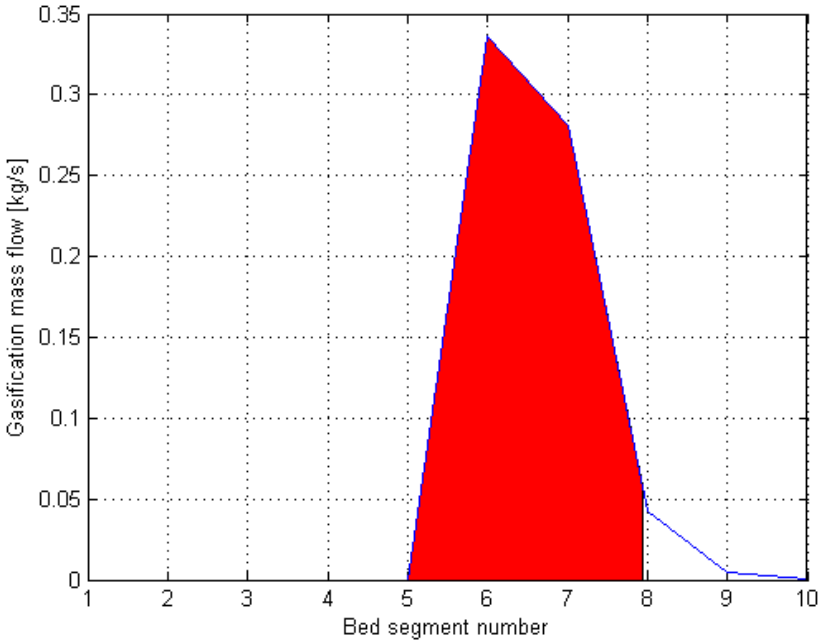

Figure 22. Char conversion mass flow. The highlighted area represents 90 % of the total mass flow, with the position of the flame front given by the position of the right edge of this area.

4.5 COMBUSTION MODEL

The combustion is modelled as a set of reactions that happen instantaneously when the gaseous fuel enters the model. The same model can be used to model both over and under-stoichiometric conditions. The implementation is based on the following assumptions:

- Fuel cannot coexist with oxygen after combustion
- CH4 combustion occurs before H2 combustion
- N2 is inert and does not react with the other species

The total combustion reaction is:

$$\alpha_i CH_4 + \beta_i CO_2 + \gamma_i CO + \omega_i H_2 + \eta_i H_2O + \phi_i O_2 \rightarrow \alpha_o CH_4 + \beta_o CO_2 + \gamma_o CO + \omega_o H_2 + \eta_o H_2O + \phi_o O_2$$

Where the Greek letters indicate the mole flow of the species and the subscripts i and o denote inlet and outlet, respectively. [Veje, 2016b]

The combustion is divided into three separate cases, depending on the stoichiometry, two under-stoichiometric and one over-stoichiometric. In the under-stoichiometric regions, the water-gas shift reaction is used to determine the ratio of carbon dioxide and, carbon monoxide, water and hydrogen, calculated from the combustion temperature. This reaction can be written as

$$CO + H_2O \rightleftarrows CO_2 + H_2$$

The following flows of carbon, hydrogen, and oxygen are introduced:

$$C = \alpha_i + \beta_i + \gamma_i - \alpha_o$$
$$H = 4\alpha_i + 2\omega_i + 2\eta_i - 4\alpha_o$$
$$O = 2\beta_i + \gamma_i + \eta_i + 2\phi_i$$

By combining the formula for the reaction, the assumptions utilized in the combustion model and the water-gas shift reaction, the analytical solution to the outflow of carbon dioxide can be calculated to be:

$$\beta_o = \frac{-b + \sqrt{b^2 - 4ac}}{2a}$$

Where a, b, and c are given by:

$$a = K_p - 1$$
$$b = K_p(C - O + 0.5H)$$
$$c = C(C - O)$$

And K_p is the equilibrium constant of the water-gas shift reaction. This holds for the under-stoichiometric cases. The mass flows of the other species in the different cases are presented next.

4.5.1 Very Limited Amount of Oxygen

In this situation, the amount of oxygen is insufficient to burn all the methane, and it is therefore present in the outgoing flow. The mole flow rates of the species leaving the segment are as follows:

$$\alpha_o = \alpha_i - 0.5\phi_i$$
$$\gamma_o = C - \beta_o$$
$$\omega_o = 0.5H - \eta_o$$
$$\eta_o = O - (2\beta_o + \gamma_o)$$
$$\phi_o = 0$$

4.5.2 Limited Amount of Oxygen

In this case, the amount of oxygen is sufficient to combust all the methane, but there is still not enough oxygen to achieve complete combustion. The mole flow rates of the species leaving the segments are:

$$\alpha_o = 0$$
$$\gamma_o = C - \beta_o$$
$$\omega_o = 0.5H - \eta_o$$
$$\eta_o = O - (2\beta_o + \gamma_o)$$
$$\phi_o = 0$$

4.5.3 Excess of Oxygen

In this final case, there is enough oxygen for complete combustion. No methane, hydrogen or carbon monoxide is leaving the segment. The flow rate for the species leaving the segments are:

$$\alpha_o = 0$$
$$\beta_o = C$$
$$\gamma_o = 0$$
$$\omega_o = 0$$
$$\eta_o = O - (2\beta_o + \gamma_o)$$
$$\phi_o = 0.5O - \beta_o - 0.5\eta_o$$

Figure 23 shows the composition of the flue gas when a fuel consisting of 95 % methane and 5 % hydrogen is combusted, as a function of λ. When no air is present, only methane and hydrogen is leaving the segment. As more air is introduced, methane is combusted, producing mostly water and carbon dioxide. The temperature determines the ratio between hydrogen and carbon monoxide in the flue gas through the water-gas shift reaction. As the air/fuel ratio is approaching $\lambda = 1$, the carbon monoxide and hydrogen are combusted as well, leaving only the products of complete combustion, carbon dioxide and water. As λ gets larger than 1, excess oxygen is seen.

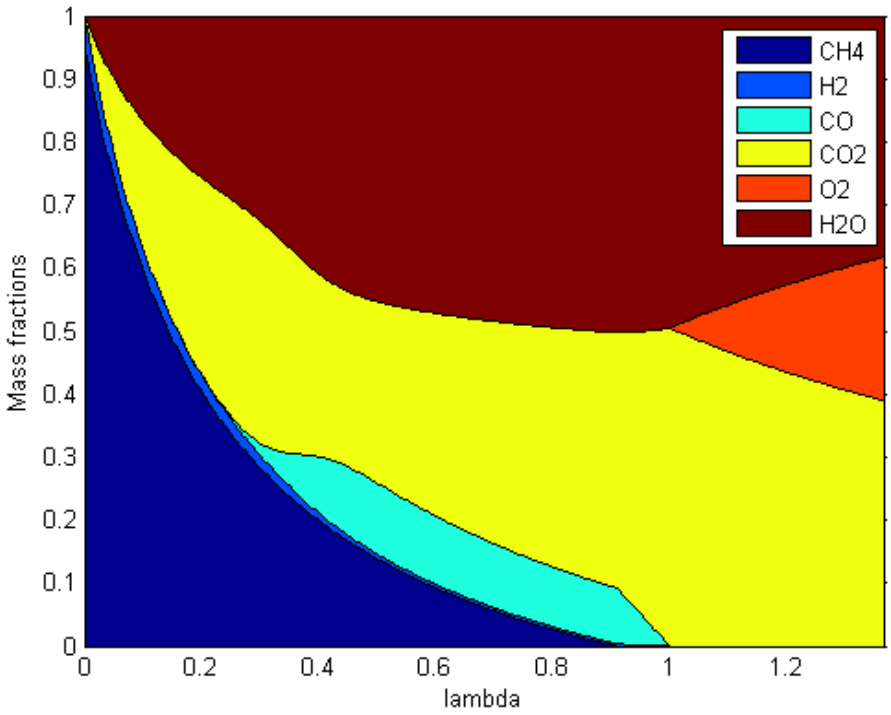

Figure 23. Gas species after combustion over varying λ.

Figure 24 shows the results of a unit test of the combustion model. Oxygen and Nitrogen in a fixed mass ratio of 1:3.29 is increased from zero to 6 kg/s and added to a gaseous fuel mixture with a fixed mass flow rate and composition. This results in an air excess number (λ) sweeping from zero to 1.37, thus covering under-stoichiometric to over-stoichiometric combustion. The topmost figure shows the combustion temperature, peaking at stoichiometric combustion (λ=1). The bottom figure shows the mass fractions of the species in the flue gas.

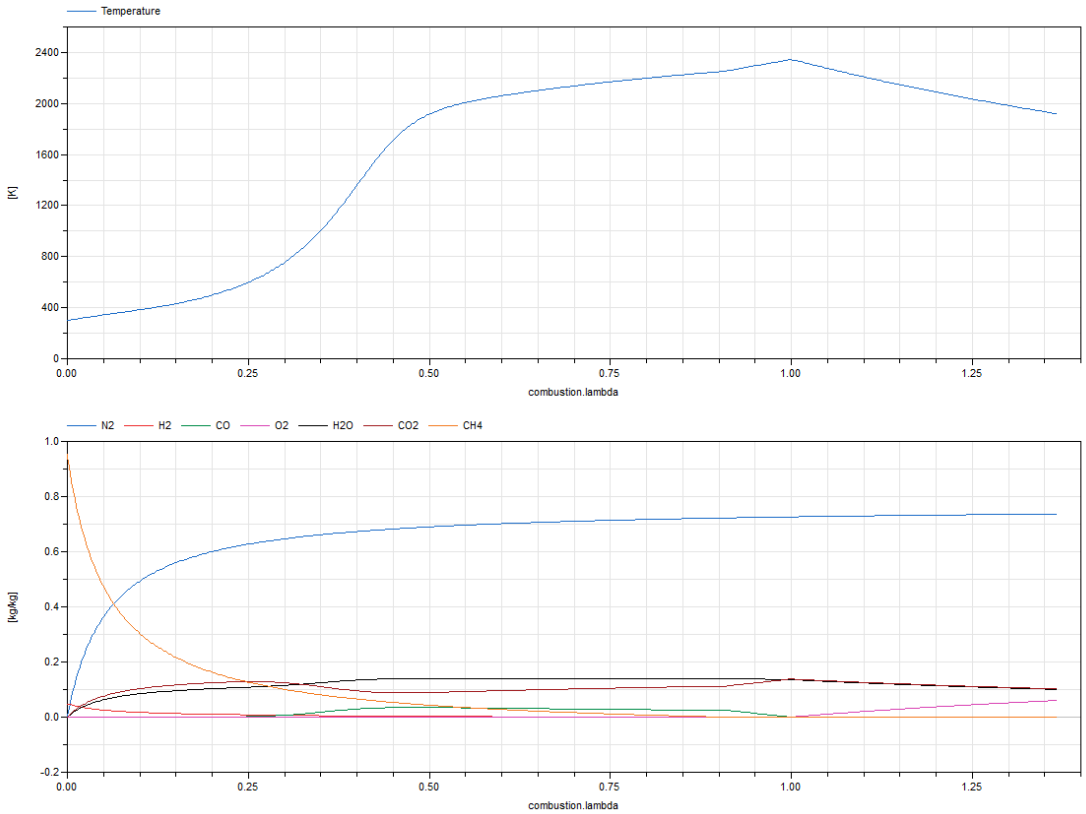

Figure 24. Plots showing combustion temperature (top) and species in flue gas as a function of λ.

4.6 GRATE MODEL

The grate beneath the fuel is discretized horizontally similarly as the bed model (from fuel entry to slag discharge). Each grate segment has a fluid pipe model (*Modelica.Fluid.Pipes.DynamicPipe*) representing the flue gas flow resistance. The pipe is connected thermally, through convective heat transfer, to a heat capacitance representing the thermal inertia of the grate metal. A constant heat transfer coefficient is chosen for reduced complexity (700 W/(m2K)). However, the heat transfer model in the dynamic pipe model can easily be interchanged with more complex versions. Thermal conduction is also assumed to take place horizontally through the grate and in an upwards direction towards the fuel. The implemented grate segment model is shown in Figure 25.

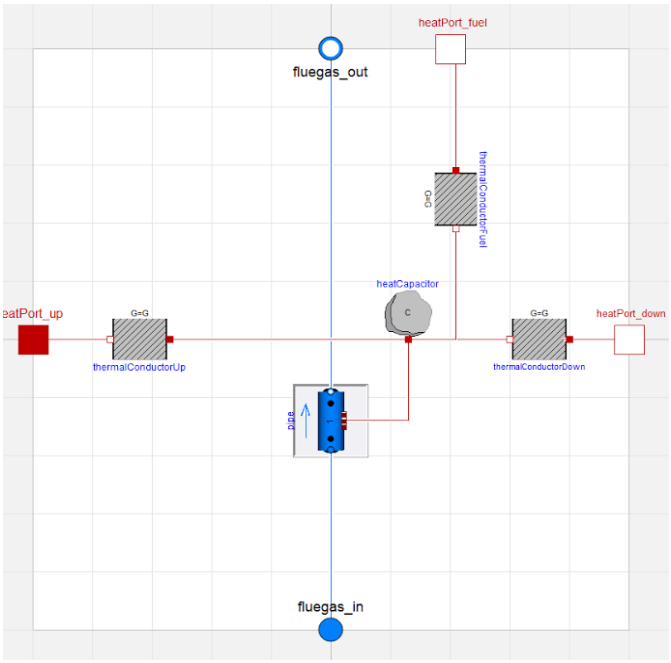

Figure 25. Grate segment model.

The dynamic equation for the heat capacity is

$$c_{p,g} l_g w_g d_g \rho_g \frac{dT}{dt} = Q_g$$

where the grate dimension is determined by l_g, w_g and d_g, the density ρ_g is set to 7900 kg/m3, Q_g is the heat transfer rate going into the heat capacity, and the specific heat capacity is a temperature dependent relation for the steel group 1 0,3 Mo (see standard DS/EN 12952-3);

$$c_{p,g} = 454.93 + 0.28139 T_g - 3.8815 * 10^{-4} (T_g - 273.15)^2 + 4.7542 * 10^{-7} (T_g - 273.15)^3$$

Each thermal conductor model adheres to the following dynamic equation;

$$k_g \frac{A_c}{d_c} \Delta T_c - Q_c$$

Where A_c is the thermal conduction surface area, d_c is the thickness of the conducting material, ΔT_c is the temperature difference across the conducting material, and k_g is the thermal conductivity of the material calculated as (steel group 1 0,3 Mo)

$$k_g = 49.83 - 1.613 * 10^{-2} (T_{avg} - 273.15) - 1.372 * 10^{-5} (T_{avg} - 273.15)^2$$

Where T_{avg} is the average temperature of the conducting material.

The grate model is then constructed by connecting n number of grate segments in parallel through the horizontal heat port connections.

4.7 FURNACE WALL MODEL

A layered wall model is implemented using a resistive-capacitive-resistive network to represent the thermal inertia of the furnace. Each layer consists of a capacity connected to a thermal resistance in each direction of heat conduction through the wall (1D heat conduction). The chosen properties for typical furnace wall material are listed in Table 4.

Table 4. Chosen furnace wall material properties. Emissivity is only provided for surfaces facing the inside of the grate boiler.

	Steel 15Mo3	Inconel 625	SIC-90 tiles	SIC concrete filling
Thickness (m)	0.005	0.002	0.030	0.030
Density (kg/m3)	7850	8440	2510	2300
Thermal conductivity (W/(mK))	50	11	11.715	4
Specific heat capacity (J/(kgK))	500	475	678	650
Emissivity	NA	0.71	0.9	NA

Most of the furnace is covered by evaporator wall, which could be steel 15Mo3. The lower part of the furnace is typically also covered with ceramic tiles and a layer of concrete filling between tiles and steel. The steel is typically covered by Inconel 625 instead of tiles in the upper part of the furnace. A constant evaporation temperature can be assumed on the other side of the furnace wall, if the boiler water pipe network is not modelled.

4.8 RADIATION HEAT TRANSFER MODEL

Heat transfer by thermal radiation is dominant inside the first flue gas pass of the boiler. The subsequent passes with superheaters are typically dominated by convective heat transfer, hence called convective passes.

Grey body radiation is illustrated in Figure 26. The incident radiation is partly reflected, absorbed, and for some materials transmitted. The radiated heat is the sum of reflected radiation and emitted radiation (Stefan-Boltzmann law).

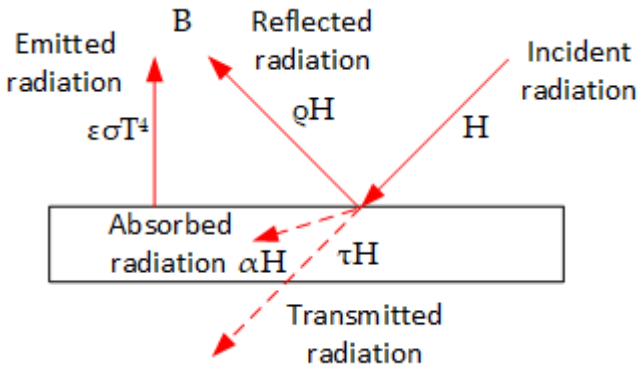

Figure 26. Grey body radiation example.

All facing surfaces in the furnace will radiate heat to each other. The complexity of the resulting network of heat transfer connections grows rapidly with increased discretization of the bed and furnace wall. The inner geometry of the furnace can also be of complex nature. A generalization and simplification of the radiation heat transfer is therefore needed and implemented in a separate model.

In the implemented radiant heat transfer model, it is assumed that the furnace can be represented by a rectangular box, as shown in Figure 27. The box is split vertically into m combustion zones, with m heat port connections in the horizontal direction going to the furnace wall and m connections to the flue gas combustion volumes inside the furnace. Furthermore, n connections are provided in the downward direction (e.g., number of bed discretizations) and k connections in the upward direction.

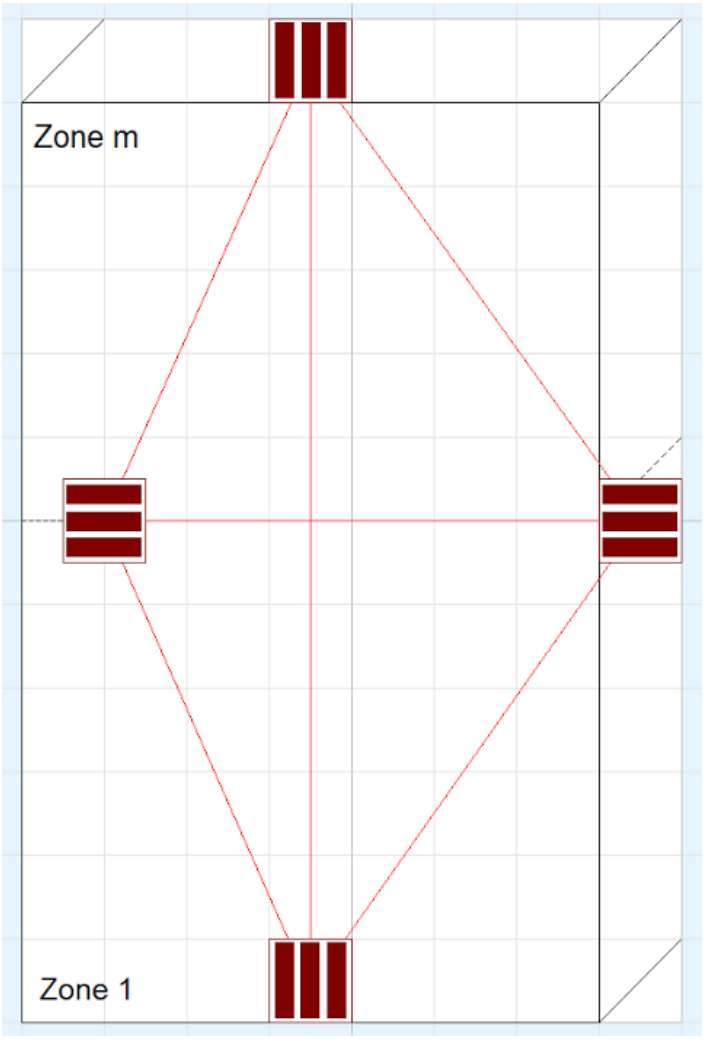

Figure 27. Illustration of the generalized furnace radiation heat transfer model.

The complete radiation of heat in the furnace is calculated by solving the following set of equations (note that the equation for the outgoing heat transfer rates for all

surfaces **B**, with dimension n+2m+k, involves element wise multiplication of vectors);

$$\mathbf{H} = \mathbf{F}\mathbf{B}$$
$$\mathbf{B} = \mathbf{A}\boldsymbol{\epsilon}\sigma\mathbf{T}^4 + \boldsymbol{\rho}\mathbf{H}$$
$$\mathbf{Q} = \mathbf{H} - \mathbf{B}$$

where the vector **H** is the incoming heat transfer rates into each surface, the square matrix **F** determines how the outgoing heat transfer rates are distributed to the facing surfaces (has zeros in the diagonal — a surface does not radiate heat to itself), the vector **A** is the surface areas, the vector $\boldsymbol{\epsilon}$ is the emissivity of each surface, σ is the Stefan-Boltzmann coefficient, the vector **T** is the surface temperatures, the vector $\boldsymbol{\rho}$ is the reflected or transmitted radiation from each surface, and finally **Q** is the resulting heat transfer into each surface element. Note that the sum of the elements in the vector **Q** is always zero.

The difficult part of deriving a radiation model is to formulate a generalization of **F** for an arbitrary number of surface discretizations. A simple version is implemented in the present work, where the outgoing radiation is distributed among all other surfaces according to their relative surface areas (view angles are thus neglected). Additionally, the following assumptions are made (see also [Ullum, 2000]);

- A gas volume absorbs and transmits energy (no reflection).
- A surface absorbs and reflects energy (no transmittance).
- Emittance = absorptance.
- Absorptance (0–1) + transmittance (0–1) + reflectance (0–1) = 1.
- Absorptance and reflectance for bed and furnace wall surfaces are constant.
- Absorptance for the gas volumes is constant (in more elaborate versions it should be a function of pressures, temperature, and mean travel length).

Figure 28 shows temperatures of heat capacities in a simulation example where they are all thermally connected with a cubic 1 m3 radiation box with downward discretization of n=4 (T_1-T_4), horizontal wall discretization of m=2 (T_5, T_6), upward discretization of k=1 (T_7), and horizontal flue gas discretization of m=2 (T_8, T_9). The chosen radiation coefficients are summarized in Table 5.

Table 5. Radiation coefficients used in simulation.

	Emittance	Reflectance	Transmittance
down (fuel bed)	0.8	0.2	0
horizontal (tile wall)	0.9	0.1	0
up (Inconel)	0.71	0.29	0
horizontal (flue gas)	0.4	0	0.6

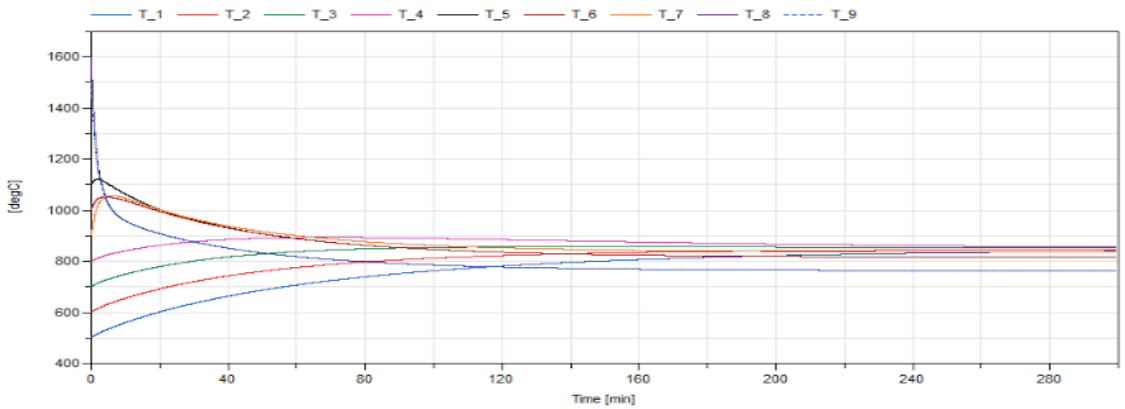

Figure 28. Furnace radiation heat transfer simulation example showing convergence of temperatures.

The radiant heat transfer between the heat capacities cause the temperatures to converge towards each other. However, there is a temperature offset caused by differences in radiation coefficients, e.g., the transmittance is high for the flue gas and these steady state temperatures (T_8 and T_9) are also lowest.

4.9 COMPLETE GRATE BOILER SIMULATION

The presented detailed grate boiler submodels have been aggregated into a complete grate boiler simulation example. A Dymola diagram view of the model is shown in Figure 29. Starting from the left, the fuel inlet flow is determined by *flowSource* with fuel composition specified by *X_source*. The fuel enters the *bed* model and is propagated along the bed with a given grate velocity (blue triangular input connector). The bed is discretized into n bed segments horizontally and vertical discretization is omitted in the example simulation model. A *grate* model (also with n segments) is thermally connected to the bed model and acts as a primary air flow resistance between the flow source *PA_source* and the bed model. The flow source air flow is split along the grate in the model represented by the light blue box (determines air distribution). The flue gas flows out of the bed segments are subsequently mixed before entering the first *combustion* model (orange box). Subsequently, secondary air is added with the *SA_source* before the flue gas enters the second combustion model (air staging). The furnace walls are represented by three layered wall segments; *furnaceWall1*, *furnaceWall2*, and *furnaceTop*. The first two segments, representing the vertical furnace walls, are made of tiles, concrete, and evaporator steel. The last segment, representing the furnace top, is made of Inconel and evaporator steel. The furnace walls are thermally connected to a constant saturation temperature on the outside, representing evaporating water in the riser tubes. All internal furnace surfaces, including the flue gas, are thermally connected through radiation heat transfer using the *radiationZone* model. *AuxiliaryBurner1*, *AuxiliaryBurner2*, and *AuxiliaryBurner3*, are added to the example providing a specified heat flow rate into the last three bed segments. This can be used during start-up if the simulation is started from cold conditions without fire on the bed. The main measurable outputs from the grate boiler simulation are furnace flue gas temperature *T_fluegas*, potential heat output *Q_heating*, flue gas oxygen concentration *O2_wet*, and the

position of the burn-out location *flameFront*. In addition to these, all internal model variables are available in the simulation.

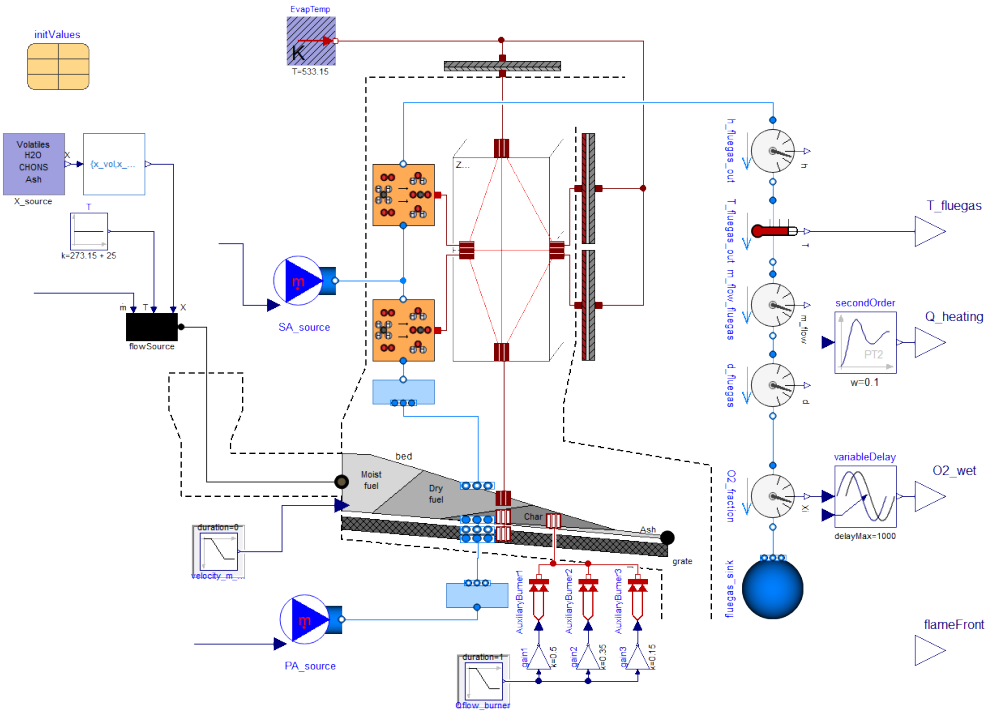

Figure 29. Dymola diagram view of complete grate boiler model simulation.

The oxygen concentration sensor is typically located after economizers and before the air preheater. This means that the measurement will be delayed with the transportation time of the flue gas through the flue gas channel (empty passes, superheater passes, etc). Models of the flue gas channel after the furnace is not part of the simulation example. However, a *variableDelay* model is added to the simulated *O2_wet* output with a delay given by the *spatialDistribution* operator in Modelica. The flue gas flow velocity v_{fg} required in the delay calculation is approximated by

$$v_{fg} = \frac{\dot{m}_{fg}}{\rho_{fg,avg} A_{cross,avg}}$$

Where $\dot{m}_{fg}$ is the mass flow rate, $\rho_{fg,avg}$ is the average flue gas density along the channel and $A_{cross,avg}$ is the average cross-sectional area of the channel.

The grate boiler heat output is normally calculated on the water/steam side. However, the water/steam part in the boiler drum, evaporators, superheaters, etc., is a complex system of pipes and heat exchangers in itself and is not part of the implemented simulation example (components from Modelica Standard Library can be used for this purpose). The heat output $Q_{heating}$ is instead calculated as

$$Q_{heating} = Q_{evap} + \dot{m}_{fg}(h_{fg,out} - h_{fg,ref})$$

where Q_{evap} is the total heat transfer through furnace walls (cooled by the evaporator) and the rest is the available heat in the flue gas when cooled down

from the furnace outlet temperature to a given reference temperature. The heat output $Q_{heating}$ is additionally passed through a second order filter to approximate the overall dynamics in the water/steam pipings.

4.10 MODEL VALIDATION

Usually, a model can be validated by directly comparing simulation results with measurements or other reference values. Since utility boilers are always very sparsely instrumented in the fuel and flue gas path, obviously, immeasurable states such as flame front, bed composition and temperatures must be validated in a different way. The key is to rely on the fidelity of the model and to assume that *if the model can reproduce measured values well, the intermediate states between boundary conditions and measured states are also reproduced well*. This approach is often taken in the field of control engineering, where it is referred to as *state estimation,* which also includes a feedback loop that continuously adjusts the model to ensure a match between measured and simulated states. In that context, it is worth noting that even if the simulated states do not exactly match the corresponding physical states, state-feedback control can still improve the process.

Nine days of data from the Sysav WtE plant in Malmö has been made available for potential model validation. The data is sampled with a 10-minute interval and the specific measurements are highlighted in Figure 30.

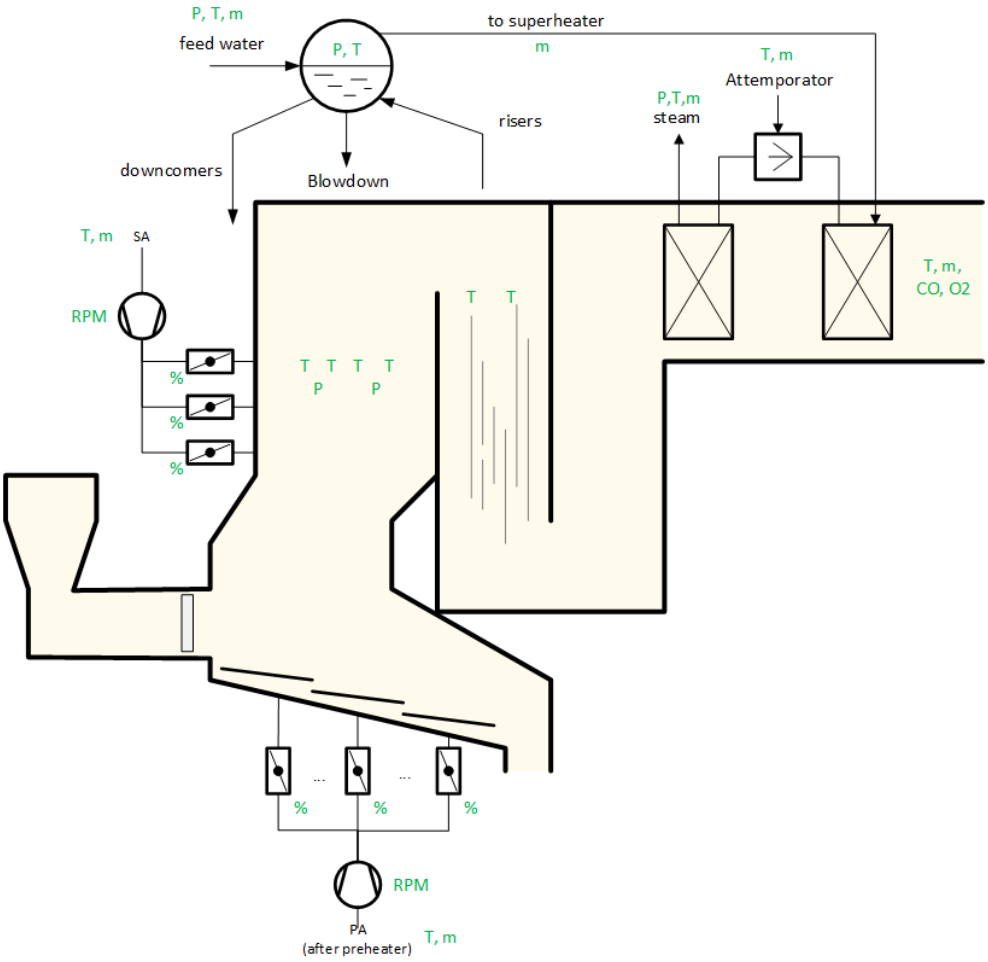

Figure 30. Simplified drawing of a Sysav grate boiler with indication of available measurements (green).

Suitable measurement data are necessary to validate the model. In this case the validation process is challenged by the fact that not all upstream boundary values for the model are measured at the Sysav plant. Particularly, the fuel flow and composition are an unknown input, which inhibits the fidelity of the validation process in the following way:

- The dynamic behaviour of the process cannot be validated since both the input and (dynamic) outputs must be known.
- The fuel movement speed on the grate also influences the dynamic response, but only grate speed in mm movement is known.
- The burn-out location (flame front) is not measured at Sysav.
- The steady state behaviour of the model, however, can be validated to some extent without the measured fuel input. This can be done by re-constructing (or back-calculating) the fuel input from downstream measurements such as oxygen contents, flue gas flow, furnace temperature etc. The norm EN-12952-15 prescribes how to do so.
- The steady state calculation also requires assumptions in terms of fuel composition (e.g., "typical" waste), heating value, and ash losses (amount of unburnt and temperature).

- The missing volatile mass fraction in the MSW fuel composition and the fact that the implemented pyrolysis model is based on biomass experiments also makes a direct comparison difficult.

However, the available measurements can be used to;

- obtain the produced heat on the steam side, which can be used to scale the model so that it approximately matches the size of the Sysav grate boiler.
  - × Two-hour average values during five steady state periods at nominal load shows an average of 81 MW on the steam side, given the measurement locations shown in figure 30.
- obtain an indication of a reasonable PA/SA combustion air split.
  - × The same periods as above shows a split of 54.8/45.2.
- compare furnace temperatures.
  - × Four temperature sensors are located inside the furnace showing an average temperature during nominal load of 958 ℃ (min 939 ℃ and max 975 ℃).

Additionally;

- the norm EN-12952-15 can be used to calculate the necessary combustion air flows at a given target O2 content in the flue gas. Applying these air flows should give the same O2 content in the flue gas for the same fuel specification in the simulation.
  - × Typical excess air ratios used in district heating furnaces fired with wood chips is in the range 1.4–1.6 corresponding to a dry O2 content in the flue gas of 6–8 %. A dry O2 content of 6 % corresponds to a wet O2 content of 4.79 % for typical wood chips with the specification given in table 1. The combustion air flow should in this case be 5.43 times higher than the fuel flow according to calculations prescribed by EN-12952-15.
- the heating value of the chosen fuel can be used to calculate the expected heat output for comparison with the simulated output.
  - × The lower heating value (LHV) of typical wood chips is approximately 10.7 MJ/kg (from 25 ℃ fuel to 150 ℃ flue gas). Any discrepancy in the result must consider the losses due to hot ash and unburnt fuel leaving the grate.

A complete grate boiler simulation has been parameterized to validate the modelling work, with boundary conditions and expected output based on the above discussion. An overview of the parametrization and boundary conditions is provided in Table 6. Note that parameters are mostly based on reasonable estimates and experience (e.g., physical dimensions that otherwise would have taken long, valuable, time to infer from drawings etc.).

Table 6. Key parameters and boundary conditions used in complete grate boiler simulation.

Description	Value	Unit	Comment
Fuel, typical wood chips	see table 1	-	
Fuel inlet flow, $\dot{m}_{fuel,in}$	7	kg/s	Gives a total heat output corresponding to Sysav
Fuel inlet temp., $T_{fuel,in}$	25	°C	For comparison of heat output with LHV
Grate velocity, v_{grate}	0.005	m/s	
PA flow, $\dot{m}_{PA}$	22.8	kg/s	60% of fuel flow multiplied with 5.43
SA flow, $\dot{m}_{SA}$	15.2	kg/s	40% of fuel flow multiplied with 5.43
Air temp., T_{PA} and T_{SA}	150	°C	For comparison of heat output with LHV
Bed discretization, n	10	-	
PA flow distribution vector	{0.03,0.03,0.05,0.05 ,0.09,0.09,0.26,0.22 ,0.1,0.08}	-	Less air in first and last part of grate (same discretization as bed)
Bed length	8	m	
Bed width	4	m	
Furnace length	6	m	
Furnace width	4	m	
Furnace height	16	m	
Cross-sectional area of flue gas channel, $A_{cross,avg}$	9	m^2	Average cross-sectional area of flue gas channel from furnace to O_2 measurement location
Flue gas channel length	70	m	
Auxiliary burner, $Q_{aux,fuel}$	3.5	MW	Distributed among the last three bed segments during the first hour of simulation
Evap. temp., T_{evap}	260	°C	Same value as in Sysav data
Init. furnace wall temp.	260	°C	Initialized to evap. temp.
Init. bed fuel temp.	25	°C	Cold initial bed

Figure 31 and Figure 32 shows simulation results from the first two hours of simulation from an initial cold bed to steady-state operation. The fuel height in each bed segment is initialized with a linearly decreasing height from 0.63 m to 0.063 m (triangular shape).

The last three segments, with auxiliary burner heat input, quickly increase in temperature starting with vaporization of water (m_{H2O} going to zero), devolatilization (m_{vol} decreasing), and ignition in the last bed segment (large increase in temperature and decrease in m_{char}). The furnace and fuel slowly begin to warm up and vaporization of water in segment 7 then leads to devolatilization in segment 8 (dry hotter fuel is transferred instead of wet). Char conversion slowly moves up the bed with ignition in segment 9 after 29 minutes, ignition in segment 8 after 51 minutes, and ignition in segment 7 after 61 minutes. Steady state temperatures are reached in a state with wet fuel on the first three segments (m_{H2O} = 448 kg), devolatized fuel on the last four segments (partly devolatized in segment

5), and almost complete char conversion after segment 8 (0.67 and 0.13 kg of char left in segment 9 and 10, respectively). The fuel flow out of the last segment (going into the slag discharge) is 0.035 kg/s and consist of 96.7 % ash.

A closer look at devolatilization reveals that it approximately starts at a fuel temperature of 200 °C and ends at 600 °C as expected. Char conversion accelerates at a fuel temperature above 800 °C. The furnace flue gas temperature $T_{fg,furnace}$ settles at a temperature of 1061 °C, which is approximately 100 °C higher than the temperatures measured at Sysav. However, the measurement at Sysav is also believed to be located closer to the top of the furnace, which could explain the small cool down (higher temperature in simulation). Small drops in $T_{fg,furnace}$ can be observed each time the water in a fuel segment vaporizes (relatively cold vapor is added to the flue gas). This effect is minimized with increasing number of bed segments.

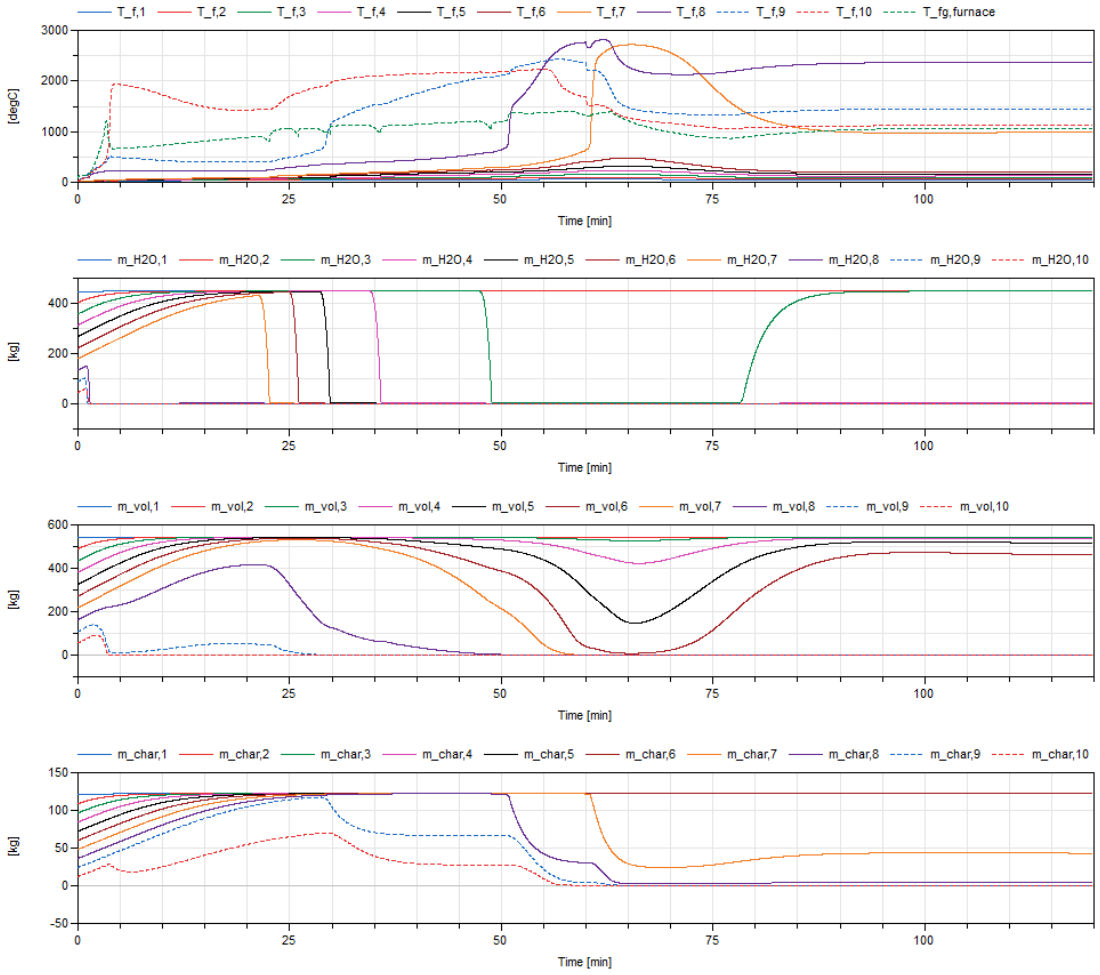

Figure 31. Temperature and proximate masses in the bed fuel segments from complete grate boiler simulation (subscript 1 is segment closest to fuel inlet). Flue gas temperature after combustion $T_{fg,furnace}$ is also shown.

The burn-out location (flame front) is initially 0.1 before char conversion starts (default value when there is no fire present). The value then goes to almost 1 when the fire starts in segment 10 (1 corresponds to a burn-out location at the end of the

bed) and slowly drops to a steady state value of 0.78 as the fire moves closer to the fuel inlet (segment 7).

The total heat output $Q_{heating}$ slowly increases as the furnace is warmed up and reaches a steady state value of 72.3 MW. Multiplying the fuel flow with an expected LHV of 10.7 MJ/kg gives 74.9 MW, which is close to the obtained heat output (note that there will be losses due to ash and unburnt fuel leaving the grate).

The flue gas O_2 mass fraction slowly decreases with increasing char conversion. The mass fraction goes to zero during peaks in char conversion in segment 7 and 8, where large amounts of char is quickly burned, while being limited by the sub-stoichiometric conditions. This also produces large amounts of CO, which consumes the remaining O_2 in the flue gas combustion above the bed. A smoother response can be obtained using a higher bed discretization, as a segment either has char conversion or not (larger volumes equals larger transients). The steady state wet O_2 mass fraction is 4.72 %, which is quite close to the expected 4.79 %.

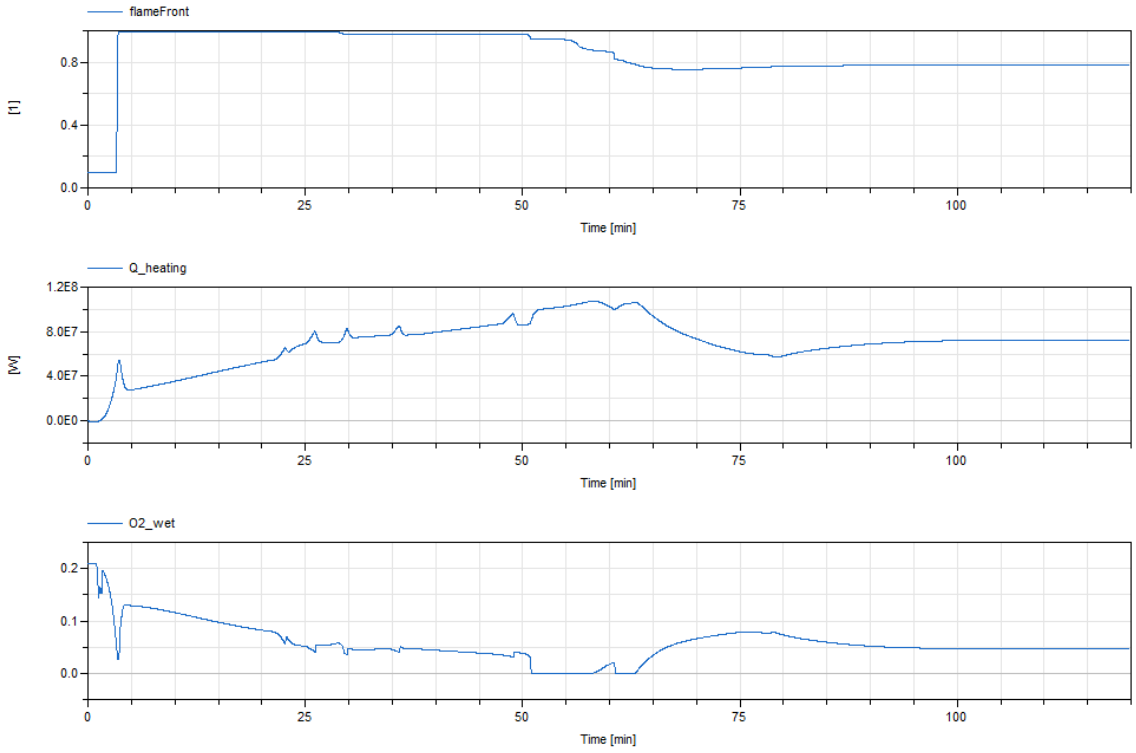

Figure 32. Burn-out location (flameFront), total heat output (Q_heating), and wet O2 mass fraction (O2_wet) from complete grate boiler simulation.

The two-hour complete grate boiler simulation example took 190 seconds to complete using Dymola 2018 on a ThinkPad T550 i7 2.60 GHz laptop. This is approximately 38 times faster than real time, when the bed is discretized into 10 segments. More could potentially be done to increase the simulation speed, but the results indicate the potential for higher discretizations within reasonable simulation time.

4.11 MODEL ROBUSTNESS

The component-oriented modelling approach, together with the physics-based modelling of Modelica, makes it is quick and easy to build aggregated models of very high complexity and fidelity by mere drag-and-drop or by parameterization. The models presented in this project is an example of this, as the connection of subcomponents based entirely on physical principles have resulted in a complete and realistic representation of a grate boiler, without a significant amount of tuning or simplifications. There are however also pitfalls with this approach, as explained in the following paragraphs. But it is the authors conviction that these issues can be resolved with additional unit testing and reasonable model simplifications.

Figure 33 shows the solver statistics for the complete grate boiler simulation model. For instance, the detailed grate boiler with "only" 10 bed segments contains around 3,000 equations and several nonlinear equation systems which need to be solved iteratively during each time step — the biggest system containing 46 unknowns before manipulation by the solver, and 19 after. The nonlinear equation systems should — if possible — be reduced or removed to speed up simulation time and increase model robustness. Complying with the staggered-grid scheme mentioned earlier is one way to increase model robustness, i.e. by breaking up the nonlinear equation systems by inserting dynamic states.

Nonlinear equation systems can be removed either by reformulating the model so that explicit formulations are used rather than implicit, or by introducing additional states. Reformulating the equations is generally the most promising of the two, as additional dynamic states in the model can increase the simulation time, especially if fast dynamics are added. However, it is often hard to find explicit formulations except for systems that are already quite small. In the system model at hand, scalar nonlinear equation systems, corresponding to enthalpy-temperature calculations for the fuel medium, could be removed by adding a corresponding explicit function, instead of the current situation, where the water fraction and the dry fuel use two separate functions. For the largest nonlinear system, there is little hope of finding a similar method, as it is introduced by the complex radiative heat transfer model. In this case, a more promising approach would probably be to search for ways to simplify the model (e.g. remove parts with little influence over the overall behaviour), rather than reformulate it.

It is important to note that systems of nonlinear equations can occur on a simulation model level and not necessarily on the component level. The connection of two numerically sound models can result in, e.g., systems of nonlinear equations if two so-called flow models are connected, or in high-index differential algebraic systems if two so-called volume models are connected. This means that one should take this into consideration when building models from components.

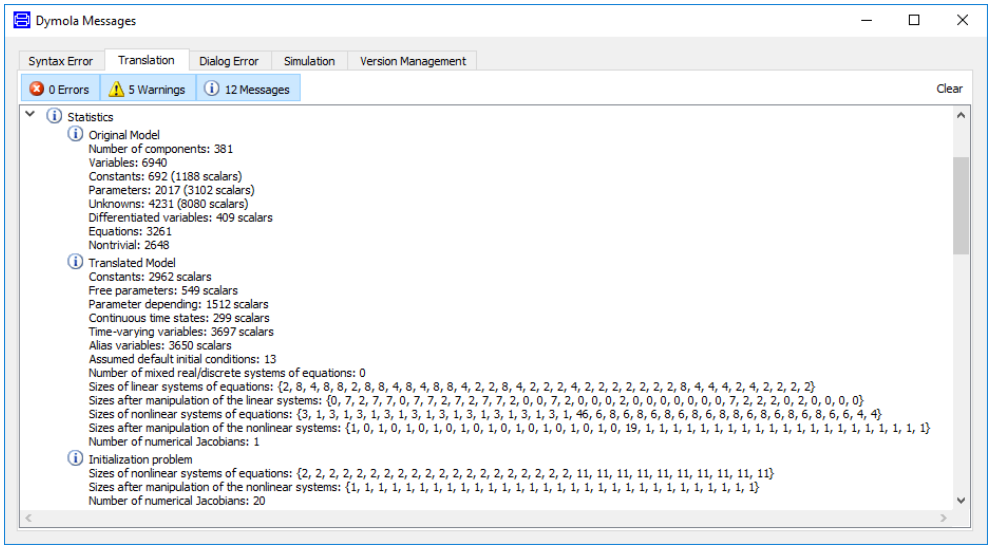

Figure 33. Solver statistics for complete grate boiler simulation model.

Another issue is the sensitivity of the model to change in parameters or inputs. In general, the aggregated model seems to be very sensitive to boundary conditions — not particularly in terms of initialization problems but rather in the way that even small step changes in e.g. input values can result in failure to simulate the model. This sensitivity has made it quite difficult to perform the intended open-loop and closed-loop simulations with the complex model.

The types of errors detected during the solution are typically related to logarithm of negative temperature, invalid water/steam table lookup values and negative mass fractions. These are typically the consequence of inadequate unit testing and lacking robustness of sub-models.

5 State Estimation

5.1 METHODS FOR STATE ESTIMATION

State estimation has the goal of reconstructing the internal states of a process based on the available measurements. This task is performed by an observer. Several different kinds of observers exist, which type to use depends on the characteristics of the process in question. Algorithms based on the Kalman filter are traditionally used for this purpose. For linear processes, the Kalman filter, which itself is linear, is optimal in the sense that the deviations between estimated and true states are minimized. For nonlinear processes, more advanced observers are often required. The Extended Kalman Filter (EKF) and the Unscented Kalman Filter (UKF) are two methods that can be used in this case.

Common for all flavours of the Kalman filtering methods is the requirement of an observable model of the process at hand. The internal states of this model, which are the basis for the state estimation, mimics the states of the real process. The observability requirement, as well as performance considerations, will in practice limit the number of states that an observer model used in this setting can have. For the detailed process developed in this project, observability analysis of a test model with a single bed segment revealed that usage of the model in a Kalman filter would be completely infeasible. More specifically, to achieve observability for just one bed segment with 15 states, approximately 10 measurement signals were needed. This analysis was conducted by looking at the observability Gramian of the linearized system, which for stable systems is positive definite whenever the system is observable [Skogestad et al., 2005].

When faced with the problem of having a model which is too complex for a traditional observer implementation, two alternative methods for the estimation task were considered, both of which are based on implementing a simpler model.

1. Developing a simplified, physics-based model of the process, capturing the key feature of how the flame front is affected by changing input signals, and how it in turn influences the available measurements. This model could be used as observer model in a setup where the detailed grate boiler model would be used as a plant.
2. Using the detailed model to derive a black-box model relating the flame front position to the available measurements in the process.

It was decided that the second alternative should be implemented, using an artificial neural network (ANN).

5.2 NEURAL NETWORKS

Some background and theory for artificial neural networks, and their application in state estimation of dynamical systems is presented in this section. For a more detailed explanation of the area of nonlinear system identification, see e.g. [Ljung, 1999].

Artificial neural networks were developed to mimic the information processing capabilities of a nervous system [Rojas, 1996]. They consist of a collection of neurons which are usually situated in layers. The neurons of each layer receive input signals from each neuron of the previous layer, which together with a bias are used to construct a weighted sum. This sum is used as input to a predefined function, the output of which is propagated to the neurons of the next layer. Feeding the first layer of neurons is a number of input signals, while the outputs from the last layer of neurons determine the output from the network. One normally separates the last layer of neurons from the rest by calling it the output layer, while all other layers are denoted as hidden layers. By finding suitable values of the weights and biases, a neural network can be used to approximate any continuous function [Hornik, 1991].

The weights and biases for each node are determined using a learning algorithm. By feeding the neural network with input signals were the correct output signal is known, the learning is handled as an optimization problem, with the objective of minimizing the difference between the output of the network and the correct output signal.

For the task of state estimation of a dynamical system, it is important to note that a neural network only functions as a static map between inputs and outputs. This means that it cannot be used as it is to represent a system with internal dynamic. A common method for circumventing this is to consider a sampled system and to introduce delayed versions of the input signals, together with the input signals at each sample time.

5.3 TOOLS AND WORKFLOW

The training of the neural network was performed in Python using the package NeuroLab [NeuroLab 0.3.5 documentation]. Simulation results for the complex model from Dymola was imported, sampled and scaled in Python and then used as input and target data in the neural network training. The capabilities of the neural network parametrization derived in training was evaluated by simulating the neural network with a different set of inputs, corresponding to other simulation results for the complex model. The weights and biases of the network were saved to a mat file.

For the implementation of the neural network observer with the complex model, the Modelica package NeuralNetwork [Codecà and Casella] was used. A network corresponding to the one trained in NeuroLab, was set up, importing the weights that were saved. To support this, the scaling of all variables was also implemented in Modelica.

5.4 NEURAL NETWORK TRAINING

Training data was generated in Modelica using amplitude modulated pseudo random input signals (APRBS). Based on analysis of the dynamics of the model, the dwell time of the signal was determined to be in the range of 1800–3600 seconds. To ensure that varying flame front positions would be present in the data, a trapezoid signal with a lower frequency was superimposed to the primary air

flow signal. Further extension of the training space was considered in terms of multiplying all inputs with a table-based gain, which would correspond to different loads of the plant. However, this was not implemented due to time constraints and stability issues with the model. The training scenario is initialized with the bed cold, followed by a ramp in fuel flow and grate speed. After the ramp and a period of constant inputs, the training is started 9000 seconds into the simulation and is conducted for 91 000 seconds or approximately 25 hours. Input signals, measurement signals and the flame front position during training are displayed in Figure 34.

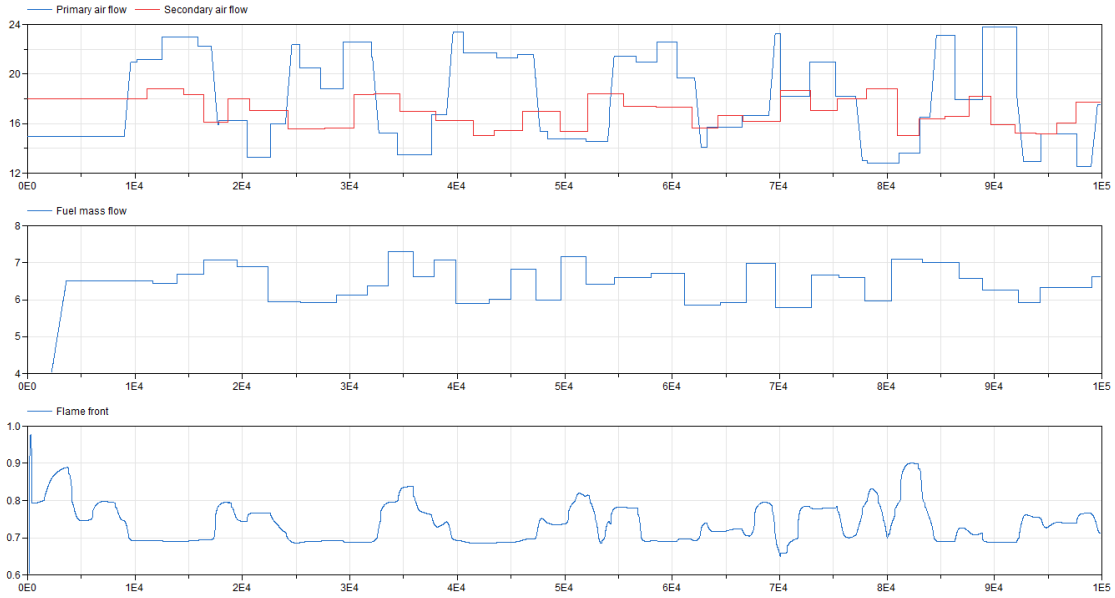

Figure 34. Air flows and fuel flows during neural network training and resulting flame front position.

During the training phase, the sum of the squared errors (SSE) in flame front position was minimized, using the Broyden-Fletcher-Goldfarb-Shanno (BFGS) algorithm, which is the default method in NeuroLab. It uses the corresponding function from SciPy [SciPy.org] for this purpose.

Different parameterizations in terms of sample time, number of input signals, number of delays and number of neurons, were considered in the neural network training. The considerations made for each of these are presented below. In all cases, the hyperbolic tangent sigmoid function is used in the hidden neuron layer and a linear function is used in the output layer.

- Sampling time: the sample time was determined to be in the order of magnitude of 100 seconds, corresponding to the typical speed of the flame front dynamics in the model. A different approach, with sampling time determined by the time constant of the total system, was also considered, but this yielded less satisfactory results. After comparing the results from generated neural networks with different sampling times, a network with a sampling time of 120 second was chosen.

- Input signals: the input signals to the neural network were decided based on matching the available measurements in the real plant, according to the list below.
  - × Primary air flow
  - × Secondary air flow
  - × Flue gas temperature
  - × Flue gas mass flow
  - × Flue gas oxygen content
- Number of delays: delayed versions of all input signals with one and two samples (together with signals without any delay) were used, resulting in 15 input signals in total for the neural network. This strategy was based on common practice in neural network modelling. Specifying the delays of different inputs differently, depending on the dynamics of the system was also considered, but the results from these experiments were inferior.
- Number of neurons: experiments were conducted with the number of neurons varying between 12 and 24 in a single layer. Tests with fewer neurons were also conducted, with less success. No clear trend in the capability of the resulting observer based on the number of neurons in this range could be observed, the best results were achieved with a network with 20 neurons.

The output from the neural network together with the flame front position for the data set that it was trained on is displayed in Figure 35. The network generally manages to follow the actual position very well, but some spikes in the results can be observed.

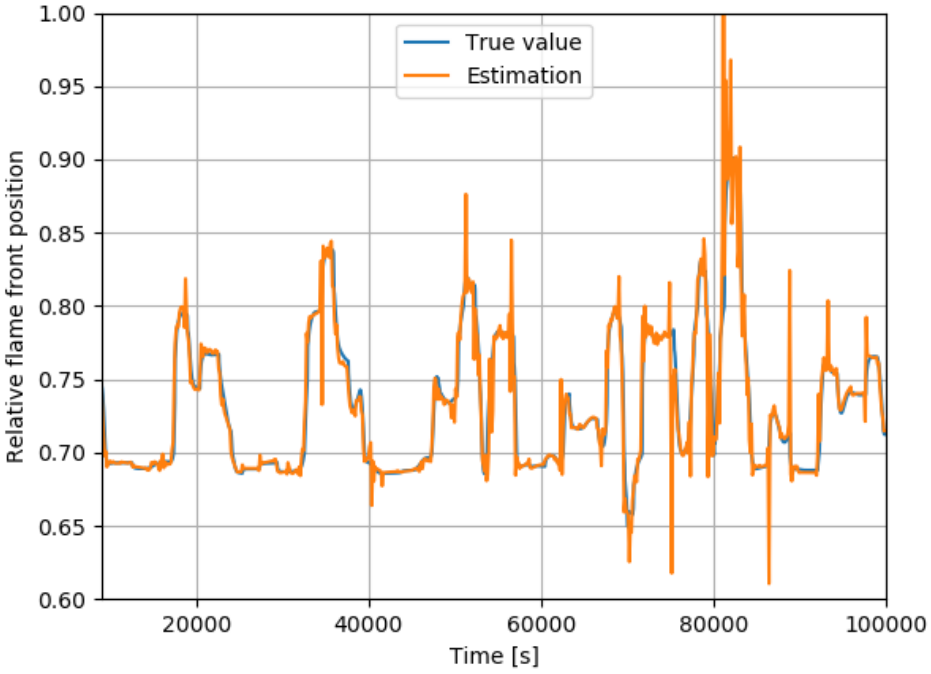

Figure 35. Neural network output for training data.

5.5 VALIDATION

The validation of the different neural network configurations was performed by comparing the network output with the flame front position in simulation for two different scenarios; one with random inputs like the training data but using a different seed and one with simple step responses. The results for these experiments are presented in Figure 36 and Figure 37. The neural network manages to capture the general dynamic responses of the system in the experiment with random input signals, but with spikes at some points in time that would need to be filtered away before potential use in feedback control. The step response experiment shows that the performance of the network for different steady state working conditions is quite varied. For the first two operating points, significant static errors can be seen, while for the last two, the estimations are very close to the true values.

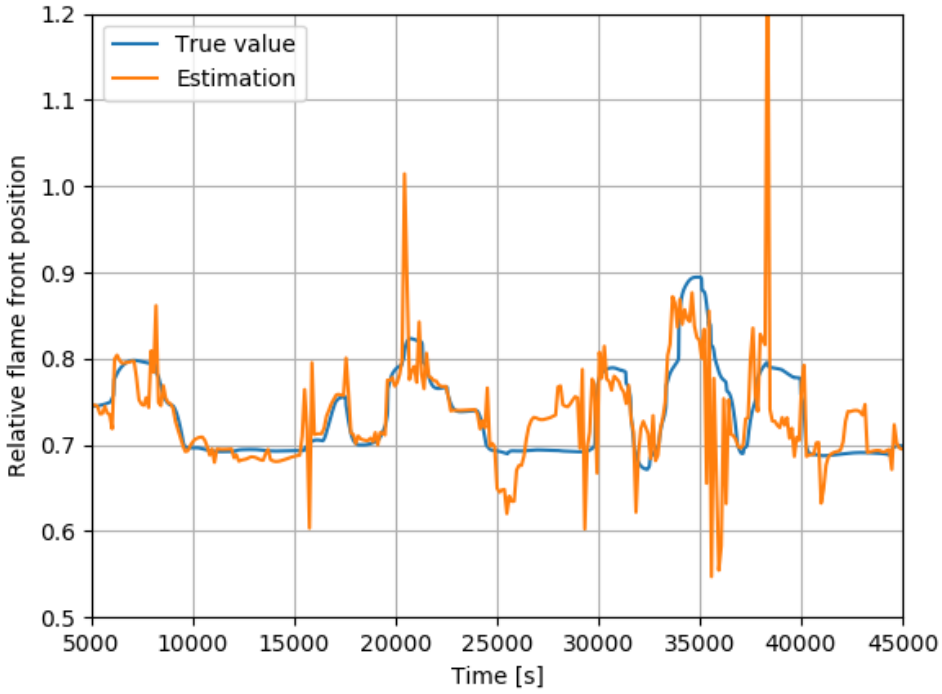

Figure 36. Comparison between neural network output flame front estimation and true value during experiment with random inputs.

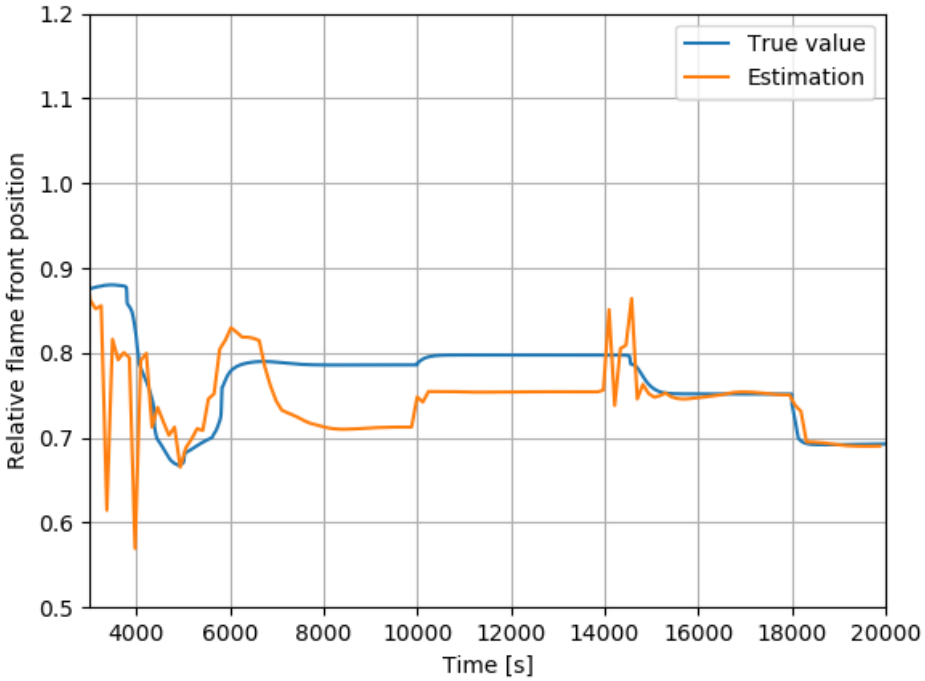

Figure 37. Comparison between neural network output flame front estimation and true value for step response experiment.

The validation revealed the difficulty of training a network so that it works well in the entire space of possible working conditions. In this project, this problem was accentuated by the following model specific issues:

- The robustness problems of the model in simulation, which specifically made training problematic, as this requires excitation of the model in many different operating conditions.
- The complex and different dynamic responses to changes in input signals. Believed to mostly be an artefact of the discretization of the bed, the response to boundary condition changes can be quite violent in terms of temperature changes in the different sections of the bed. In some situation the system also appears to reach a cyclic behaviour, where the flame front moves back and forth, instead of reaching a steady state, when certain combinations of boundary conditions are used. An obvious way to reduce this problem is to increase the spatial discretization of the bed and introduce vertical discretization.

It is however believed that, with additional efforts to improve the neural network setup, such as sampling time and number of delays for each input signal, significantly better results would be possible.

6 Extended Grate Boiler Control

The overall purpose of this project is to improve grate combustion by controlling the flame front to optimize the utilization of the grate. This is a general desire from the industry using grate boilers.

The closed-loop boiler control must be able to utilize the additional information about the flame front, provided by the soft sensor and this can be done, for example, by taking the following pragmatic approach

1. If the flame front is too close to the slag discharge, reduce the fuel flow and increase the primary air flow.
2. If the flame front is too close to the fuel inlet, increase fuel flow and decrease primary air flow.

A suggested extension of the generic control scheme in Figure 14 is shown in Figure 38. The blue dashed contour indicates the added changes.

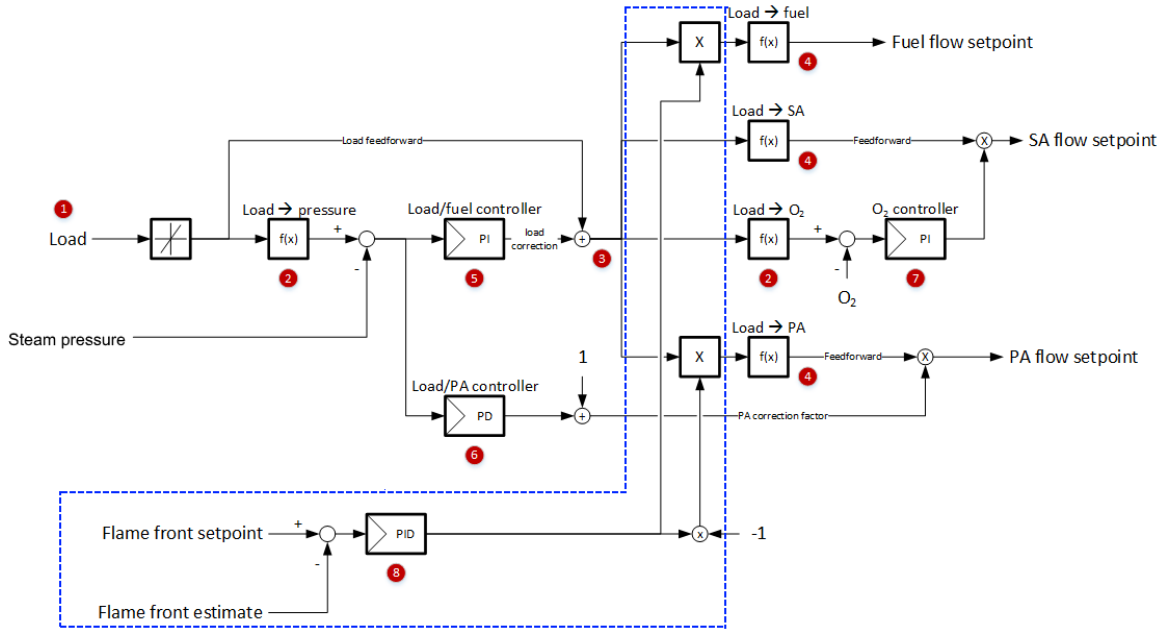

Figure 38. Extended grate control, utilizing flame front information.

The flame front estimate is compared with a flame front setpoint. Obviously, the two must have identical units which could be a distance (meters) from fuel inlet or a percentage of the grate length (e.g. 80 %). The deviation between setpoint and measurement is used in a PID controller ⑧, e.g., with an output in the range ±0.2. A control signal >1 means that the flame front is too close to the fuel inlet and a control signal <1 means that it too close to the slag discharge. The control signal is then either added to or subtracted from 1 to generate two multiplicative correction factors to apply to the fuel and primary air flow setpoints, respectively.

6.1 CLOSED-LOOP CONTROL

To show its validity, a comparison between the generic control scheme, shown in figure 14, and the extended scheme shown in figure 38 has been performed on the simplified grate model. Although it doesn't display all the transient details and nonlinearities of the complex model, the differences in step responses will justify the proposed concept.

6.2 LOAD CHANGE WITHOUT FLAME FRONT CONTROL

Figure 39 shows the responses from a step change in boiler load reflected in the following process variables. The control structure is the generic grate boiler control shown in Figure 14.

3. The topmost figure shows the flame front, defined as the distance from the fuel inlet, is constant, 10 meters, until the load step at t=200 seconds. The dynamic coordination of air and fuel inputs causes the flame front to retract a bit before starting a steady increase. If the model is simulated for long time, the flame front will converge on a value of about 10.3 meters (not shown).
4. The second figure shows that the fuel, primary and secondary air flows all jump to a higher than initial value. The transient behaviour of fuel and primary air after the load step is caused by the load feedback controller. The transient behaviour of the secondary air flow is caused by the oxygen controller.
5. The third figure shows the flue gas oxygen contents and its corresponding, unchanged, setpoint. The oxygen controller manages to maintain the O2 contents after the load change.
6. The bottom figure shows the flue gas temperature and the boiler load (expressed as heat release) and its setpoint. The load follows its reference nicely (see discussion about simplified model) while the temperature overshoots and slowly converges to a temperature higher than the initial value.

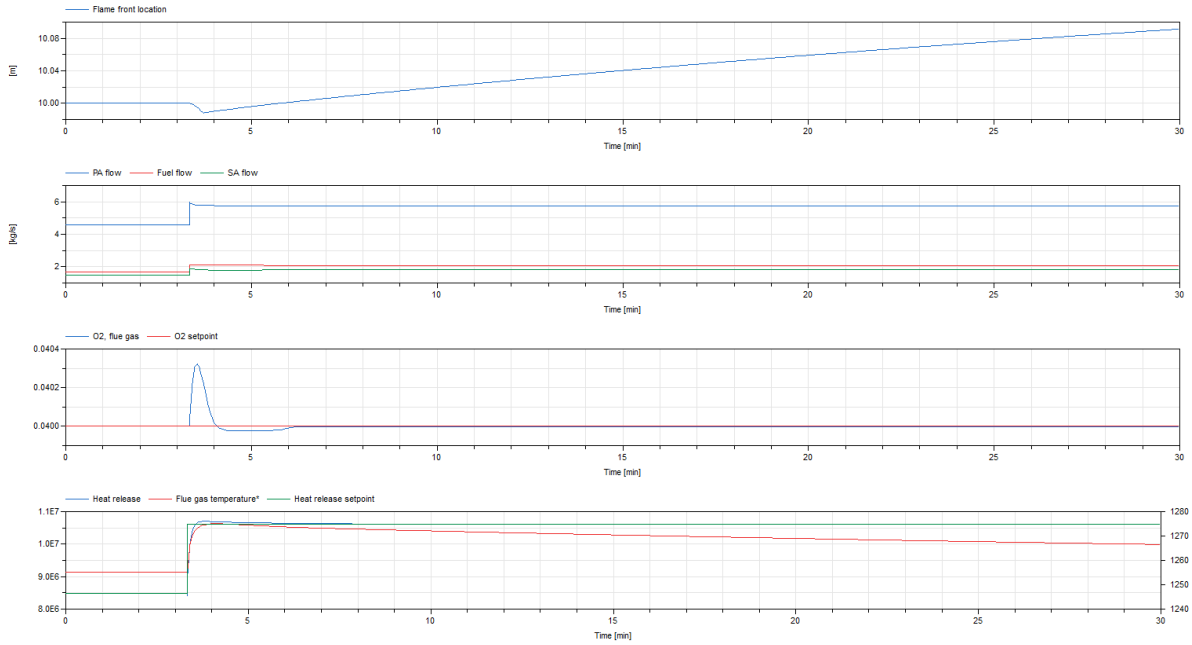

Figure 39. Closed-loop control without flame front control.

Apart from the uncontrolled flame front the generic grate control works well, despite of its simplicity.

6.3 LOAD CHANGE WITH FLAME FRONT CONTROL

Figure 40 shows the responses from the same step change in boiler load as shown in Figure 39. The difference is the control of the flame front with the extended grate control from Figure 38.

The topmost figure shows the flame front position and its setpoint of 10 meters. After the load change at t=200 seconds the flame front is disturbed by the jump in fuel and air flow and after a transition of 5–10 minutes the flame front is returned to its setpoint. The flame front controller in this case is tuned by trial and error in the simulation and keeps the flame front within 1 centimetre of its setpoint. This control quality should of course not be expected in a real plant.

The remaining plots in figure 40 show that fuel and air flow, O_2 contents, heat release and flue gas temperature show similar stable behaviour as in the closed-loop response without flame front control.

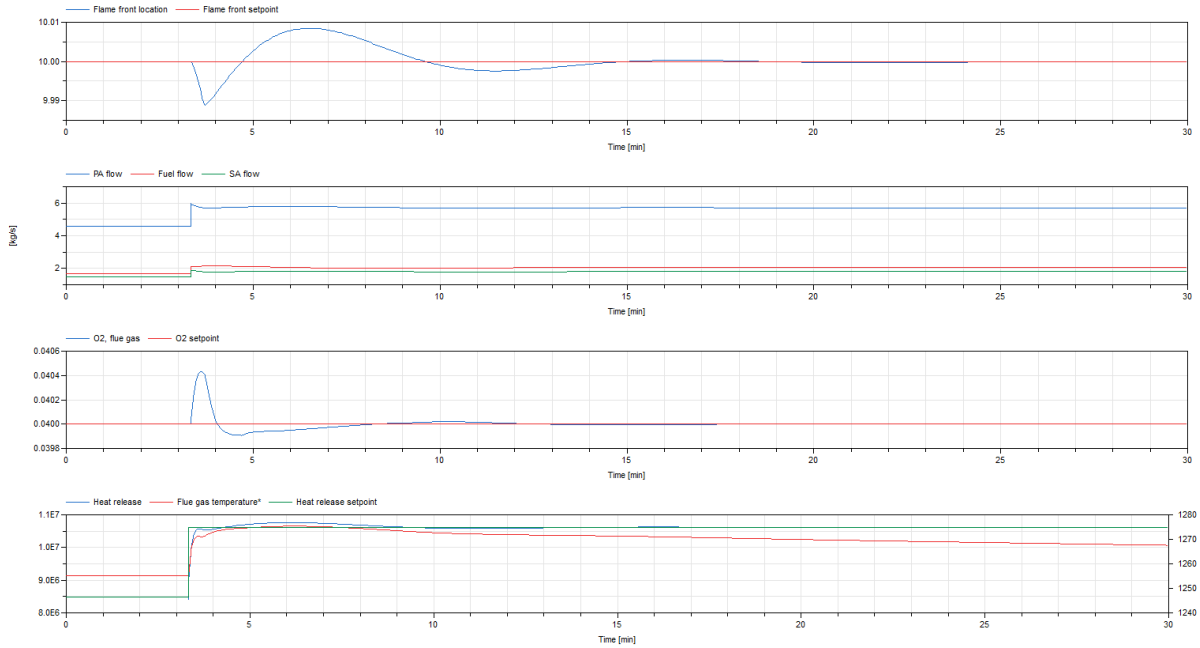

Figure 40. Closed-loop control with flame front control.

7 Summary and Conclusions

A highly complex grate boiler model has been developed, using physics-based modelling. The model contains a bed model discretized along the grate, combustion models, a discretized grate model and boundary conditions for fuel, gas and heat flows.

A soft sensor has been implemented based on an artificial neural network, trained using simulation results from the complex model. Validation of the soft sensor shows that it is likely possible to extract the flame front position from the available measurements.

A reference control system has been implemented and extended to enable use of the estimated flame front position. Its usefulness is verified using a simplified grate boiler model.

7.1 CONCLUSIONS

7.1.1 Modelling

The project has shown that physics-based modelling in Modelica is a viable method for representing the complex processes that occur in a grate boiler. As measurements of key signals was not available, such as fuel composition, fuel flow and flame front position, a detailed quantitative validation of the model was not possible, but the qualitative behaviour is reasonable. The modelling effort has revealed both strengths and difficulties in this modelling approach. The main takeaway is the potential of the method, as the connection of subcomponents based directly on physical principles with very little simplifications, have resulted in a highly complex model, which displays a behaviour that is aligned with the authors expectations of the process. The main difficulty has been the robustness problems in simulation of dynamic scenarios. The nature of these problems is a combination of the following:

- Nonlinear equations: With highly nonlinear equations such as radiant heat transfer, chemical reaction rates, pressure/flow relations connected without dynamic states to “separate” them several nonlinear equations must be solved simultaneous during each solver step. The solution of these equation systems usually relies on a quasi-Newton solver, requiring at least C1 continuity and much care should be taken when implementing discontinuities like IF-statements, MAX/MIN functions etc.
- Model topology: Following the staggered-grid approach when constructing large models is usually beneficial for the simulation time, initialization and robustness of a model. It basically means that the nonlinear equations mentioned above are decoupled in an alternating grid of so-called flow models and volume models and often only the volume models contain dynamic states. When aggregating a large model from components, however, it can be a challenge to strictly follow this scheme.

- Model stiffness: One challenge of rigorously following the staggered-grid scheme is that many dynamic states are introduced. If the time constants of these dynamics differ by several orders of magnitude simulation speed will slow down.
- Unit testing: Years of experience in component-oriented modelling has shown that rigorous testing of submodels or components is paramount! A component flaw (discontinuity, limited validity range, coding error etc.) can remain undetected during many applications of the component in question. However, at some point — usually in a complex context — it will surface making debugging tedious.

Despite the mentioned difficulties with the model, a highly flexible modelling approach has been introduced which allows us to easily reconfigure the model or adapt it to any other plant. For example, fuel drying, pyrolysis, combustion, radiative heat transfer etc. have been implemented in a way by which it is easy to replace the model equations with simpler or more complex equations using a "building block" approach.

7.1.2 Soft Sensor

The following general steps are suggested for implementing a soft sensor in a real plant:

1. Develop a model of sufficient complexity to capture all relevant dynamics of the process, in all relevant operating conditions.
2. Tune the model to match measurement data from the plant.
3. Develop a simplified model; black-box, grey-box or physics based, which captures the relation between flame front position and measured signals, based on the behaviour of the complex model.
4. Extend the control system of the plant with flame front information provided by the simplified model.

To some degree depending on the method for deriving the simplified model, the complex model is generally needed for increasing the amount of information that can be conveyed to the simplified model, compared to using measurement data alone. If for instance a neural network is used, it would be challenging to use measurements from the real plant as training data. The reason for this is that it would be infeasible to use PRBS signals as inputs to the real plant, which means that the training data in this case would be close to normal operation. This in turn could easily result in insufficient excitation of the system in the training phase which would result in unreliable estimations from the neural network in operation. The complex model is also important for validating the performance of the simplified model.

In this project, the limited amount of tuning that was possible makes it hard to know whether the complex model is sufficient to represent the dynamics of the real plant. This is of crucial importance if a neural network is used as the simplified model, as any significant mismatch between the model and the plant could result in large errors in the estimations.

The simplified model is needed for the practical implementation. Since it is derived from the complex model it cannot produce better estimations than that model does, but the complex model will often be too complex for implementation in a control system, as was observed in this project and the unscented Kalman filter that was the initial observer approach. The validation of the simplified model against the real plant could be performed by manually monitoring the flame front position at discrete points in time and comparing this data with the output of the soft sensor, when it is fed with measurements from the plant.

The neural network approach used for the simplified model in this project has proven to be a relatively easy to use method for estimating unknown process states. Taking results from simulation of a Modelica model in Dymola into NeuroLab, generating the weights and biases for the network and then bringing this data back into the Modelica environment constituted a relatively smooth workflow. The method itself seems capable of retrieving the desired states from a simulation model, but this has been somewhat hard to verify due to problems with generating enough training data and insufficient time to find the optimal setup for the network. The observability of the flame front position, however uncertain, still is an important result from the project as it indicates that other methods also could be used to determine the position.

The limitations in the results achieved with the work-flow presented above in this project should be seen in the light of the small amount of measurements that were both available in the plant and used in the observer model. For a plant with more available measurements, both the task of model validation and deriving an observer could potentially be simplified significantly. Furthermore, providing just a rough estimate of the flame front position, e.g., too far back, normal, or too close to slag discharge, and using this information in feedback control, would be an improvement in itself.

7.1.3 Flame Front Position Control

An extension to the generic grate control scheme has been proposed utilizing the estimated flame front position. A PID controller can use the estimate to produce a multiplicative correction of fuel and primary air flow setpoints, increasing the primary air to fuel ratio if the flame front is too close to the slag discharge.

A comparison of closed-loop simulations with the preliminary grate boiler model with and without flame front position control proved the validity of the proposed control concept.

7.2 FUTURE WORK

7.2.1 Modelling

First and foremost, the robustness issues of the model should be addressed. This should be a combination of improving the numerical properties of the (sub)models and of simplifying the existing model.

Numerical Improvements

In terms of numerical improvements, the following could be considered.

- On a component level, the entire range of sub-models, components and functions in the grate boiler model library should undergo rigorous unit testing to reveal situations where the numerics of the model code in question have hard times. For example, the char conversion model must be able to produce numerically valid results regardless of the boundary conditions applied to it — even with wrong boundary values (negative temperature, mass fraction etc.). This sort of robustness will ensure that bad calculations are not propagated onwards to adjacent models. Additionally, exceeding the scope of validity for a given model or function could produce a warning.
- On an overall model level great care should be taken about complying with the staggered-grid scheme to avoid direct connection of volume models since this can result in initialization problem. Also, connection of nonlinear flow-models should be avoided and should, preferably, be de-coupled with a dynamic element.

Model Simplifications

In terms of model simplifications, the following could be considered.

- Heat transfer model: A highly complex radiative model is used to represent the heat transfer between combustion, bed and furnace walls. The model introduces a large nonlinear equation system. By simplifying this area of the model, performance and stability improvements could be achieved.
- The simulation results in this project show that the different processes considered in the bed segment seldom occurs in parallel, meaning that most of the submodels in each bed segments are inactive during most of the simulation. The observations suggest that alternative modelling approaches might be more suitable in terms of simulation speed. One option is a moving boundary model, where the sequences are assumed to happen in series. This kind of model would have significantly fewer states than the current implementation.

7.2.2 Soft Sensor

The next step towards implementing a soft sensor in a real plant would be to investigate the implementational steps presented in Section 7.1.2 more thoroughly.

Perhaps most important of these is an improved validation of the complex model of the plant. However, only a limited amount of dynamic measurement data is typically available for this kind of plant, which will be a challenge in the validation process. As correct estimation of the flame front position specifically is crucial for the success of the overall method, one suggestion is to adapt the model to a plant where this is already measured, to verify that the modelling approach captures the dynamics of the flame front to an acceptable degree. Without this measurement available, regular manual inspection through the looking glass during a limited time (e.g. once every few minutes for a few hours), could be considered as an alternative way of producing data for comparison with the output of the model. To

analyse the neural network approach specifically, more systematically and rigorously trained network models need to be evaluated in a larger set of operating conditions. That would reveal if the measurements used in this project are sufficient to estimate the flame front position with sufficient accuracy in all relevant working conditions. The effect of adding more measurement signals could also be worth investigating, as it is expected that this will simplify the task.

As the results of this project indicate that the flame front position is in fact observable based on the available measurements, other estimation techniques should also be considered, which do not have the same requirements as a neural network in terms of training.

8 Bibliography

[Andersen et al., 2005] Observer-Based Fuel Control Using Oxygen Measurement — A study based on a first-principles model of a pulverized coal fired Benson boiler, Palle Andersen, Jan Dimon Bendtsen, Jan Henrik Mortensen, Rene Just Nielsen, Tom Søndergaard Pedersen, Värmeforsk P4-318.

[Bauer et al., 2010] *Modelling of Grate Combustion in a Medium Scale Biomass Furnace for Control Purposes*, Robert Bauer, Markus Gölles, Thomas Brunner, Nicolaos Dourdoumas and Ingwald Obernberger, Biomass and Bioenergy, 34, pp. 417-427, 2010.

[Bech et al., 1996] *Mathematical Modeling of Straw Bale Combustion in Cigar Burners*, Niels Bech, Lars Wolff and Lars Germann, Energy & Fuels, 10, pp. 276-283, 1996.

[Blasi et al., 2001] *Pyrolytic Behavior and Products of Some Wood Varieties*, Colomba D. Blasi, Carmen Branca, Antonio Santoro and Elier G. Hernandez, Combustion and Flame, 124, pp. 165-177, 2001.

[Brandt et al., 1997] *Decomposition of Tar in Pyrolysis Gas by Partial Oxidation and Thermal Cracking*, P. Brandt and Ulrik Henriksen, Part 2. EFP-97 journal nr. 1383/97-0015, 1997.

[Channiwali et al., 2002] *A Unified Correlation for Estimating HHV of Solid, Liquid, and Gaseous Fuels*, S. A. Channiwali and P. P. Parikh, Fuel, 81 (8), pp. 1051-1063, 2002.

[Codecà and Casella] *Neural Network Library in Modelica*, Fabio Codecà and Fransesco Casella, 5th Modelica Conference, 2006

[DK06] *Træfyringens teori*, Videnscenter for halm- og flisfyring, 2006.

[Dupont et al., 2014] *Heat Capacity Measurements of Various Biomass Types and Pyrolysis Residues,* Capucine Dupont, Rodica Chiriac, Guillaume Gauthier and Francois Toche, Fuel, 115, pp. 644-651, 2014.

[Henriksen et al., 1991] *Pyrolyse og forgasning af halm*, Ulrik Henriksen et al., Danmarks Tekniske Universitet, Delrapport 4. (RE 91-3), 1991.

[Hobbs et al., 1992] *Prediction of Effluent Compositions for Fixed-bed Coal Gasifiers*, Michael L. Hobbs, Predrag T. Radulovic, L. D. Smoot, Fuel, 71 (10), pp. 1177-1194, 1992.

[Hornik, 1991] Approximation Capabilities of Multilayer Feedforward Networks, Kurt Hornik, Neural Networks, 4, 1991.

[Kujik, 2008] *Grate Furnace Combustion - a Model for the Solid Fuel Layer*, Hans A. J. A. van Kuijk, Technische Universiteit Eindhoven, 2008.

[Laurendeau, 1978] *Heterogeneous Kinetics of Coal Char Gasification and Combustion*, Normand M Laurendeau, Progress in Energy and Combustion Science, 4, 1978.

[Ljung, 1999] System Identification: Theory for the User (2nd Edition), Lennart Ljung, Prentice-Hall, 1999

[McBride et al., 2002] *NASA Glenn Coefficients for Calculating Thermodynamic Properties of Individual Species*, Bonnie J. McBride, Dr. Michael J. Zehe, and Sanford Gordon, 2002

[NeuroLab 0.3.5 documentation] https://pythonhosted.org/neurolab/

[Neves et al., 2011] *Characterization and Prediction of Biomass Pyrolysis Products*, Daniel Neves, Henrik Thunman, Arlindo Matos, Luís Tarelho and Alberto Gómez-Barea, Progress in Energy and Combustion Science, 37, pp. 611-630, 2011.

[Paces et al., 2011] *Modeling of a Grate-firing Biomass Furnace for Real-time Applications*, Nicole Paces and Martin Kozek, Proceedings of the MMMse, 2011.

[Ramström et al., 2004] Metodik för modellering av förbränningsrost med systemidentifiering, svart- og grålådemodeller, Erik Ramström et al., Värmeforsk, 2004.

[Ramström et al., 2005] Framtagande av en dynamisk rostmodell för en rörlig förbränningsrost, Erik Ramström et al., Värmeforsk, 2005.

[Rojas, 1996] *Neural Networks: A Systematic Introduction*, Raul Rojas, Springer Science & Business Media, 1996

[Sadaka et al., 2009] *Biomass Combustion*, Sammy Sadaka and Donald M. Johnson, University of Arkansas, 2009.

[SciPy.org] https://www.scipy.org/

[Skogestad et al., 2005] *Multivariable Feedback Control*, Sigurd Skogestad and Ian Postlethwaite, Wiley, 2005.

[Tanner et al., 2016] *Kinetics of CO2 and Steam Gasification of Victorian Brown Coal Chars*, Joanne Tanner and Sankar Bhattacharya, Chemical Engineering Journal, 285, pp. 331-340, 2016

[Thunman et al., 2001] *Composition of Volatile Gases and Thermochemical Properties of Wood for Modeling of Fixed or Fluidized Beds*, Henrik Thunman, Fredrik Niklasson, Filip Johnsson, and Bo Leckner. Energy & Fuels, 15, pp. 1488–1497, 2001.

[Ullum, 2000] *Modellering af biomassefyret kedel* - Halmkedlen på Enstedværkets blok 3, Thorvald U. Ullum, Danmarks Tekniske Universitet, 2000.

[Veje, 2016a] *Preparation for Fixed Grate Modelling in Modelica*, Johannes Veje, Aalborg University Esbjerg, 2016.

[Veje, 2016b] *Dynamic Model of a Fixed Grate Combustion in Modelica*, Johannes Veje, Aalborg University Esbjerg, 2016.

[Wagner et al, 2000] The IAPWS Industrial Formulation 1997 for the Thermodynamic Properties of Water and Steam, J. Enf. Gas Turbines Power 122, 150-182

[Yin et al., 2008] *Mathematical Modeling and Experimental Study of Biomass Combustion in a Thermal 108 MW Grate-Fired Boiler*, Chungen Yin, Lasse Rosendahl,

Søren K. Kær, Sønnik Clausen, Søren L. Hvid and Torben Hille, Energy and Fuels, 22 (2), pp. 1380-1390, 2008.

GRATE BOILER MODELING FOR SOFT SENSOR BASED CONTROL

In response to the increasing flexibility requirements of thermal power plants, this report describes how an improved flame front position control can be achieved for grate boilers. The flame front position affects the performance of the plant significantly, but it is generally not measured directly, as this requires cameras and advanced image processing. A soft sensor, which uses existing measurements to estimate the flame front position, is therefore suggested.

Utilizing the physics-based modelling approach of Modelica, a detailed grate boiler model has been developed for this purpose. By combining the model with black-box modelling techniques, a soft sensor implementation is presented. Experimental results in simulation indicate that methods based on this approach could be used to improve the control of grate boilers, without the need for new expensive equipment.

Energiforsk is the Swedish Energy Research Centre – an industrially owned body dedicated to meeting the common energy challenges faced by industries, authorities and society. Our vision is to be hub of Swedish energy research and our mission is to make the world of energy smarter!

Energiforsk

Energimyndigheten